電気シグナルで誘導される細胞応答の測定システムの構築と定量的解析

Construction of measurement system and quantitative analysis for electric signal-induced cellular response

大阪大学大学院生命機能研究科

ナノ生体科学講座

ソフトバイオシステム研究室

佐藤　雅之

2008 年 9 月　博士学位論文

論　文　内　容　の　要　旨

〔　題　　名　〕

Construction of measurement system and quantitative analysis for electric signal-induced cellular response

（電気シグナルで誘導される細胞応答の測定システムの構築と定量的解析）

学位申請者　　佐藤　雅之

外部刺激に対する細胞の応答には、集団平均では見えてこない個々の細胞ごとのばらつきが存在する。これは細胞の応答が単に外部刺激の影響を受けるだけでなく、細胞内情報伝達ネットワークの状態に依存しているためであると考えられる。そこで、このような細胞内情報処理過程を研究するためには、細胞内情報伝達ネットワークの状態をモニターしながら、高精度に制御された入力刺激に対する細胞の応答を一細胞ごとに定量的に計測することが必要となる。入力の精度が高ければ高いほど、細胞内情報処理システムの状態を反映した応答を定量的に計測することができるため、入力刺激の厳密な制御は細胞内情報伝達の仕組みを調べる上で重要である。こうした高精度の入力刺激の制御が容易な手法として、電気刺激の利用が考えられる。実際、様々な細胞は電位勾配を認識して方向性のある運動を示す走電性 (electrotaxis, galvanotaxis)と呼ばれる性質を持つ。そこで、制御された入力刺激として電場を用い、応答として細胞運動を計測することで、上記要請に適う系を構築可能である。本研究は高速かつ低ノイズで電位勾配を発生させることができる実験系を開発し、走電性応答における入出力関係を明らかにした。また、このような入出力関係を実現するメカニズムを明らかにするために、走電性応答に関与している細胞内情報伝達経路を同定した。

走化性研究のモデル生物である細胞性粘菌*Dictyostelium discoideum*は直流電場下で陰極側へ移動運動する。細胞に与える電位勾配を大きくするにつれて、陰極側へ向かう移動の効率が高くなった。そこで電位勾配（入力）と走電性効率（出力）の関係を明らかにするために、細胞の陰極側への移動運動を陰極方向への平均変位速度（Mean Cathodal Displacement Speed、MCSと呼ぶ）により、定量化した。その結果、MCSは電位勾配の大きさE に対してシグモイダルに変化し、その入出力関係は以下の式で記述できることがわかった。

$$MCS = V_{\max}\left\{\frac{E^2}{E^2 + K_E^2}\right\}$$

ここで、V_{max}は陰極方向への最大平均変位速度である。K_EはMCSが50%となる電位勾配であり、細胞の電場感受性の指標となる。また、走電性効率は電位勾配の二乗に影響を受けることがわかった。様々な実験条件下における走電性効率は、この電場感受性K_Eを用いることで議論できる。一例として、細胞性粘菌の走化性誘引物質として働くcAMPの効果を調べた。細胞外液にcAMPを加えると走化性経路の細胞内情報伝達ネットワークが活性化されるが、このとき走電性効率が高くなることが観察された。上式から、cAMP存在下では電場感受性K_Eは約1.3倍高くなり、細胞がより低い電位勾配を認識できるようになることを示している。これは走化性経路の活性化が何からの方法で走電性効率の上昇に寄与していることを示唆している。このように、細胞の走電性応答における入出力関係は上式に従う。

次に、走電性応答の入出力関係を実現している細胞内情報伝達経路を同定することを試みた。その結果、阻害剤と変異体株を用いた実験から、走化性経路として知られるグアニル酸シクラーゼとPI3キナーゼ依存性経路が走電性応答における細胞内情報伝達経路であることを見出した。PI3キナーゼの活性が抑制されたとき、運動性に大きな変化は見られなかったが、電場方向のセンシング効率が著しく低下した。次に、グアニル酸シクラーゼ依存性経路の分子群をノックアウトしたところ、同様に走電性効率が低下した。さらに詳細な解析から、グアニル酸シクラーゼの酵素活性産物であるcGMPが

走電性応答における運動方向決定に重要であることがわかった。PI3キナーゼとcGMP依存性経路の活性を同時に抑制したところ、走電性応答の運動方向が陰極から陽極側へと反転した。これらの結果はPI3キナーゼとcGMP依存性経路が走電性応答の運動方向を決定する因子であることを示している。
細胞内情報伝達経路の構成要素であるタンパク質分子は熱ゆらぎや発現量の少数性からくる数ゆらぎなどによってたえずゆらぎに晒されている。しかしながら、細胞は安定にその機能を実現している。したがって、細胞内情報伝達経路は何らかの仕組みでゆらぎを抑制もしくは利用している可能性がある。本研究で得られた結果をもとに、今後は走電性情報伝達分子のダイナミクスをモニターしながら、外部から積極的に変調した入力を加えることで、細胞内情報処理の仕組みを明らかにしたい。

“Only connect …”

E. M. Forster

Contents

1, Introduction

1.1 Preface

Cells exist in a noisy environment. Since the size of a cell is only 10-100μm, both thermal fluctuations and the collision of water molecules can directly alter activity or structure of protein, which in turn can affect downstream intracellular signaling molecules and cellular function. The number of signaling molecules in a cell is estimated to range from a few hundred to a few thousand molecules. Thus, if a cell is cubic with a length of 1-10 μm, its volume is 1-1000 μm^3, which contains 10^{10}-10^{13} water molecules, meaning that a 1nM concentration of intracellular signaling molecules potentiates 0.6-600 molecules in the cell. To sustain a steady concentration, the number of intracellular signaling molecules must fluctuate with the cell size. Consequently, noise affects various cell functions including ion channel gating, neural firing rate, cytoskeleton dynamics, bacteria flagella rotation, gene expression and chemotactic signaling, all of which are modulated by signaling molecules [1-6]. In particular, since intracellular signaling cascades contain many feedback loops, the influence of noise is often amplified [7,8]. However, despite this noise amplification, cells function stably suggesting mechanisms that suppress and/or utilize noise. To clarify these mechanisms, I sought to examine the role of noise in intracellular signaling cascades by quantitatively measuring the relationship between the input and output under various conditions (Fig.1-1). In a uniform condition or in the absence of an external signal, cells migrate in random directions or show slow morphological change. These observations reflect the innate internal activity of a signaling cascade (Fig.1-1A). When an external signal is presented, cells show some responses such as directional migration, rapid morphological change and protein synthesis (Fig. 1-1B). In this case, the output is composed of the aforementioned internal activity and additional activity corresponding to the response. Specific external signal conditions (*e.g.* strength, speed, or periodicity) may synchronize with the internal time scale of the signaling components, enhancing or diminishing the output (Fig.1-1C). Additionally, a signal effect can be manipulated by genetic or pharmacological manipulation (Fig.1-1D). This last feature is very useful in identifying the roles of specific components in an intracellular signaling cascade. Taking

advantage of this, I applied a series of electrical inputs and analyzed the corresponding outputs, expressed as cell migration.

1.2 Bioelectricity

Here, I used an electric signal as a precise and stable input stimulation method allowing us to manipulate parameters such as strength, speed and waveform. Because a protein is a polymer chain with a charge, its structure should respond to an electric signal. Such structural changes affect molecule recognition and enzyme activity. In fact, it has been reported that particular electric field frequencies increase ion pump activity and promote cytoskeleton depolymerization in living cells [9,10]. Also application of electric field to the cells induces membrane potential change [11]. The function of the cell membrane includes selective permeation or active transport of ions or substrates; sensing, amplifying and transmiting an environmental signal; energy conversion; and recognition of cell-cell interaction. Therefore, changes in membrane potential potentially have many biological implications.

Long history of bioelectricity has clarified the importance of electric signal on many physiological phenomena including embryogenesis, neurogenesis, wound healing and regeneration [12-15] (Fig. 1-2). These physiological electric fields are thought to be generated in general by a simple mechanism where an asymmetric ion distribution through a thin membrane, which generates a large electro-chemical gradient. For example, consider a biological cell membrane with 5 nm thickness. Since cells maintain a membrane potential around -60mV, the strength of the electric gradient can reach ～ 120000 V/cm. Once the membrane permeates ions through a pore, ions flow to achieve an equilibrium state leading to an electric field. The most important point here is that this is not limited to the case of a single cell. *In vivo*, a cell itself can behave as a boundary. The surface of most organs is covered with a sheet of epithelial cells whose thickness is about ～20 μm and are tightly connected to each other by tight junctions [13]. This sheet's impermeability is so strong that even ion or water molecules cannot pass freely. Typical epithelial cells constitute a monolayer with Na^+ channels localized on the apical plasma membrane and K^+ channels and Na/K–ATPase pumps localized on the basolateral membrane (Fig. 1-3). Consequently, this system sustains an asymmetric ion distribution resulting in an electrical gradient. Such an electrical gradient is referred to as trans epithelial cells potential (TEP). A vibrating electrode system, which can detect small electric fields, has clarified that TEPs exists in various regions *in vivo*

including the prostatic epithelial duct, amphibian neural tube and in wounded skin. Furthermore, electric field strengths have been measured as 5 V/cm in the duct, 0.45-16 V/cm in the tube, and 1.5-2.0 V/cm in a wound [16-18]. Consider the case of wounded skin where the ion flow forms an “injury current” that generates an electric field, as first described by Emil DuBois-Reymond about one century ago [19]. It has been gradually realized that such physiological electric fields affect cellular functions such as the cell cycle, cell division and protein synthesis [20-22], all of which are pertinent to wound healing. One typical cell response to an electric field is directed cell migration, also known as electrotaxis or galvanotaxis, which describes the phenomenon where cells sense an electric field and migrate towards the anode or cathode [12-14]. A variety of cells can show electrotaxis. The migration direction and threshold of electrotaxis are dependent on the cell type as summarized in Table 1. However, the following questions remain largely unanswered. What kind of signaling molecules are involved in electrotaxis? How do cells sense the electric field direction? And how do they integrate this sensing into the motile apparatus for directional cell migration? Answering these questions is necessary to utilize electrical signals when investigating intracellular signaling pathways quantitatively.

Table 1 Property of electrotaxis in various cells

Cell type	Response direction	Threshold [V/cm]	Reference
Neural crest cells			
Quail	Cathode	0.1	Nuccitelli & Erickson (1983)
Xenopus	Cathode	0.1	Stump & Robinson (1983)
Fibroblasts			
Mouse NIH3T3 and SV101	Cathode	ND	Brown & Loew (1994)
Cornea			
Rat epithelial	Cathode	ND	Song et al. (2002)
Rabbit epithelial	Cathode	4	Soong et al. (1990)
Rabbit endothelial	Anode	2	Chang et al. (1996)
Bovine	Cathode	1	Zhao et al. (1996)
Human	Cathode	1	Farboud et al. (2000)
Lens			
Bovine	Cathode/Anode	0.5/1.5-2	Wang et al. (2003)
Human granulocyte	Anode	1	Rapp et al. (1988)
Human leukocyte	Cathode/Anode	ND	Fukushima et al. (1953)
Human macrophage	Anode	ND	Cho et al. (2002)
Rat prostate cancer cell line	Cathode	0.1	Djamgoz et al. (2001)
Epidermal cells			
Xenopus embryo	Cathode	ND	Luther et al. (1983)
Fish scale	Cathode	0.5	Cooper & Schliwa (1986)
Human skin	Cathode	0.1	Nishimura et al. (1996)
Neurons			
Xenopus	Cathode	>2.5	Patel & Poo (1982)
Mouse	No	0.5	De Boni & Anderchek (1986)
Zebrafish	No	1	Cormie & robinson (2007)
Melanocyte	No	1	Grahn et al. (2003)
Amoebae			
Amoebae proteus	Cathode	<3	Korohoda et al. (2000)
Dictyostelium discoideum	Cathode	1-2	Sato et al. (2007)

ND: Not determined. This table is based on reference 13.

In the section of response direction, “No” means random cell migration.

1.3 *Dictyostelium discoideum*

Model organism

Dictyostelium discoideum have been used to investigate various cell biology systems including cell movement, cell division, differentiation and chemotaxis [23-27]. Because *Dictyostelium* cells also exhibit strong electrotactic movement towards the cathode in a direct current electric field (dcEF), here I used *Dictyostelium* cells as a model organism for investigating the mechanism behind the interaction between an electric signal and living cells [28,29]. Compared to mammalian cells, *Dictyostelium* cells have many experimental advantages. For example, there is a wealth of knowledge regarding the chemotactic signaling pathway of *Dictyostelium* cells. Because both chemotaxis and electrotaxis exhibit directed cell migration, there is a possibility that the signaling pathways are shared to some extent. Several chemotactic signaling components like G protein coupled receptor, hetero trimeric G proteins, the Ras family, PI3-kinase and PTEN have been identified while actin, myosin Ⅱ and many related proteins have been identified as components of the motile apparatus [23-27]. Also, established genetic techniques make this organism more attractive. *Dictyostelium* cells are haploid creatures meaning homologous recombination occurs frequently such that mutant or knockout cells are easier to produce than in mammalian cells. Unlike mammalian cells, *Dictyostelium* cells show highly motile activity meaning exposure time to the electric field can be minimized (Mammalian cells; 1-5 μm/hours, *Dictyostelium* cells; 600-900 μm/hours). This allows us to minimize heating and exposure to toxic byproducts from the electrode. Finally, we can obtain a cell population whose response to the environment and motility is synchronized. This is important when measuring the input-output relationship of a cellular system quantitatively. Thus, *Dictyostelium* cells are an attractive organism for investigating the mechanism of electrotaxis as well as chemotaxis.

Life cycle

Here, we briefly introduce the lifecycle of *Dictyostelium discoideum* (Fig. 1-3). In a nutrient rich condition, *Dictyostelium* cells posses a round shape and proliferate, but with low motile activity (vegetative stage). When the nutrient is removed, they enter the

developmental stage leading to offspring (developmental stage). As development progresses (typically about 4 hours later), the cells become chemotactic competent cells, taking a polarized polarization shape and showing increased motile activity. They can sense extracellular cAMP emitted by other neighboring cells and move towards a higher concentration area causing aggregation. Afterwards, about 10^5 cells form a multi-cellular organism, called a slug and move to a more habitable area determined by temperature and humidity. Finally, the slug morphs into a fruiting body. The fruiting body consists of mainly two parts, a stalk and a spore [24,27]. When environmental conditions are adequate, cells spread from the spore and start to proliferate again. In all experiments in this study, only starved cells were used.

Possible meaning of electrotaxis in *Dictyostelium* cells

Electric potentials have been found on the surface of multicellular system such as skin, embryos and neural tubes. Therefore, the effects of electric signal in *Dictyostelium* cells may be applied to these multicellular systems. It has been already demonstrated that ions flow during the multicellular stage of *Dictyostelium* cells as Jaffe *et al*. demonstrated Ca^{2+} efflux at the center of a slug and influx at the tail and head regions by using a vibrating electrode system [30]. Recently, along with confirming these results, Reid *et al*. also detected ion flux at the mound stage as shown in Fig. 1-3 [31]. One characteristic of multicellular stages is the appearance of differentiated cells. In *Dictyostelium* cells, differentiation at the multicellular stage determines the position of the cell within a slug or mound. For example, the tip of a cell within a slug becomes the spore while the remainder becomes the stalk. Additionally, some researchers have pointed out the relationship between cell differentiation and its electrical property [32]. Yabuno reported that the electrical property of membrane of differentiated cells was different from undifferentiated one [33,34]. Since it has been suggested that electrical property of cells affects the electrotactic response, there is a strong possibility that the electric signal may sort cells by manipulating the electrotactic movement efficiency among differentiated cells within the slug or mound stage.

References

[**1**] Berg OG (1978) A model for the statistical fluctuations of protein numbers in a microbial population. *J Theor Biol* **71**:587-603.

[**2**] Simon SM, Peskin CS, Oster GF (1992) What drives the translocation of proteins? *Proc Natl Acad Sci U S A.* **89**:3770-3774.

[**3**] Allen C, Stevens CF (1994) An evaluation of causes for unreliability of synaptic transmission. *Proc Natl Acad Sci U S A* **91**:10380-10383.

[**4**] van Oudenaarden A, Theriot JA (1999) Cooperative symmetry-breaking by actin polymerization in a model for cell motility. *Nat Cell Biol* **1**:493-499.

[**5**] White JA, Rubinstein JT, Kay AR (2000) Channel noise in neurons. *Trends Neurosci* **23**:131-137.

[**6**] Korobkova E, Emonet T, Vilar JM, Shimizu TS, Cluzel P (2004). From molecular noise to behavioural variability in a single bacterium. *Nature* **428**:574-578.

[**7**] Shibata T, Fujimoto K (2004) Noisy signal amplification in ultrasensitive signal transduction. *Proc Natl Acad Sci U S A* **102**:331–336.

[**8**] Ueda M, Shibata T (2007) Stochastic signal processing and transduction in chemotactic response of eukaryotic cells. Biophys J **93**:11-20.

[**9**] Cho MR, Thatte HS, Lee RC, Golan DE (1994) Induced redistribution of cell surface receptors by alternating current electric fields. *FASEB J* **8**:771-776.

[**10**] Cho MR, Thatte HS, Lee RC, Golan DE (1996) Reorganization of microfilament structure induced by ac electric fields. *FASEB J* **10**:1552-1558.

[**11**] Hassan N, Chatterjee I, Publicover NG, Craviso GL (2002) Mapping membrane-potential perturbations of chromaffin cells exposed to electric fields. *Plasma Science, IEEE Transactions on*. **30**:1516- 1524.

[12] Robinson KR (1985) The responses of cells to electrical fields: a review. *J Cell Biol* **101**:2023-2027.

[**13**] Nuccitelli R (2003) A role for endogenous electric fields in wound healing. *Curr Top Dev Biol* **58**:1-26.

[**14**] Mycielska ME and Djamgoz MB (2004) Cellular mechanisms of direct-current electric field effects: galvanotaxis and metastatic disease. *J Cell Sci* **117**:1631-1639.

[**15**] McCaig CD, Rajnicek AM, Song B, Zhao M (2005) Controlling cell behavior

electrically: current views and future potential. *Physiol Rev* **85**:943-978.

[**16**] Szatkowski M, Mycielska M, Knowles R, Kho AL, Djamgoz MB (2000) Electrophysiological recordings from the rat prostate gland in vitro: identified single-cell and transepithelial (lumen) potentials. *BJU Int* **86**:1068-1075.

[**17**] McCaig CD, Rajnicek AM, Song B, Zhao M (2002). Has electrical growth cone guidance found its potential? *Trends Neurosci* **25**:354-359.

[**18**] Nuccitelli R, Nuccitelli P, Ramlatchan S, Sanger R, Smith PJ (2008) Imaging the electric field associated with mouse and human skin wounds. *Wound Repair Regen* **16**:432-441.

[**19**] DuBois-Reymond E (1843) Vorla¨ufiger Abriss einer Untersuchung uber den sogenannten Froschstrom und die electomotorischen Fische. *Ann. Phy. U. Chem*. **58**:1–30.

[**20**] Wang E, Yin Y, Zhao M, Forrester JV, McCaig CD (2003) Physiological electric fields control the G1/S phase cell cycle checkpoint to inhibit endothelial cell proliferation. *FASEB J* **17**:458-460.

[**21**] Song B, Zhao M, Forrester JV, McCaig CD (2002) Electrical cues regulate the orientation and frequency of cell division and the rate of wound healing in vivo. *Proc Natl Acad Sci U S A* **99**:13577-13582.

[**22**] McLeod KJ, Lee RC, Ehrlich HP (1987) Frequency dependence of electric field modulation of fibroblast protein synthesis. *Science* **236**:1465-1469.

[**23**] Fukui Y (1993) Toward a new concept of cell motility: cytoskeletal dynamics in amoeboid movement and cell division. *Int Rev Cytol* **144**:85-127.

[**24**] Maeda Y, Inouye K, Takeuchi I (Eds.) (1997) Dictyostelium: A Model System for Cell and Developmental Biology. Universal Academy Press, Tokyo.

[**25**] Parent CA and Devreotes PN (1999) A cell's sense of direction. *Science* **284**, 765-770.

[**26**] Van Haastert PJ and Devreotes PN (2004) Chemotaxis: signalling the way forward. *Nat Rev Mol Cell Biol* **5**:626-634.

[**27**] Eichinger L et al. (2005) The genome of the social amoeba Dictyostelium discoideum. *Nature* **435**:43-57.

[**28**] Zhao M, Jin T, McCaig CD, Forrester JV, Devreotes PN (2002) Genetic analysis of the role of G protein-coupled receptor signaling in electrotaxis. *J Cell Biol* **157**:921-927.

[**29**] Sato MJ, Ueda M, Takagi H, Watanabe TM, Yanagida T, Ueda M (2007) Input-output relationship in galvanotactic response of Dictyostelium cells. *Biosystems* **88**:261-272.

[**30**] Kühtreiber WM, Jaffe LF (1990) Detection of extracellular calcium gradients with a calcium-specific vibrating electrode. *J Cell Biol* **110**:1565-1573.

[**31**] Reid B, Nuccitelli R, Zhao M (2007) Non-invasive measurement of bioelectric currents with a vibrating probe. *Nat Protoc* **2**:661-669.

[**32**] Guitard M, Leyvraz C, Hummler E (2004) A nonconventional look at ionic fluxes in the skin: lessons from genetically modified mice. *News Physiol Sci* **19**:75-79.

[**33**] Yabuno K (1970) Changes in electronegativity of the cell surface during the development of the cell surface during the development of the cellular slime mold, Dictyostelium discoideum. *Dev Growth Differ* **12**:229-239.

[**34**] Yabuno K (1971) Changes in cellular adhesiveness during the development of the slime mold Dictyostelium discoideum. *Dev Growth Differ* **13**:181-190.

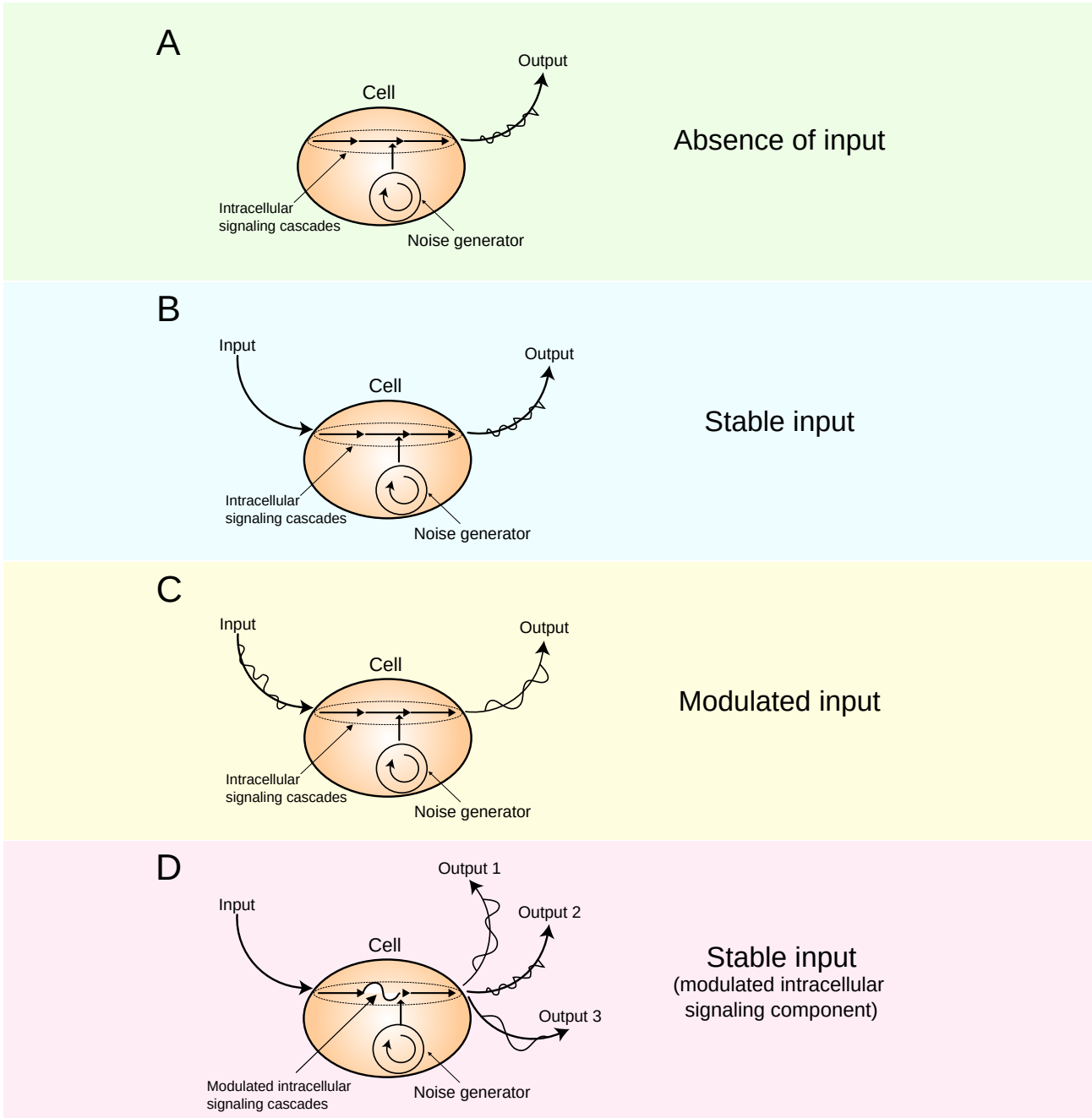

Fig.1-1 Investigation of logic of intracellular signaling from input-output relationship.
Cells migrate in random direction even when an external signal is absent (**A**). When stable input is applied, cells show a coordinated output which contains the rich information about intracellular signaling cascade (**B**). (**C**) Modulated inputs can change the property of intracellular signalig cascades positively or negatively. This can be controlled by using genetic manipulation technique or pharmacological treatment (**D**).

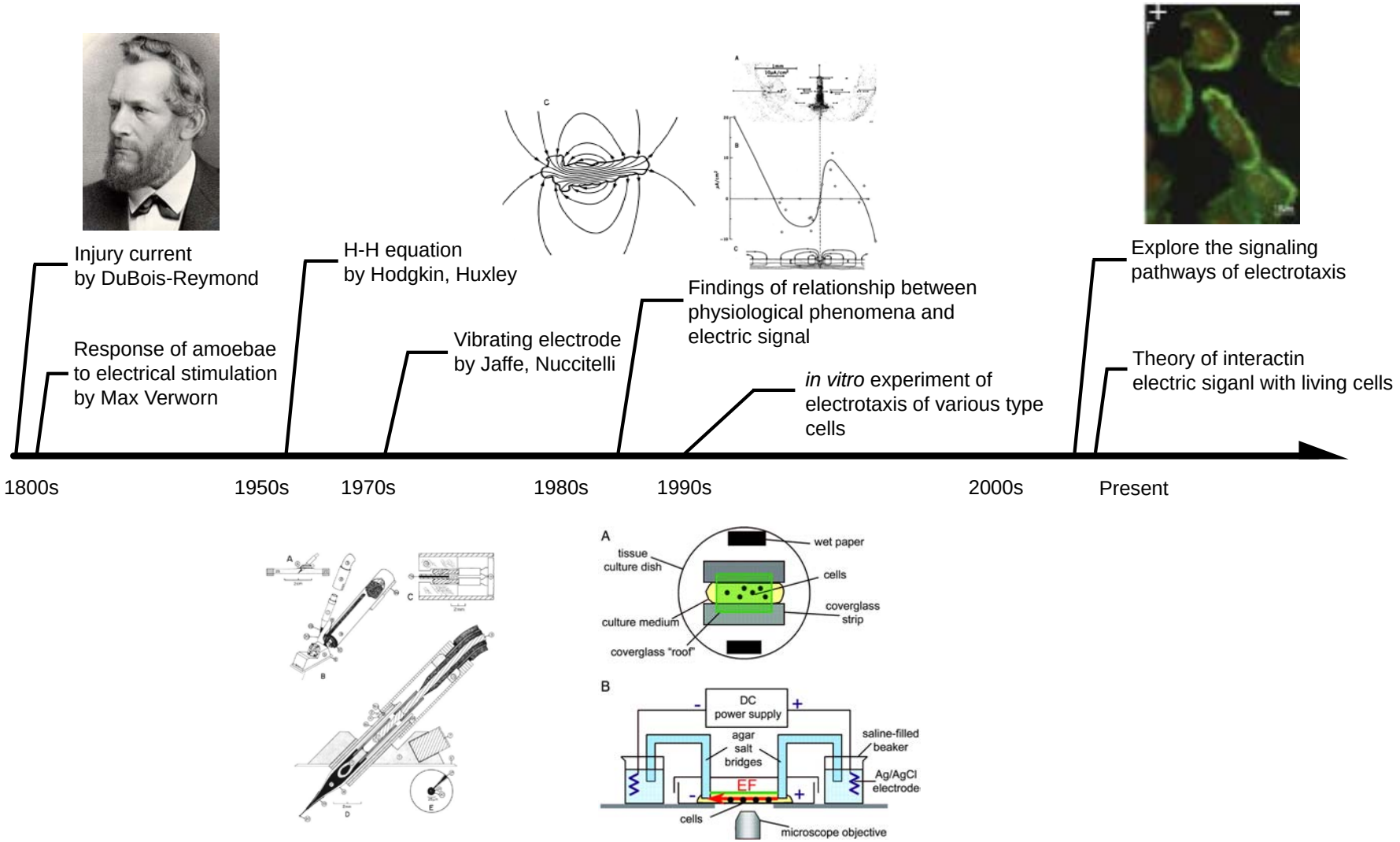

Fig.1-2 History of Bioelectricity.

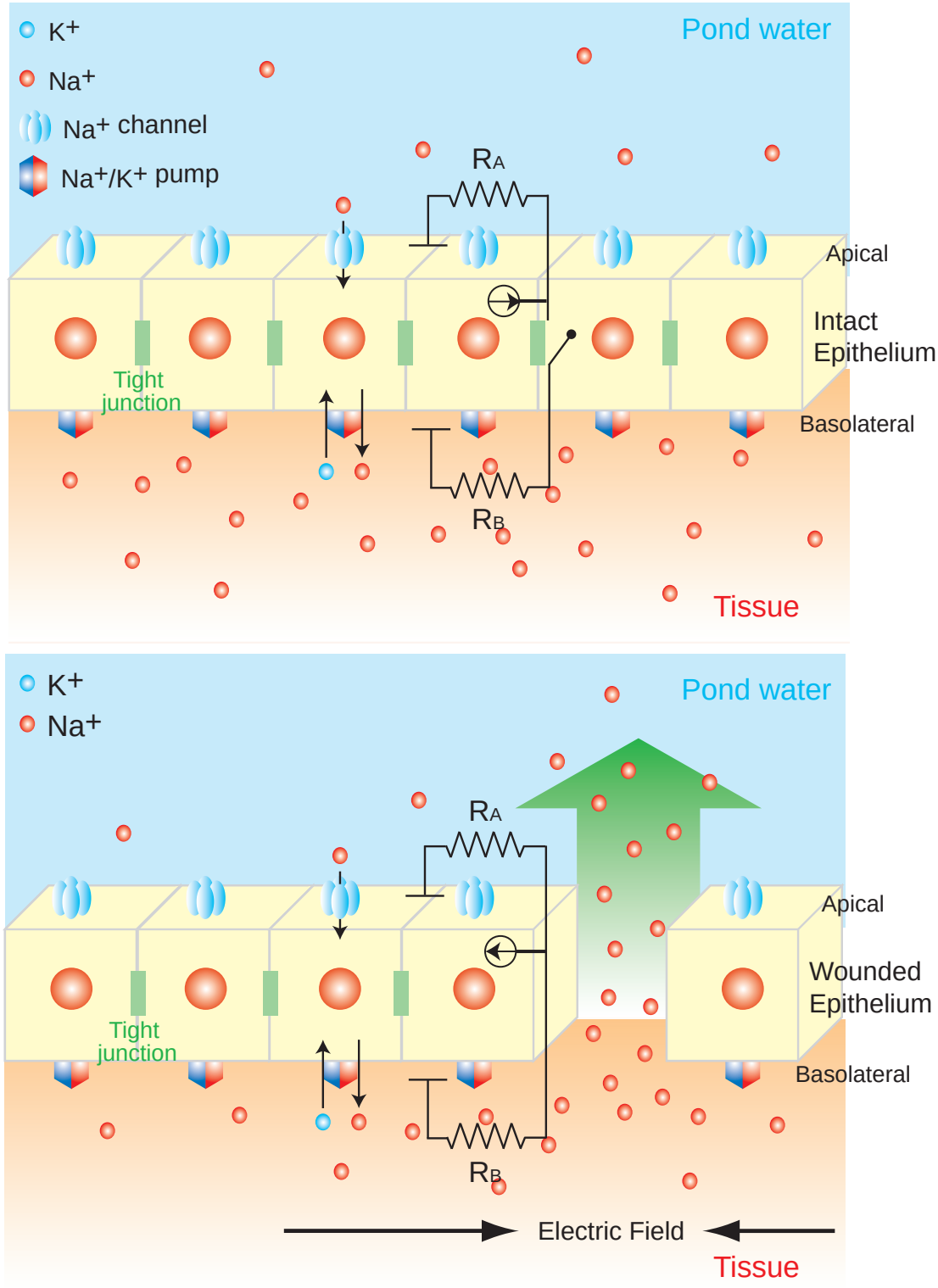

Fig.1-3 Biological battery. Schematic representation of the skin epitheria of a frog. Note that in the case of humans, a wound is exposed to air instead of the pond water. R_A and R_B are resistances of apical and basolateral area, respectively. (**Upper**) The combined activities of Na^+ channels and Na^+/K^+ pumps create a charge differential resulting in the inside of the skin having a high electric potential (red region) with respect to the outside (Blue region). This charge difference is known as a trans-epitheial potential (TEP). The whole system behaves as a biological battery. The unidirectional transport of Na^+ across epitherial sheet precludes the completion of the circuit. (**Lower**) Generation of an electric field by a wound. When epitherial sheet is broken, ion leakage causes in an outward-directed current and creates an electric field. Since positive charge (Na^+) flows towards the site of the wounded area, the wounded area is defined as the cathode pole.

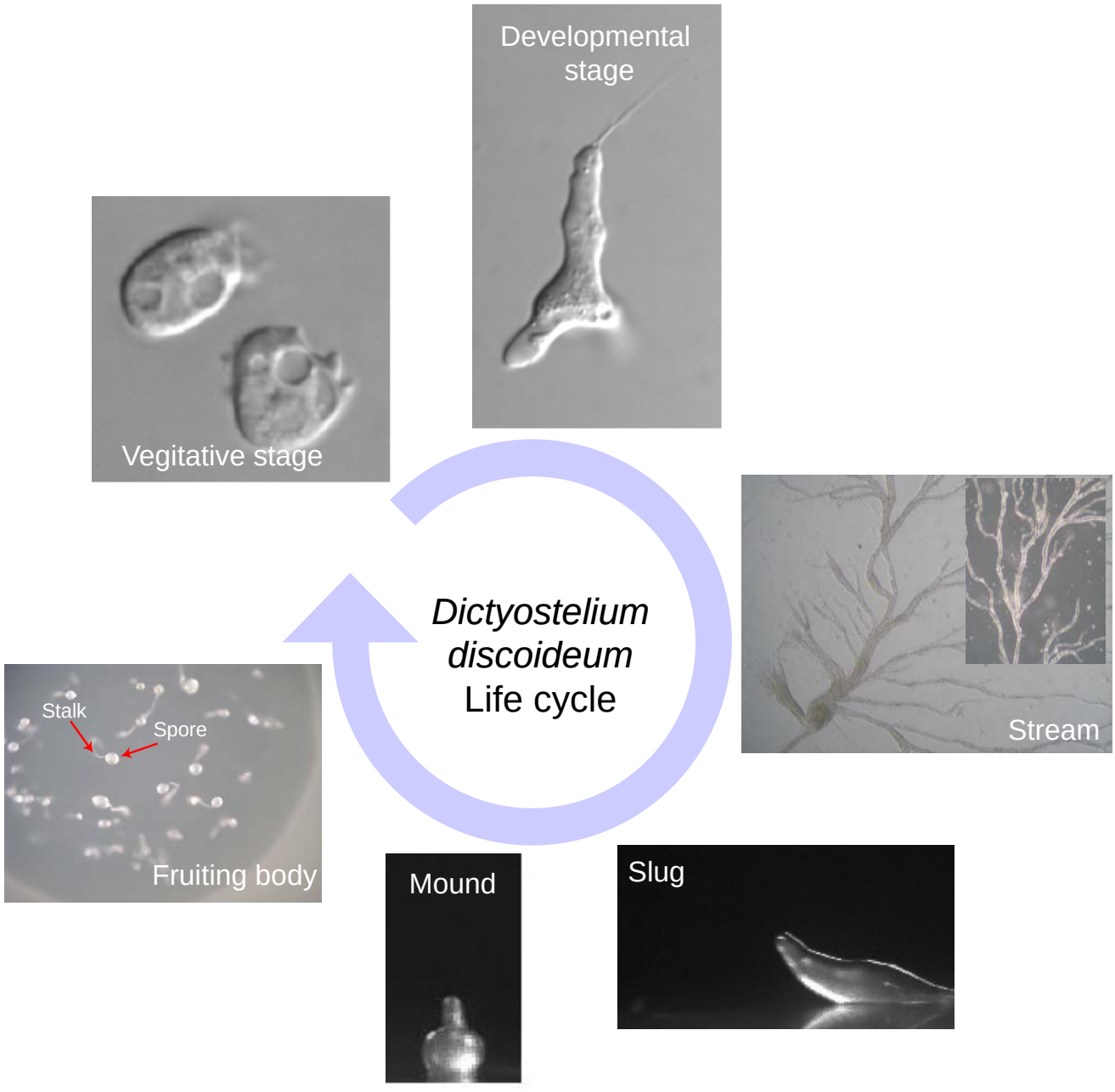

Fig.1-4 Life cycle of *Dictyostleium discoideum*. At the vegetative and early developmental stage, cells behave as a single cell. At later developmental stage, about 10^5 cells aggregete and form multicellular organism, slug. Slug moves to a region suitable for the fruiting body at the end of developmental stage. Fruiting body is resistant for dry or heat. When condition improve, cells spread from the spore and start the vegitative stage again.

2, Methods & Materials

2.1 Cell preparation

For electrotactic assays, Ax2 cell line was used as the wild type. Ax2 cells were grown on a culture dish (Petridish, ϕ=90 mm, height=20 mm, INA-OPTIKA) filled with 10 ml HL5 medium (30.8 g glucose, 14.3 g yeast extract, 28.6 g proteose peptone, 0.485 g/l KH_2PO_4, 1.28 g/l $Na_2HPO_4 \cdot 12H_2O$, 0.2 μg/ml folic acid, 0.06 μg/ml Vitamin B_{12} in total 2 liter) with 10 μg/ml streptomycin [1]. Cells were grown in a static culture condition at 21 ^{o}C. Particular attention was given to avoid a confluent culture condition since a high cell density risks generating a heterogeneous population. In addition to the wild type, the following 7 knockout cell lines were used including guanylyl cyclase double knockout cells (*gca*$^{-}$/*sgc*$^{-}$), soluble guanylyl cyclase deletion catalytic domain in *gca*$^{-}$/*sgc*$^{-}$ cells (sgcΔcat in *gca*$^{-}$/*sgc*$^{-}$), guanylyl cyclase deletion N-terminus domain in *gca*$^{-}$/*sgc*$^{-}$ cells (sgcΔN in *gca*$^{-}$/*sgc*$^{-}$), cyclic GMP binding protein A and B null cells (*gbpA*$^{-}$/*gbpB*$^{-}$), cyclic GMP binding protein C and D null cells (*gbpC*$^{-}$/*gbpD*$^{-}$), cyclic GMP binding protein C null cells (*gbpC*$^{-}$) and a series of KI mutant cells (KI-5, KI-8, KI-10). Except for the KI mutants, knockout cell lines were grown in HL5 culture medium supplemented with 10 μg/ml streptomycin lines. Selection markers for each cell are summarized in Table 2. KI mutant cells could not grow in HL5 culture medium. Therefore, these cells were grown on a 5LP plate (0.5% lactose, 0.5% proteose peptone, 1.5% agar) with *Escherichia coli* B/r at 21 ^{o}C [2].

To examine the behavior of molecules involved in the electrotactic signaling pathway, guanylyl cyclase (GC) and phosphatidylinositol-3-OH kinase (PI3K) dependent signaling molecules fused to green fluorescent protein (GEP) were observed by fluorescence imaging. sGC-GFP in GC-double null cells and GbpC-GFP in GbpC null cells were gifts from Dr. Peter Van Haastert. The GFP fused $PH_{Akt/PKB}$-domain plasmid was a gift from Dr. Taro Q. P. Uyeda. The PI3K2-GFP plasmids were constructed in our laboratory. These plasmids were introduced into the cells by electroporation (Electro Square Porator, ECM830, BTX) at a rate of one pulse per

second (voltage 500 V, 15 pulses, 100 μs pulses). Again, selection markers for each cell line are summarized in Table 2.

Table 2 Cell lines for electrotactic assay

Cell type	Selection marker (concentration)	cAMP pulse stimulation time [hr]	Resource
gca⁻/sgc⁻	Blasticidin S (10 μg/ml)	3	Dicty Stock Center[1)]
sgc Δ cat in *gca⁻/sgc⁻*	G418 (10 μg/ml)	3	Van Haastert Lab.[2)]
sgc Δ N in *gca⁻/sgc⁻*	G418 (10 μg/ml)	3	Van Haastert Lab.[2)]
gbpA⁻/gbpB⁻	Blasticidin S (10 μg/ml)	6	Dicty Stock Center[1)]
gbpC⁻/gbpD⁻	Blasticidin S (10 μg/ml)	6	Dicty Stock Center[1)]
gbpC⁻	Blasticidin S (10 μg/ml)	3	Van Haastert Lab.[2)]
sGC-GFP in *gca⁻/sgc⁻*	G418 (10 μg/ml)	5	Van Haastert Lab.[2)]
GbpC-GFP in *gbpC⁻*	G418 (10 μg/ml)	4	Van Haastert Lab.[2)]
PI3K2-GFP / PTEN-Halo in Ax2	G418 (10 μg/ml) Blasticidin S (10 μg/ml)	3	-
$PH_{Akt/PKB}$-GFP in Ax2	G418 (10 μg/ml)	3	-

1) Dicty Stock Center; http://dictybase.org/StockCenter/StockCenter.html

2) Van Haastert Laboratory; http://www.rug.nl/gbb/research/researchgroups/cellBiochemistry/index

To shift from the vegetative to starvation stage, all cell lines were treated as follows:

1) HL5 was removed by aspiration. 10 ml developmental buffer（DB, 10 mM Na/K PO_4, 2 mM $MgSO_4$, 0.2 mM $CaCl_2$）was added.
2) 1 min after, DB was removed and 3 ml DB was added.
3) Cells were peeled away from the dish by pipette and placed in a centrifuge tube (15 ml, centrifuge tube, IWAKI).
4) Additional 2 ml DB was added into the dish to extract residual by the same procedure in 3. (Total 5 ml cell suspension)
5) Centrifugation (2-3 min, 4 ^{o}C, 1500 rpm).
6) After removing the supernatant by aspiration, 5 ml DB was added and gently mixed the cell pellet by using a pipette.

7) Centrifugation (2-3 min, 4 ^{o}C, 1500 rpm).
8) Operation 6 and 7 were repeated twice.
9) Cell density was adjusted to 5x10^{6} cells/ml by adding DB.
10) 1 ml cell suspension was injected into the plastic culture dish (35 mm, Iwaki) and placed on an incubator at 21 ^{o}C for 1 hour.
11) After 1 hour, cells were pulse stimulated with 100 nM cAMP at 6 min intervals for 3-5 hours on a rotating shaker (SL3D, SeouLin Bioscience). This pulse stimulation system was constructed with a timer and liquid flow pump (SJ-1211, ATTO). The pulse stimulation accelerated cell synchronization. As a result, the cell population shifted to the developmental stage faster (about 3 hours) than that of untreated cells (normally 5 hours-).
12) After 3-5 hours, cells were removed from the dish by using a pipette and correct in a centrifuge tube.
13) Centrifugation (2-3 min, 4 ^{o}C, 1500 rpm).
14) After removing the supernatant by aspiration, 5 ml DB was added and mixed gently with the cell pellet by using a pipette.
15) Operation 13 and14 were repeated twice.
16) 6 ml DB was added to the cell pellet and gently mixed. This dilution made the cell density appropriate for observing single cell migration in an electrotactic chamber.
17) After mixing the cell suspension with ligands such as cAMP or inhibitors, 75 μl of the cell suspension was injected into an electrotactic chamber from one well (Fig. 2-1A). Caffeine was added to reduce cell-cell interactions by inhibiting adenylyl cyclase activity, except in KI mutant cell lines [3].
18) After 10 min, the inside of the chamber was washed with DB containing the same composition from operation 17 three times to remove the non-adhered cells.
19) A salt bridge was set into the chamber well. After adding 40 μl DB into the other well, a salt bridge was placed there as well.
20) After 20 min, the attachment and motile activity of the cells were observed. The electric field was then applied.

After cAMP pulse stimulation, the cells became chemotactic competent cells and often

started to aggregate. Once cells form a multicellular organism, they cannot be used for electrotactic assays. So, we delayed development by keeping cells at a low temperature (4 ^{o}C). This treatment kept the cells in an ideal condition for electrotactic experiments for 3-4 hours.

1) After cAMP pulse stimulation, the cell density was adjust to 5x10^{6} cells/ml.
2) The cell suspension (650 μl) was placed into the culture plate (24 well plate, Nunclon™ Δ surface) at 4 ^{o}C.
3) Before use, cells were removed from the plate by using a pipette.
4) Temperature was raised to 21 ^{o}C for 20-30 min resulting in active cell motility.

2.2 Equipment for electrotactic assay

The electrotactic assay system is shown in Fig. 2-1.

(1) Microscope and image capturing

Cells in the chamber were observed with an inverted microscope, Olympus IX-71, equipped with differential interference contrast (DIC) optics or phase contrast (PH) optics. The objective lens depended on the optics (UPIanApo, 20x/0.8, oil, LVCPIanFLN; 20x/0.45 Ph1, Olympus for DIC and LUCPIanFLN; 20x/0.45 Ph1, Olympus for PH). Images were captured with a cooled CCD camera (Micro Max, Princeton Instruments.inc) through the relay lens (x2.5). MetaMorph (Molecular Devices) was used to control the CCD camera. Data acquisition started 5 min after applying electric field to the cells. Images were acquired at 5 sec intervals for 20-30 min. To visualize GFP fused proteins, cells were examined through an inverted microscope (TE2000-PFS, Nikon) with an Apo TIRF 60×/1.49 oil immersion lens. Confocal images were obtained using a CSU10 scanner unit (Yokogawa) at an excitation wavelength of 488nm from a DPSS laser (Sapphire 488-200 CDRH, COHERENT) with an EM-CCD camera (Andor technology ixon+ DU-897). A barrier filter was used to detect emissions greater than 522 nm. The image was captured with Andor IQ software.

(2) Electrotactic assay chamber

Figure 2-1A illustrates the configuration of the electrotactic assay chamber. The chamber requires certain properties. 1) The substrate of the chamber does not harm the

cells; 2) The dimension of chamber is constructed in a highly reproducible manner; and 3) Unavoidable joule heating generated by applying the electric field to the insulator is minimized. To satisfy these demands, we made an silicon chamber (CX-32-2297-No1,No2, Shin-Etsu Silicones or SYLGARD 184 Silicone Elastomer kit, Dow Corning). No.1 and No.2 liquids were mixed at a weight ratio of 1:10 in a 15 ml centrifuge tube. After mixing these thoroughly, they were centrifuged to release trapped air from within the mixed gel (20 min, 4 ^{o}C, 1500 rpm). The gel was then gently introduced into a wax-block mold that was processed by using a milling machine. The gel containing mold was placed in an incubator at 37 ^{o}C overnight. The next day, the mold was heated (60 min, 90 ^{o}C) in a drying oven (DO-300A, As ONE). After cooling down, the silicone chamber was removed from the mold and preserved in 100% EtOH. Before use, the chamber was washed with miliQ. At the bottom of the chamber was a 40x50 mm coverslip. Above the chamber, a 10x18 mm coverslip was placed (Fig. 2-1A). The coverslips were sonicated in 70 % EtOH for 15 min, washed 10 times with miliQ and blow dried. In every experiment, a new glass coverslip was used. To attach the chamber to the bottom coverslip, vaseline (white, high pure, Wako) was painted on the bottom of chamber uniformly. To seal, we gently pressed the chamber from above. Next, the upper area of the chamber was also painted with vaseline uniformly. The second coverslip was placed on the chamber and this was also pressed gently from above. Final volume of the cell attached apace between coverslips was 20x3x0.25 mm^3 (length x width x height). The completed chamber was placed on the microscope stage via a silicon sheet to suppress slipping (Fig. 2-1A). To keep chamber moist, wet papers surrounded chamber and whole apparatus was enclosed with modified plastic dish (Fig. 2-1D). This chamber was not harmful to cells in DB and allowed for long periods of observation. Moreover, the chamber was constructed in a highly reproducible manner because of the mold. To minimize the joule heating, the volume to surface area ratio in the chamber was adjusted carefully to resemble that from other electrotactic experimental systems [4]. In addition, since all experiments were done in a temperature-controlled room (21 ^{o}C), temperature change was minimal (<1 ^{o}C) meaning little Joule heating in our experimental system was due to rapid heat dissipation from the glass surface of the chamber.

(3) Salt bridge

Because several byproducts generated on the electrode surface by applying a voltage are toxic to cells, electrodes should be separated from the cell attached area. Therefore, electric fields were applied to the cells through the salt bridges. Solution containing 100 ml DB and 2 g agarose for electrophoresis (Nnacalai tesque) was stirred and warm up repeatedly until gel to be invisible. Next, as shown in Fig.2-2, a silicon tube (ϕ =8 mm) was connected to a modified glass tube to remove gel from the beaker (Fig. 2-2). Immediately, the glass tube was cooled using a water flow. Too rapid cooling makes an opening between the gel and glass tube. Since this should be avoided in order to perform a stable electric field application, salt bridges were first sunk in miliQ at room temperature and then preserved at 4 ^{o}C. Just before using, excess gel was cut and removed by a razor.

(4) Generation of electric fields

An electrical field generation system was developed to apply electric field to cells at a high speed and with low noise (Fig. 2-1B). A function generator (Type 8025, Tabor Electronics) transmitted an optimal electric signal, made by a wave generator (ARB-software, Tabor Electronics) through a bipolar voltage amplifier (BOP500M, KEPCO or A400, FLC electronics). The electric signal was passed through the Ag/AgCl electrodes and salt bridges. The rising time of the voltage generation by the bipolar power supply was within 30 μsec while the changing rate of the supplying voltage and load were 0.0005 % and 0.0005% at constant voltage, respectively. The ripple and noise was less than 10 mV (rms) at 10-100V. These properties insured a fast and highly stable electric field.

(5) Manufacture of Ag/AgCl electrode

Ag/AgCl electrodes are preferred for their stability, easy manufacturing and easy handling. For these reasons, Ag/AgCl electrodes have been widely used in electro-chemistry and biology. Here, the silver line (circular section; 0.8 mm diameter; Nilaco) was used connected to the copper line. The silver line was immersed in sodium hypochlorite solution, NaClO (Wako), overnight to coat the AgCl thin layer. Before use, Ag/AgCl electrodes were washed with miliQ well.

(6) Electric field strength measurement

The circuit of the experimental system is drawn in Fig.2-3A. In electrotactic experiments, the electric field strength is often calculated by Ohm's law. However, since direct measurement of the electric field strength is more reliable, as described by Nuccitteli and Erickson, here the electric field strength was measured directly by a Pt electrode connected to a high impedance probe [5]. If the internal resistance of the measurement system is not sufficiently large, current flows into it. In such cases, when the measurement system is connected to the sample, the combined resistance (R_{cmp}), which consists of the measurement system resistance (R_m) and the chamber resistance (R_s), is lower than the actual value meaning that the electric field is not accurately measured. Thus, one needs to know the internal resistance of the measurement system

in order to accurately measure the field strength. The combined resistance can be expressed as

$$R_{cmp} = \frac{R_s R_m}{R_s + R_m} \tag{2.1}$$

Here, R_s and R_m represent the resistance of the chamber and measurement system, respectively. The relationship between R_m/R_s and R_{cmp}/R_s can be expressed by rewriting equation (2.1),

$$\frac{R_{cmp}}{R_s} = \frac{R_m}{R_s + R_m} = \frac{\left(\frac{R_m}{R_s}\right)}{1 + \left(\frac{R_m}{R_s}\right)} \tag{2.2}$$

The plot of this equation is shown in Fig. 2-3B. When R_m/R_s is 100, the measurement system has little impact on the field strength. Since the resistance of chamber area was measured to be around 200 kΩ, ideal resistance of measurement system is 20 MΩ. Here digital multimeter (10 MΩ internal resistance, 50 resistance ratio, Type R6341B, ADVANTEST) or digital oscilloscope (10 MΩ internal resistance, Type TDS2014, Tektronix) was used to measure the electric field strength. When these measuring systems were connected to the chamber, it was predicted that the voltage decreased by about 2% voltage. However, such tiny changes can be ignored. The current meter (digital multi meter, SC-7401 IWATSU) was placed in series to monitor the stability of the applied electric field during the experiments. Thus, although such a high resistance system that includes the solution makes precise measurements difficult in general, I could measure the electric field strength in my system within 2% accuracy.

2.3 Analysis of cell migration

(1) Analysis

Data acquisition began 5 min after applying the electric field. Cell images were acquired at 5 sec intervals for 20-30 min. To analyze the motile activities of the cells under electric fields, cell images were processed automatically by using lab-developed software called “Tsuiseki-kun” developed by Dr. T. Watanabe in which images are converted into binary images by setting an optimal threshold value for brightness. The center position of the brightness of the cells was determined in X,Y-coordinates. Not all cells in the view were analyze for the whole observation time. Cells which were observed for a short time (less than half the observation time) and interacted with other cells were removed from the analysis. Next, the two dimension coordinate data was processed using a Perl-language program to evaluate cell migration. This was done by calculating positional change, which include motile properties such as migration velocity, cell motility efficiency, directedness and asymmetric index (Fig. 2.4A). Migration velocity was calculated by dividing the total path length of cell migration (trajectory) by the observed time. Cell motility efficiency was defined as the ratio of the net displacement to the total path length, so that the efficiency becomes unity when a cell moves along a straight line in one direction. Directedness of a cell with respect to the electric field was defined as $\cos\theta$, where θ is the angle between the direction of the cell’s net displacement and the direction of the electric field. Average directedness for the cell population was obtained by calculating $\frac{1}{n}\sum_{i=1}^{n}(\cos\theta)i$, where n is the total number of cells analyzed. Thus, a randomly moving population of cells will have an average directionality of zero. When all the cells migrate toward the cathode, the directionality will have unity. The asymmetric index was defined as the ratio of the total number of cathode biased cells to the total number of anode biased cells at the end of electric field application.

(2) Mean displacement analysis

Mean displacement analysis was introduced to quantify the bias degree of directed cell migration. Here, each cells are considered as a single particle that moves randomly in

two dimensions.

Definitions

N - total steps

τ - time for one step

l - distance of one step

T - observation time

k_x - number of steps towards the positive X-axis (see Fig. 2-4B)

p_x- probability of migration towards plus direction in X-axis

q_x - probability of migration towards minus direction in X-axis (p_x+q_x=1)

Assume a particle is positioned at the origin. Here, only steps towards the X-direction are considered. After N steps, the position of the particle along the X-axis can be expressed as $X = \left(k_x - \left(N - k_x\right)\right) \cdot l$. Therefore,

$$X = (2k_x - N) \cdot l \tag{2.3}$$

Because N and l are constant, mean displacement, $\langle X \rangle$ can be expressed as

$$\langle X \rangle = \left(2\langle k_x \rangle - N\right) \cdot l \tag{2.4}$$

Here, the degree of bias degree, b, is introduced as follow,

$$p_x - q_x = b \tag{2.5}$$

Therefore, we obtain,

$$p_x = \frac{b+1}{2} \tag{2.6}$$

Also, by definition,

$$T = N \cdot \tau \tag{2.7}$$

$$\langle k_x \rangle = N \cdot p_x \tag{2.8}$$

Using (2-6), (2-7) and (2-8), (2-4) can be rewritten as $\langle X \rangle = b \cdot \frac{l}{\tau} \cdot T$, where $\frac{l}{\tau}$ represents the migration velocity of one step, which I call v such that

$$\langle X \rangle = b \cdot v \cdot T \tag{2.9}$$

Equation (2.9) tells us that the mean displacement $\langle X \rangle$ linearly depends on time when the extent of bias on cell migration is constant with time. The mean displacement $\langle X \rangle$ can be obtained experimentally by measuring the positional changes of cells under an electric field. When $\langle X \rangle$ is plotted as a function of time, the slope bv reflects the extent of the bias. Because the velocity of cell migration was almost constant in the presence of an electric field (See chapter 3.1), the migration velocity, v, can be assumed to be constant. The same analysis can be applied to the cell's migration along the y-axis. Therefore, by analyzing the dependency of the slope bv on electric field strength, the extent of the bias on the directional migration induced by an electric field can be obtained. This analysis provides the input-output relationship to electrotactic response. Here I refer to the slope bv as mean cathodal displacement speed (*MCS*).

References

[**1**] Watts DJ, Ashworth JM (1970) Growth of myxameobae of the cellular slime mould Dictyostelium discoideum in axenic culture. *Biochem J* **119**:171-174.

[**2**] Kuwayama H, Ishida S, Van Haastert PJ (1993) Non-chemotactic Dictyostelium discoideum mutants with altered cGMP signal transduction. *J Cell Biol* **123**:1453-1462.

[**3**] Brenner M, Thoms SD (1984) Caffeine blocks activation of cyclic AMP synthesis in Dictyostelium discoideum. *Dev Biol* **101**:136-146.

[**4**] Korohoda W, Mycielska M, Janda E, Madeja Z (2000) Immediate and long-term galvanotactic responses of Amoeba proteus to dc electric fields. *Cell Motil Cytoskeleton* **45**:10-26.

[**5**] Erickson CA, Nuccitelli R (1984) Embryonic fibroblast motility and orientation can be influenced by physiological electric fields. *J Cell Biol* **98**:296-307.

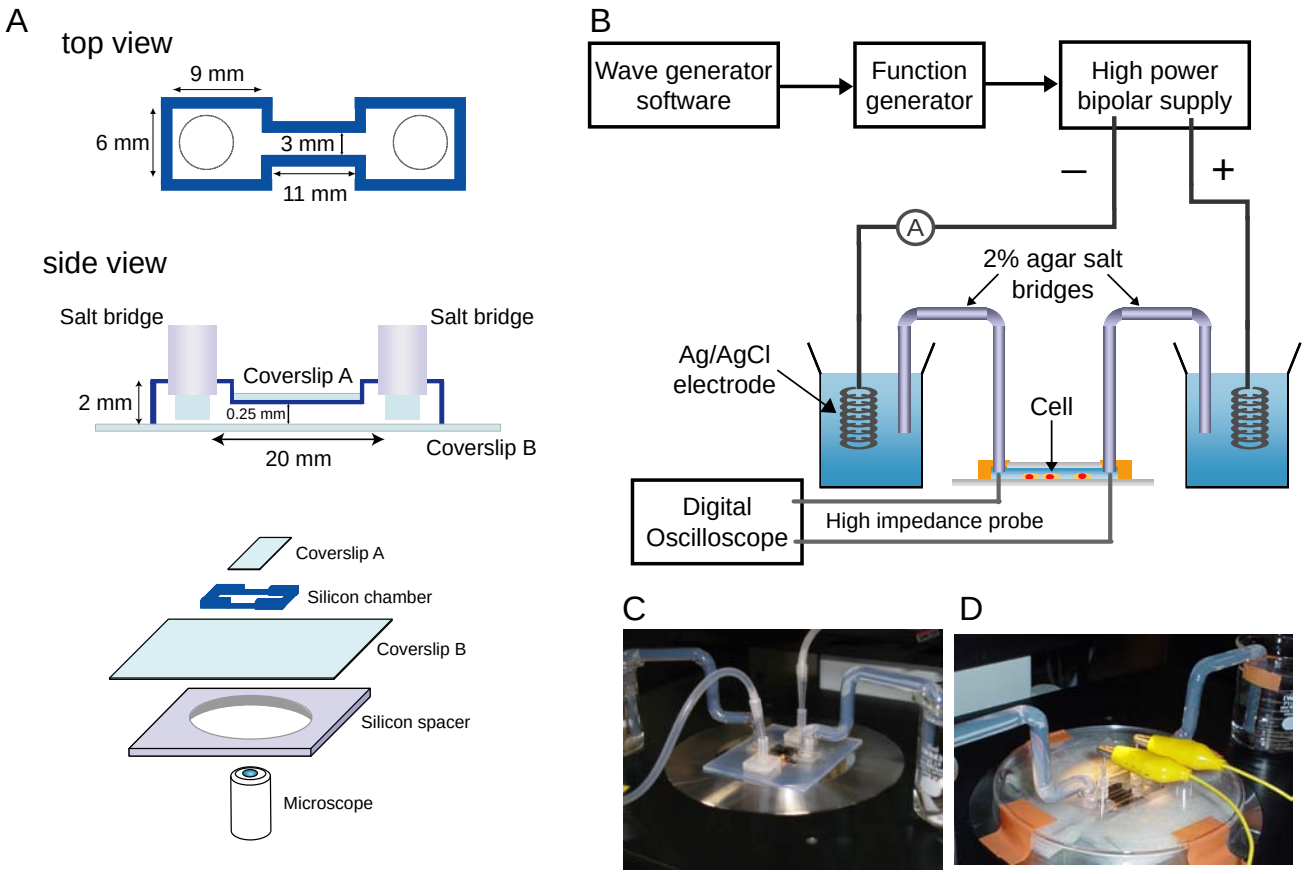

Fig.2-1 Experimental setup for electrotactic assay

(**A**) Configuration of electrotaxtic assay chamber. Electric fields were generated between salt bridges. Cell behaviors were observed by an inverted microscope and recorded by a CCD camera connected to a personal computer. (**B**) Apparatus for electric field application. "A" denotes digital multimeter (ampere mode). Pictures represent cross-current flow chamber (**C**) and normal experimental setup for electrotactic assay (**D**).

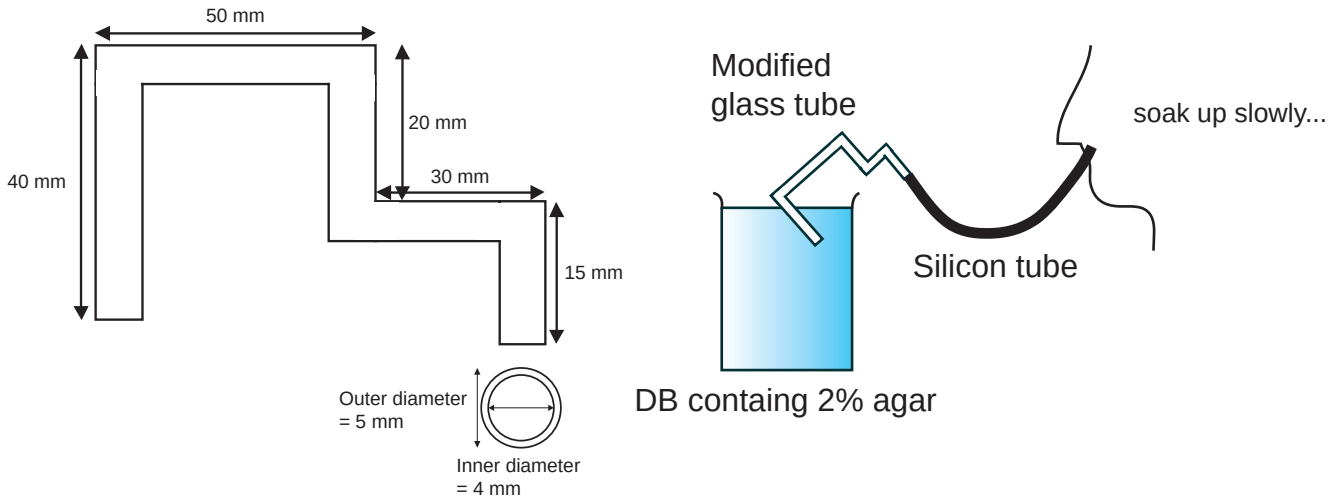

Fig.2-2 Construction of salt bridge

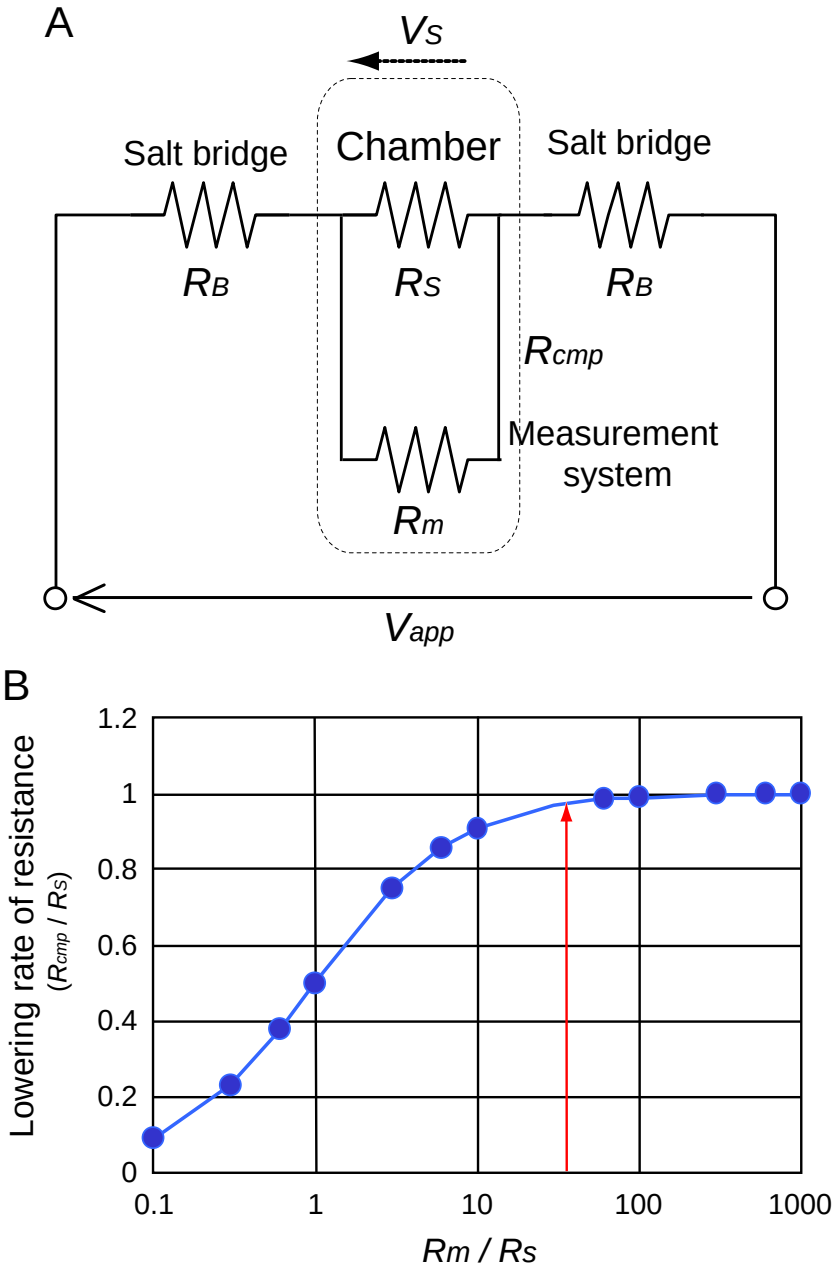

Fig.2-3 Experimental setup of the electrotactic assay

(**A**) Circuit of the experimental system for electrotactic assays. V_S and V_{app} represent applied voltage for the sample and whole system, respectively. R_B and R_S indicate the resistance of the salt bridge and the chamber, respectively. R_m is the internal resistance of the measurement system. Combined resistance, R_{cmp}, is a sum of R_S and R_m. Current of this system can be expressed by $V_{app}=I \cdot (2R_B+R_{cmp})$.
(**B**) When the ratio of resistance of the measurement system and the chamber (R_m/R_S) is 100, connection of the measurement system does not cause voltage decline. Actual resistance of chamber was almost 200 kΩ.Therfore, the measurement system with 20 MΩ internal resistance is ideal. Red arrow indicates the value of R_m/R_S in this system.

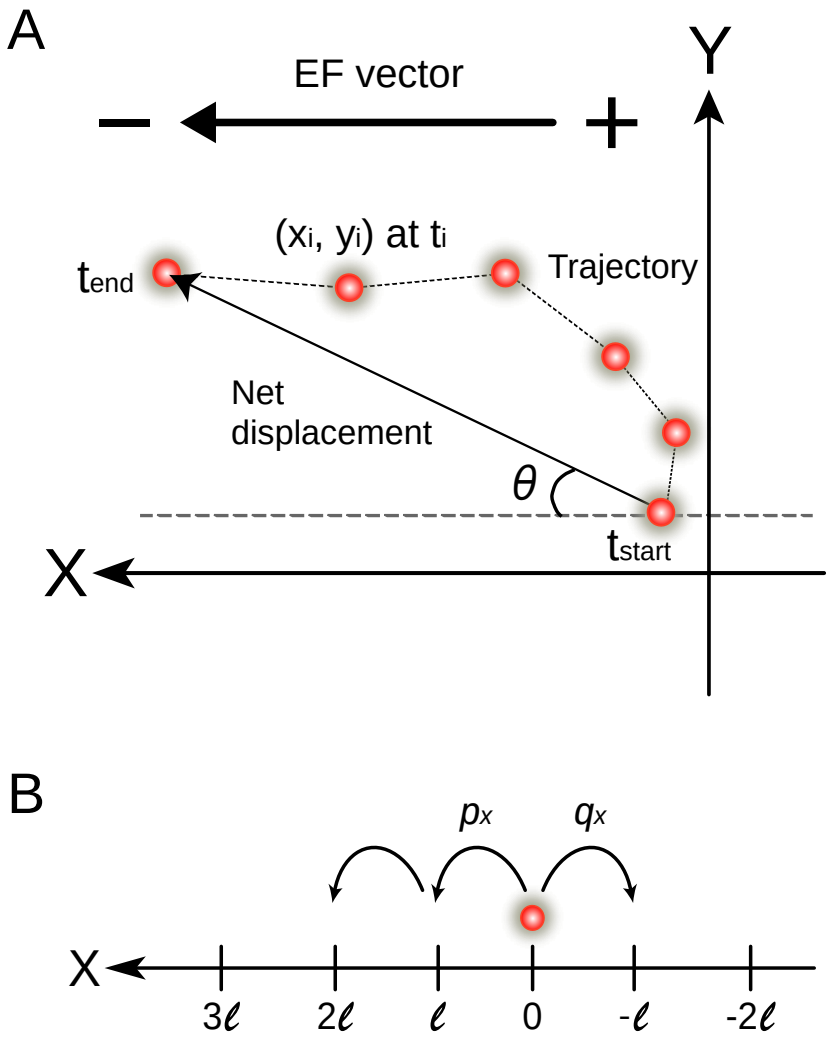

Fig.2-4 Cell migration analysis
(**A**) The geometric center of the cell is represented in X,Y-coordinates by red circles. The X axis denotes the direction of the electric field. Net displacement and total path length of the cell are expressed by an arrow and dashed line, respectively. (**B**) Particles undergoing one-dimentional random movement with a bias. The X axis denotes the direction of the electric field. Step size is *l* with a constant time interval t. Probabilities towards X and the opposite direction are p_x and q_x for each step, respectively. The bias can be expressed by the difference between p_x and q_x.

3, Results

3.1 Input-output relationship in the electrotactic response of *Dictyostelium* cells

Abstract

Under a direct current electric field, *Dictyostelium* cells exhibit migration towards the cathode. To determine the input-output relationship of the cell's electrotactic response, I developed an experimental instrument in which electric signals applied to the cells are highly reproducible and the motile response are analyzed quantitatively. With no electric field, the cells moved randomly in all directions. Upon applying an electric field, cell migration velocity became about 1.3 times faster than those in the absence of an electric field. Such kinetic effects of electric fields on the migration were observed for cells stimulated between 0.25 to 10 V/cm of the field strength. The directions of cell migrations were biased toward the cathode in a positive manner with field strength, showing electrotactic response in a dose-dependent manner. Quantitative analysis of the relationship between field strengths and directional movements revealed that the biased movements of the cells depend on the square of electric field strength, which can be described by one simple phenomenological equation. The threshold strength for the electrotaxis was between 0.25 and 1 V/cm. Electrotactic efficiency reached to half-maximum at 2.6 V/cm, which corresponds to an approximately 8 mV voltage difference between the cathode and anode direction of 10-μm wide, round cells. Based on these results, possible mechanisms of electrotaxis in *Dictyostelium* cells were discussed. This development of experimental system, together with its good microscopic accessibility for intracellular signaling molecules, makes *Dictyostelium* cells attractive as a model organism for elucidating stochastic processes in the signaling systems responsible for cell motility and its regulations.

3.1.1 Introduction

Living cells can sense and respond to environmental signals flexibly and adaptively through dynamic processes in intracellular signaling networks. Recently, studies examining stochastic processes in living cells in various biological signaling systems including transcriptional regulatory networks and chemotactic signaling networks [1-11] have found that intracellular molecular processes are noisy. Hence, a fundamental question regarding the intracellular signal transduction is, “How do stochastically-operating biomolecular networks work reliably to process environmental signals under stochastic and thermal noise”? To gain insights into the signaling mechanisms, it is important to reveal a quantitative relationship between signal inputs and the corresponding output in living cells. For this purpose, signal inputs should be applied to cells in a highly reliable and reproducible manner and the output response of the cells should be measured and analyzed quantitatively. One of the best experimental systems for elucidating the quantitative relationship between signal inputs and outputs is to measure the cell directional motile response to a given electric signal. This phenomenon is known as electrotaxis or galvanotaxis [12, 13].

Since electrotaxis in living cells was first described over a century ago [14, 15], this fascinating response has been found in various cell types including neurons, fibroblasts, leukocytes, macrophages, neural crest cells, cancer cells and slime molds [16-19]. The social amoeba *Dictyostelium discoideum*, a well known chemotactic model organism, also exhibits strong electrotaxis [20,21]. Cells can move preferentially toward the cathode or anode under direct current electric fields. In developing and regenerating animals, the importance of electric signals on tissue generation and maintenance has been gradually realized. In fact, electrotaxis is thought to have important roles in various physiological processes such as embryogenesis, neurogenesis, regeneration, wound healing and metastasis (18,22-26). This response includes intracellular signaling processes by which cell migration is somehow biased directionally in response to the electric field. Because cell migration depends on the actin cytoskeleton and its regulatory proteins, electric signals ultimately give rise to various intracellular signals that stimulate actin polymerization at the leading edge of the cells for pseudopod

formation and myosin II assembly at the rear for tail retraction. Still, the underlying molecular mechanisms of electrotaxis remain largely unknown.

Dictyostelium discoideum is a well-established model organism for elucidating the molecular mechanisms and regulation of amoeboid movements [27-32]. Besides the general advantages of this organism in molecular and cellular biology, which include well-established genetic engineering techniques, advanced microscopic techniques and complete sequences of the genome, there are several specific reasons to use this model for cellular motility research. For example, *Dictyostelium* cells exhibit fast amoeboid movements with a velocity of 10~20 μm/min on glass substrates; their motile behaviors have been well documented by microscopic observations [33-35]; and they exhibit remarkable chemotaxis at the aggregation stage during their life cycle. Upon starvation, *Dictyostelium* cells start to undergo their developmental program and then become chemotactic-competent at the aggregation stage. About one hundred thousand of the competent cells moves directionally toward the aggregation center by chemotactic migration and then form one aggregate, which is an essential process for the generation of spores (See Fig. 1-3). Because *Dictyostelium* cells are highly synchronized during the developmental progress, more than 99% of these cells can exhibit chemotaxis at the aggregation stage, making it possible to prepare highly homogeneous cell populations. These advantages make *Dictyostelium* cells attractive as a model system for cellular motility as they have already offered tremendous insight in the roles of actin cytoskeleton and microtubule systems on cellular motility [27,36-40]. Multiple molecular components required for chemotactic response in *Dictyostelium* cells have been identified including G protein-coupled receptors, hetero trimeric G proteins, Ras proteins, phospholipase A2 (PLA2), phophatidylinsitol-3-OH kinases (PI3K), tumor suppressor phosphatase and tensin homolog (PTEN) and guanylyl cyclases [31,41-44]. Furthermore, imaging analysis of cytoskeletal proteins and their regulatory molecules by fluorescence microscopy has revealed the dynamic behaviors of these molecules in response to chemotactic stimulation. In one particular case, the signaling molecules have been observed at the single molecule level in living cells, demonstrating the stochastic nature of molecules in intracellular signaling processes [3,11]. Thus, *Dictyostelium* is a preferred model organism for elucidating the molecular mechanisms of electrotaxis.

Here I report the input-output relationship quantitatively in the electrotactic response of *Dictyostelium* cells. Results revealed that the relationship can be described by one simple phenomenological equation and that the electrotactic efficiency of the cells depends on the square of the electric field strength.

3.1.2 Electrotaxis of *Dictyostelium* cells

Cells were prepared from a population adopting the aggregation stage of the *Dictyostelium* lifecycle. The cells had an obvious morphological polarity with one pseudopod at the leading edge and one tapered tail at the rear end, which is typical of chemotactic competent cells (Fig. 3-1A). The cell size was about 20 μm long and 7 μm wide. Trajectories of cell migration were tracked in the absence or presence of dcEFs semi-automatically and analyzed (Fig.3-1B). With no electric field, cells moved randomly in all directions with a migration velocity of 11.6$\pm$ 0.8 μm/min (n=36) (Fig. 3-1C and 3-4A). We first studied the effects of relatively larger field strength on the cell's behaviors because the response was easier to detect.

Upon application of a 10 V/cm dcEF, cells exhibited cathodal migration, like that reported by Zhao et al. (2002) (Fig. 3-1D). The cells adhered on the substrate and moved with a migration velocity of 16.4 $\pm$ 0.7 μm/min (n=58). The cell shapes were indistinguishable from those in no electric field. Cells sometimes moved perpendicular to the electric fields or in the anodal direction, but such cells would eventually reorient themselves by extending a pseudopod toward the cathode. When the electric field was reversed, the cells transiently ceased their movements and within a minute reoriented themselves toward the new cathode. In polarized cells with one pseuodpod and one tail at their opposite sides, the reorientation was achieved by U-turn with maintaining their morphological polarity in most case (Fig. 3-2A). Cells with multiple pseudopods reoriented by adjusting the pseudopod extensions to the direction of the new cathode (Fig. 3-2A, See No3 and No5). Such reorientation was achieved within minutes of reversing the electric field (Fig. 3-2B). Thus, *Dictyostelium* cells follow the directional changes of the electric fields.

3.1.3 Effects of electro-osmotic flow on electrotaxis

To establish whether the directional migration of cells were caused by electric fields and not by artifacts such as a chemical gradient in the medium, fluid flow, or temperature changes, cross-current fluid flow experiments were done in which the medium was flowed across the chamber in the direction perpendicular to the electric field (Fig. 2-1D). In the absence of cross-current fluid flow, electric osmotic flows (EOF) were clearly observed when microsphere beads were included in the chamber (0.9 μm diameter; polyacrolein microspheres, Poly science. Inc.)(Fig. 3-3A and B). The movements of the beads reflect the fluid flow because the effects of the electric osmotic flow are much stronger than that of electrophoresis. Thus, from these results, the charge of the beads can be ignored. The water layer just above the surface of the coverslip where cells were placed flowed toward the cathode, while the upper water layer flowed toward the anode. The flow rates of the surface layer and upper layer at 10 V/cm were 5.5 $\pm$ 0.5 μm/sec (n=22) and 8.2 $\pm$ 0.9 μm/sec (n=22), respectively (Fig.3-3C). A 60 μm/sec cross-current fluid flow was applied to the cells in the chamber, which is a rate much larger than that of the EOF. In this situation, cells still moved towards the cathode, parallel to the electric field. Cell migration analysis revealed that the motile properties such as migration velocity, cell motility efficiency, directedness and asymmetric index were not affected by the cross-current fluid flow, indicating that cells have no sensitivity to fluid flow. Furthermore, since the medium was continuously exchanged by the application of cross-current fluid flow, this experiment also demonstrates that any field-induced changes in the medium such as chemical gradients and temperature changes have no significant effects on the directional movements of cells under an electric field. Under an electric field, cells sometimes aggregated with each other because of chemotaxis. Thus, cells were treated with 4mM caffeine, which inhibits adenylate cyclase activation and thereby excludes chemotaxis towards cAMP gradients but also has no effect on cathodal migration (See ref.[3] in chapter2).

Because *Dictyostelium* cells have been known to exhibit shear flow-induced directional motility [45], we further examined the effects of electric osmotic flow on cell motility by estimating the strength of shear stress applied to the cells. By observing beads in the flow induced by electric osmosis, the height and the velocity of the flowed

layer at the glass surface was estimated to be about 50 μm and 5.5 μm/sec at an electric field of 10 V/cm. Because the width of the chamber was 3 mm, the flow rates of the medium around the cells were calculated to be about 8.3 x 10^{-7} ml/sec (50 μm x 3 mm x 5.5 μm/sec). Shear stress, σ [Pa], is given by the following equation [46,47],

$$\sigma = \frac{6\mu Q}{bh^2} \tag{3.1}$$

, where μ is fluid viscosity [Pa·sec], Q is flow rate [ml/sec], b is chamber width [cm], and h is the height of the fluid layer [cm]. The sheer stress was calculated to be 0.66 mPa assuming the viscosity of water was 1.002 mPa·sec at 20 ^{o}C and a field-induced flow of 8.3 x 10^{-7} ml/sec. This value is three magnitudes lower than the reported *Dictyostelium* cell threshold for shear stress (0.8 Pa) [45], indicating that shear stress has virtually no effect on cell motility in these electric field experiments. Thus, it is unlikely that the directional migration of the *Dictyostelium* cells was mediated by field-induced changes in the medium.

The electrotactic response of *Dictyostelium* cells was dose-dependent for electric field strength. With increasing electric field strength, the migration of the cells towards the cathode became more obvious. I analyzed migration velocity, cell motility efficiency, directedness and asymmetric index to examine the effects of electric fields on cell motility. Directedness increased with increasing field strength (Fig. 3-4C). The threshold stimulation to induce biased movement was between 0.25 and 1 V/cm. Asymmetric index also showed that cells were biased from 0.5 V/cm (Fig. 3-4D). Both directedness and asymmetric index reached maximum at 7 V/cm and became constant for further increases in field strength up to 20 V/cm (data not shown). Cell motility efficiency also exhibited similar dose-dependency, indicating the efficiency or persistency of cell movements became higher with increasing electric field strength (Fig. 3-4B). On the other hand, migration velocities were independent of electric field strength and had a range of about 13 ~ 16 μm/min (Fig. 3-4A). It should be noted that the migration velocity of the cells exposed to electric fields as low as 0.25 V/cm was ~ 1.3 times faster than those without electric field, which represents the kinetic effects of the electric fields. Such effect has been reported in other cell types [48, 49], although the underlying mechanisms remain unknown. Thus, applying electric fields to cells causes migration velocity to accelerate, but not in a dose-dependent manner. Thus, electric fields affect the directionality but not the motility in a dose dependent manner.

3.1.4 Description of electrotactic movement by a phenomenological equation

In general, motile cells move spontaneously in random directions even when extracellular directional cues are absent. The tactic response of cells is a process by which the random movement of cells is somehow biased along with extracellular directional cues, as shown in *Dictyostelium* cells (Fig. 3-1C). In the presence of an electric field, the movement is biased. To determine the relationship between electric field strength and electrotactic efficiency, the extent of the bias on cell movements induced by an electric field were quantified. Here we used mean displacement analysis (See "cell migration analysis" in chapter2).

$$\langle X(t) \rangle = b \frac{l}{\tau} t = bvt \qquad (2.9)$$

Equation (2.9) tells us that the mean displacement, $\langle X(t) \rangle$, linearly depends on time when the extent of the bias on cell migration is constant with time. $\langle X(t) \rangle$ can be obtained experimentally by measuring the positional changes of the cells under an electric field. When $\langle X(t) \rangle$ is plotted as a function of time, the slope, bv, reflects the extent of the bias. Because the velocity of cell migration was almost constant in the presence of an electric field (Fig. 3-4A), the migration velocity, v, can be assumed to be constant. The same analysis can be applied to the cell's migration along the y axis. Therefore, by analyzing the dependency of bv on electric field strength, the extent of the bias on the directional migration induced by an electric field can be obtained. This analysis provides the input-output relationship to an electrotactic response. Here we refer to the slope bv as mean cathodal displacement speed (*MCS*).

Fig. 3-5A and B show the mean displacements of the cells along the x axis $\langle X(t) \rangle$ and y axis $\langle Y(t) \rangle$, parallel and perpendicular to the electric fields, respectively. $\langle X(t) \rangle$ increased almost linearly with time, indicating that the *MCS* is constant at a given electric field strength during the observation time. In other words, the cell movements were biased constantly towards the cathode. The *MCS* became larger with

increasing electric field strength, indicating the electrotactic migrations of *Dictyostelium* cells are biased in a dose-dependent manner. On the other hand, $\langle Y(t) \rangle$ remained zero irrespective of electric field strength, indicating that the cell migrations were not biased toward the direction perpendicular to the electric field.

Fig. 3-5C shows the dependence of *MCS* on electric field strength. Interestingly, the dependence was not linear to field strength but rather sigmoidal. The relationship between field strength and *MCS* can be fitted to the following Hill like equation,

$$MCS = V_{\max} \frac{E^n}{K_E^n + E^n} \tag{3.2}$$

, where $V_{\max}$ is maximum *MCS*, E is electric field strength, n is sigmoid number, and K_E is the electric field strength where *MCS* reaches to half-maximum and hence represents the electric field sensitivity of the cells. The experimental data can be fitted well to equation (3.2) with $n = 2$, leading to K_E = 2.6 V/cm and V_{max} = 9.2 μm/min. Thus, the electrotaxis of the cells are affected by the square of the electric field strength.

3.1.5 Effects of cAMP on electrotaxis

Dictyostelium cells became chemotactic competent cells at the starved stage, where cells can sense the chemoattractant, cAMP by the specified receptor cAR1, which then activates the chemotactic signaling pathways [41,42]. Upstream components of these pathways such as cAR1 and hetero trimeric G proteins are not essential for exhibiting electrotaxis [20]. However, since both chemotaxis and electrotaxis induce directed cell migration, some synergetic effects of cAMP stimulation on electrotaxis were examined by adding 1μM cAMP in the electrotactic assay chamber uniformly. Similar to the no cAMP results, cell migration velocities were not dependent on the applied electric field strength (Fig.3-6A), while cell motility efficiency, directedness and asymmetric index increased with increasing field strength (Fig. 3-6 B-D). From 0.75 V/cm, directedness and asymmetric index were higher than that of no cAMP, indicating that cells can sense electric field gradients at a lower range (Fig. 3-6C and D). This enhanced sensitivity was confirmed by mean displacement analysis, where K_E was 1.77 V/cm and 1.41 V/cm in the absence or presence of cAMP, respectively (Fig. 3-7A). This means the sensitivity for to electric signal increased about 1.3 times in the presence of cAMP. Thus, although the synergy between the two mechanisms is unknown, activating the chemotactic signaling pathway increases the sensitivity of the cells to the electric signal.

When the direction of the electric field was reversed, the delay of the response was observed in both the absence and presence of cAMP. However, the delay time was longer in the presence of cAMP taking approximately 5 min longer to reach the same directedness (Fig. 3-7B). I should note that the addition of cAMP induces more clear polarized shapes than no cAMP (data not shown). Similar responses were reported by Swanson and Taylor (1982) where strong polarization induced by cAMP stimulation decreased the flexibility of cell migration reorientation [50].

3.1.6 Defective electrotaxis

Sprawled and round morphological cells were sometimes observed under 10V/cm dcEF (Fig. 3-8A). In these cells, it was difficult to distinguish the leading edge from the tail. These cells often changed their morphology dramatically and recovered their polarized shape within a few minutes (Fig. 3-8B). Although the number of these cells was quite low, they are worth noting since they could not show electrotaxis, as migration was independent of the direction of dcEF. (Fig. 3-8C). These cells migrated in one direction and showed relatively long and persistent migration.

3.1.7 Discussion

In the present investigation, we report the input-output relationship for electrotaxis in *Dictyostelium* cells as described by equation (3.2) with n=2. Cell movement under electric fields was biased with the square of the electric field strength. I also found the cell migration kinetics were sensitive to electric fields as low as 0.25 V/cm.

Cell migration was biased constantly with time in a given electric field (Fig. 3-4B-D), which was obvious when the cells were exposed to relatively larger field strengths (> 2 V/cm). This suggests that some intracellular processes are generated in cells immediately after field application and maintained to modulate constant migration. If such modulation processes were generated gradually following field application, the extent of the bias would also increase gradually, leading to a non-linear relation with the mean displacement $\langle X(t) \rangle$. In fact, this did occur at field strengths near the threshold stimulation (0.5 ~ 2 V/cm). For example, at 0.75 and 2 V/cm, the slope of the mean displacement became steeper at 400 and 200 sec after field application, respectively, suggesting that some motility modulation may occur in this time window due to the continuous application of the electric field (Fig. 3-5A). Further investigations of temporal changes in $\langle X(t) \rangle$ are required because n, which describes the electric field dependency value, may change with time. This is important when trying to understand the mechanisms modulating cell motility in response to electric stimulation. Additionally, it is important to investigate the fluctuation of the cell trajectory. In our experiments, trajectory paths of cell migration generally had fluctuations at all electric field strengths including 10 V/cm (Fig. 3-1D). Since input signals were almost constant in time, these fluctuations may reflect the stochastic properties of the intracellular signaling. However, even without temporal analysis, it is still obvious that the electrotactic efficiency has a non-linear dependency with the electric field strength. Such non-linearity can be expressed by the sigmoid number n. It would be interesting to see whether the input-output relationship similar to that reported here can be observed in other cell types.

What are the possible mechanisms described by the non-linear dependency of electrotaxis on the electric field? It has been demonstrated that electric field applications to living cells induce membrane potential changes [51-53]. In general, the membrane

potentials induced by external electric fields for a spherical shaped cell can be expressed by the following equation,

$$V_\theta = \Delta\Psi_0 + 1.5r \cdot E \cdot \cos\theta \tag{3.3}$$

where θ is the angle with respect to electric fields (Fig. 3-9A), V_θ is the membrane potential [mV] at θ, r is the cell radius (~5 μm for *Dictyostelium* cells), and E is the electric field strength [mV/μm]. The resting membrane potential, $\Delta\Psi_0$, of *Dictyostelium* cells is about -47 mV [54]. The potential changes in a cell are largest at both the anodal-facing side ($\theta = 0^o$) and cathodal-facing side ($\theta = 180^o$), while the potential changes at the site perpendicular to the electric field ($\theta = 90^o or -90^o$) are zero. The anodal-facing side is hyperpolarized while the cathodal-facing side is depolarized [51-53]. Thus, the potentials have a gradient along the membrane surface from the cathodal to anodal sides in a sinusoidal manner. These membrane potential changes have been thought to be important for inducing ion currents or gradients in cells via ion channels or ion pumps along the membranes. Voltage-sensitive enzymes may also be modulated by the electric field application [55,56]. However, such external electric field-induced membrane potential changes cannot explain the non-linear dependency of electrotaxis in *Dictyostelium* cells since the membrane potentials are linearly related to electric field strength as expressed in equation (3.3). The relationship between membrane potential changes and cell motility changes should have some non-linearity. One explanation is that some voltage-sensitive molecules that operate in a non-linear manner with membrane potential changes might be involved in electrotactic signaling to modulate cell motility.

According to equation (3.3), the voltage difference was estimated to be about 8 mV between the cathodal- and anodal-facing sides in a 10 μm wide cell at a field strength of 2.6 V/cm, which is where the electrotactic efficiency reaches half-maximum. At the threshold stimulation, the voltage difference was between 1.1 and 3 mV. Also, kinetic effects of the electric field application on cell migration speed were caused by a field strength of 0.4 mV between both ends of the cells. Although these estimations have many uncertainties, it implies that the electric signal strengths required for cell motility modulation are comparable to the spontaneous fluctuations in membrane potentials that are derived from thermal fluctuations of ion channels or ion pumps found along the membranes [57-59]. Whatever mechanisms are responsible for detecting the electric field, cells can achieve electrotactic and electrokinetic signaling at the level of thermal and stochastic noise. It is plausible that the spontaneous generation of polarized morphology and responsiveness of *Dictyostelium* cells may also involve endogenous changes in the membrane potential [54].

As an alternative mechanism, it has been proposed that electric field application produces an asymmetric distribution of receptors or ion channels by electrophoresis on the cell membrane surface [60-62]. Migration of *Dictyostelium* cells was biased within 30 seconds after the field application, which was obvious at larger field strength ranges. At high field strength ranges, the electrotactic response lag was minimal. Such fast responses to electric field applications in *Dictyostelium* cell are similar to that of metastatic cancer cells or *Amoeba proteus* [48,63]. The electrotactic responses of all three cell types were too fast for the redistribution of the membrane proteins to be involved in the initial phase [64,65]. On the other hand, as previously discussed by Korohoda (2000), polarized cells show polar distributions of negative charges along the membrane surfaces where the mobility of ions are much faster than that in bulk solution [66-68]. Consequently, an asymmetric distribution of ions on the cell membrane surface or some other small molecules may be involved in the initial phase of electrotaxis in *Dictyostelium* cells.

It is thought that certain intracellular signaling molecules are involved in electrotactic signaling [69-71]. One of the mediators for electrotaxis is calcium and its related signaling molecules [72,73]. Adding the calcium chelator EGTA (1mM) to the extracellular medium of electrotaxis *Dictyostelium* cells led to no observable changes

suggesting no involvement of extracellular calcium (data not shown). Zhao et al (2002) reports that G protein-coupled receptor signaling responsible for chemotaxis is not essential for electrotaxis in *Dictyostelium* cells. cAMP stimulate chemotaxis in *Dictyostelium* cells is mediated by the G protein-coupled receptors cARs and the corresponding coupled hetero trimeric G protein composed of the $G\alpha_2$ subunit and $G\beta\gamma$ complex. Knockout mutants of cARs and the $G\alpha_2$ subunit exhibited similar electrotaxis as wild type cells while mutant cells lacking the $G\beta$ subunit exhibit slightly suppressed electrotaxis (Zhao et al., 2002). Furthermore, neither the receptor nor any downstream signaling proteins such as CRAC, a PH_{CRAC}-domain-containing protein, are localized at the leading edge of the pseudopods in response to electric stimulation. These results suggest that sensing and the signal transduction for electrotaxis are largely independent of G protein-coupled receptor signaling. In our experimental system, we used developed cells prepared from the aggregation stage of the *Dictyostelium* lifecycle. Because the cAMP receptor and G protein knockout has a defect in the developmental progression, the electrotactic efficiency of the knockout mutants cannot be compared with that of wild type cells in our system. Instead, we examined the effects of cAMP addition on electrotaxis specifically because it can activate the G protein-coupled receptor signaling system. I found that cells tend to show enhanced electrotaxis in the presence of cAMP (Fig. 3-6 and 3-7). The activation of chemotactic signaling pathways may have some synergetic effects on the directional movements of cells under an electric field. One possible explanation of the cAMP effect is a change in membrane potential through the activity of ion channels or morphological change. It has reported that the addition of cAMP induces hyperpolarization of membrane potential [54], which in turn potentially affects electrotactic efficiency. Alternatively, cAMP affects cell morphology. I noted that the addition of cAMP induced strong cell polarization, influencing cell shape. The effects of an external dcEF on the membrane potential of spheroidal cells are different from that of spherical cells [74] (Fig. 3-9B) as both the cathode and anode membrane potential changes are larger according to equation (3.4). These differences in membrane potential may potentially enhance the electrotactic efficiency.

$$V_\theta = -47[mV] - E \times \frac{R_1^2 - R_2^2}{R_1 - \frac{R_2^2}{\sqrt{R_1^2 - R_2^2}} \log \frac{R_1 + \sqrt{R_1^2 - R_2^2}}{R_2}} \times \frac{R_2 \cos\theta}{\sqrt{R_1^2 \sin^2\theta + R_2^2 \cos^2\theta}} \quad (3.4)$$

The defective electrotactic cells may be explained by the differentiation progress of *Dictyostelium* cells. Migration and morphological characteristics of these abnormal cells resemble those of prestalk cells (called, T1 cells) [29]. Since sensitivity to cAMP by these cells was quite low at the initial developmental stage, these cells started to aggregate later. At the end of the starved stage, these cells become stalk cells. These cells also exhibited defects in their electrotactic response (Fig. 3-8C). In a dcEF, these cells migrated randomly suggesting that there is a relationship between differentiation and electrotactic response if these cells are a prestalk cells. It is important to investigate the correlation between differentiation and electrotaxis to fully comprehend the meaning of electrotactic responses in *Dictyostelium* cells. Technical developments to combine between electric field application and single molecule imaging techniques are underway.

References

[**1**] Becskei A and Serrano L (2000) Engineering stability in gene networks by autoregulation. *Nature* **405**:590-593.

[**2**] Thattai M and van Oudenaarden A (2001) Intrinsic noise in gene regulatory networks. *Proc Natl Acad Sci U S A* **98**:8614-8619.

[**3**] Ueda M, Sako Y, Tanaka T, Devreotes P, Yanagida T (2001) Single-molecule analysis of chemotactic signaling in Dictyostelium cells. *Science* **294**:864-867.

[**4**] Elowitz MB, Levine AJ, Siggia ED, Swain PS (2002) Stochastic gene expression in a single cell. *Science* **297**:1183-1186.

[**5**] Blake WJ, KAErn M, Cantor CR, Collins JJ (2003) Noise in eukaryotic gene expression. *Nature* **422**:633-637.

[**6**] Paulsson J (2004) Summing up the noise in gene networks. *Nature* **427**:415-418.

[**7**] Raser JM and O'Shea EK (2004) Control of stochasticity in eukaryotic gene expression. *Science* **304**:1811-1814.

[**8**] Korobkova E, Emonet T, Vilar JM, Shimizu TS, Cluzel P (2004). From molecular noise to behavioural variability in a single bacterium. *Nature* **428**:574-578.

[**9**] Hooshangi S, Thiberge S, Weiss R (2005) Ultrasensitivity and noise propagation in a synthetic transcriptional cascade. *Proc Natl Acad Sci U S A* **102**:3581-3586.

[**10**] Shibata T and Fujimoto K (2005) Noisy signal amplification in ultrasensitive signal transduction. *Proc Natl Acad Sci U S A* **102**:331–336.

[**11**] Matsuoka S, Iijima M, Watanabe TM, Kuwayama H, Yanagida T, Devreotes PN, Ueda M (2006) Single-molecule analysis of chemoattractant-stimulated membrane recruitment of a PH-domain-containing protein. *J Cell Sci* **119**:1071-1079.

[**12**] Rapp B, de Boisfleury-Chevance A, Gruler H. (1988) Galvanotaxis of human granulocytes. Dose-response curve. *Eur Biophys J* **16**:313-319.

[**13**] Gruler H, Nuccitelli R (1991) Neural crest cell galvanotaxis: new data and a novel approach to the analysis of both galvanotaxis and chemotaxis. *Cell Motil Cytoskeleton* **19**:121-133.

[**14**] Verworn M (1889) Die polare Erregung der Protisten durch den galvanischen Strom Pfluegers *Arch Desante Physiol* **45**:1-36.

[**15**] Dineur E (1891) Note sur la sensibilité des leucocytes à l’electricité. *Bull Séances*

Soc Belge Microsc **18**:113-118.

[**16**] Nuccitelli R, Poo MM, Jaffe LF (1977) Relations between ameboid movement and membrane-controlled electrical currents. *J Gen Physiol* **69**:743-763.

[**17**] Robinson KR (1985) The responses of cells to electrical fields: a review. *J Cell Biol* **101**:2023-2027.

[**18**] Mycielska ME and Djamgoz MB (2004) Cellular mechanisms of direct-current electric field effects: galvanotaxis and metastatic disease. *J Cell Sci* **117**:1631-1639.

[**19**] McCaig CD, Rajnicek AM, Song B, Zhao M (2005) Controlling cell behavior electrically: current views and future potential. *Physiol Rev* **85**:943-978.

[**20**] Zhao M, Jin T, McCaig CD, Forrester JV, Devreotes PN (2002) Genetic analysis of the role of G protein-coupled receptor signaling in electrotaxis. *J Cell Biol* **157**:921-927.

[**21**] Sato MJ, Ueda M, Takagi H, Watanabe TM, Yanagida T, Ueda M (2007) Input-output relationship in galvanotactic response of Dictyostelium cells. *Biosystems* **88**:261-272.

[**22**] Jaffe LF and Stern CD (1979) Strong electrical currents leave the primitive streak of chick embryos. *Science* **206**:569-571.

[**23**] McCaig CD, Rajnicek AM, Song B, Zhao M (2002). Has electrical growth cone guidance found its potential? *Trends Neurosci* **25**:354-359.

[**24**] Nuccitelli R (2003) A role for endogenous electric fields in wound healing. *Curr Top Dev Biol* **58**:1-26.

[**25**] Pu J, McCaig CD, Cao L, Zhao Z, Segall JE, Zhao M (2007) EGF receptor signalling is essential for electric-field-directed migration of breast cancer cells. *J Cell Sci* **120**:3395-3403.

[**26**] Adams DS, Masi A, Levin M (2007) H+ pump-dependent changes in membrane voltage are an early mechanism necessary and sufficient to induce Xenopus tail regeneration. *Development* **134**:1323-1335.

[**27**] Segall JE and Gerisch G (1989) Genetic approaches to cytoskeleton function and the control of cell motility. *Curr Opin Cell Biol* **1**:44-50.

[**28**] Schleicher M and Noegel AA (1992) Dynamics of the Dictyostelium cytoskeleton during chemotaxis. *New Biol* **4**:461-472.

[**29**] Maeda Y, Inouye K, Takeuchi I (Eds.) (1997) Dictyostelium: A Model System for Cell and Developmental Biology. Universal Academy Press, Tokyo.

[**30**] Eichinger L, Lee SS, Schleicher M (1999) Dictyostelium as model system for studies of the actin cytoskeleton by molecular genetics. *Microsc Res Tech* **47**:124-134.

[**31**] Van Haastert PJ and Devreotes PN (2004) Chemotaxis: signalling the way forward. *Nat Rev Mol Cell Biol* **5**:626-634.

[**32**] Eichinger L et al. (2005) The genome of the social amoeba Dictyostelium discoideum. *Nature* **435**:43-57.

[**33**] Fukui Y (1993) Toward a new concept of cell motility: cytoskeletal dynamics in amoeboid movement and cell division. *Int Rev Cytol* **144**:85-127.

[**34**] Soll DR, Wessels D, Voss E, Johnson O (2001) Computer-assisted systems for the analysis of amoeboid cell motility. *Methods Mol Biol* **161**:45-58.

[**35**] Fukui Y (2002) Mechanistics of amoeboid locomotion: signal to forces. *Cell Biol Int* **26**:933-944.

[**36**] Schliwa M, Euteneuer U, Graf R, Ueda M (1999) Centrosomes, microtubules and cell migration. *Biochem Soc Symp* **65**: Postland Press, London, 223-231.

[**37**] Graf R, Brusis N, Daunderer C, Euteneuer U, Hestermann A, Schliwa M, Ueda M (2000) Comparative structural, molecular, and functional aspects of the Dictyostelium discoideum centrosome. *Curr Top Dev Biol* **49**:161-185.

[**38**] Noegel AA and Schleicher M (2000) The actin cytoskeleton of Dictyostelium: a story told by mutants. *J Cell Sci* **113**:759-766.

[**39**] Koonce MP and Khodjakov A (2002) Dynamic microtubules in Dictyostelium. *J Muscle Res Cell Motil* **23**:613-619.

[**40**] Yumura S and Uyeda TQ (2003) Myosins and cell dynamics in cellular slime molds. *Int Rev Cytol* **224**:173-225.

[**41**] Parent CA and Devreotes PN (1999) A cell's sense of direction. *Science* **284**:765-770.

[**42**] Parent CA (2004) Making all the right moves: chemotaxis in neutrophils and Dictyostelium. *Curr Opin Cell Biol* **16**:4-13.

[**43**] Chen L, Iijima M, Tang M, Landree MA, Huang YE, Xiong Y, Iglesias PA, Devreotes PN (2007) PLA2 and PI3K/PTEN pathways act in parallel to mediate chemotaxis. *Dev Cell* **12**:603-614.

[**44**] Veltman DM, Keizer-Gunnik I, Van Haastert PJ (2008) Four key signaling pathways mediating chemotaxis in Dictyostelium discoideum. *J Cell Biol*. **180**:747-753.

[**45**] Decave E, Rieu D, Dalous J, Fache S, Brechet Y, Fourcade B, Satre M, Bruckert F (2003) Shear flow-induced motility of Dictyostelium discoideum cells on solid substrate. *J Cell Sci* **116**:4331-4343.

[**46**] Albuquerque ML., Waters CM, Savla U, Schnaper HW, Flozak AS (2000) Shear stress enhances human endothelial cell wound closure in vitro. *Am J Physiol Heart Circ Physiol* **279**:H293-302.

[**47**] Levesque MJ and Nerem RM (1985) The elongation and orientation of cultured endothelial cells in response to shear stress *J Biomech Eng* **107**:341-347.

[**48**] Korohoda W, Mycielska M, Janda E, Madeja Z (2000) Immediate and long-term galvanotactic responses of Amoeba proteus to dc electric fields. *Cell Motil Cytoskeleton* **45**:10-26.

[**49**] Finkelstein E, Chang W, Chao PH, Gruber D, Minden A, Hung CT, Bulinski JC (2004) Roles of microtubules, cell polarity and adhesion in electric-field-mediated motility of 3T3 fibroblasts. *J Cell Sci* **117**:1533-1545.

[**50**] Swanson JA, Taylor DL (1982) Local and spatially coordinated movements in Dictyostelium discoideum amoebae during chemotaxis. *Cell* **28**:225-232.

[**51**] Hibino M, Shigemori M, Itoh H, Nagayama K, and Kinosita K Jr (1991) Membrane conductance of an electroporated cell analyzed by submicrosecond imaging of transmembrane potential. *Biophys J* **59**:209-220.

[**52**] Hibino M, Itoh H, Kinosita K Jr (1993) Time courses of cell electroporation as revealed by submicrosecond imaging of transmembrane potential. *Biophys J* **64**:1789-1800.

[**53**] Hassan N, Chatterjee I, Publicover NG, Craviso GL (2002) Mapping membrane-potential perturbations of chromaffin cells exposed to electric fields. *Plasma Science, IEEE Transactions on* **30**:1516-1524.

[**54**] Van Duijn B and Wang M (1990) Chemoattractant-induced membrane hyperpolarization in Dictyostelium discoideum A possible role for cyclic GMP *FEBS Lett* **275**:201-204.

[**55**] Ben-Chaim Y, Tour O, Dascal N, Parnas I, Parnas H (2003) The M2 muscarinic G-protein-coupled receptor is voltage-sensitive. *J Biol Chem* **278**:22482-22491.

[**56**] Murata Y, Iwasaki H, Sasaki M, Inaba K, Okamura Y (2005) Phosphoinositide phosphatase activity coupled to an intrinsic voltage sensor. *Nature* **435**:1239-1243.

[**57**] Cooper MS and Schliwa M (1986) Motility of cultured fish epidermal cells in the presence and absence of direct current electric fields. *J Cell Biol* **102**: 1384-1399.

[**58**] Weaver JC and Astumian RD (1990) The response of living cells to very weak electric fields: the thermal noise limit. *Science* **247**:459-462.

[**59**] Oosawa F (2001) Spontaneous signal generation in living cells. *Bull Math Biol* **63**:643-654.

[**60**] Poo M and Robinson KR (1977) Electrophoresis of concanavalin A receptors along embryonic muscle cell membrane. *Nature* **265**:602-605.

[**61**] McLaughlin S and Poo MM (1981) The role of electro-osmosis in the electric-field-induced movement of charged macromolecules on the surfaces of cells. *Biophys J* **34**:85-93.

[**62**] Poo M (1981) In situ electrophoresis of membrane components. *Annu Rev Biophys Bioeng* **10**:245-276.

[**63**] Djamgoz MBA, Mycielska M, Madeja Z, Fraser SP, Korohoda W (2001) Directional movement of rat prostate cancer cells in direct-current electric field: involvement of voltagegated Na+ channel activity. *J Cell Sci* **114**:2697-2705.

[**64**] Jaffe LF (1977) Electrophoresis along cell membranes. *Nature* **265**:600-602.

[**65**] Fang KS, Ionides E, Oster G, Nuccitelli R, Isseroff RR (1999) Epidermal growth factor receptor relocalization and kinase activity are necessary for directional migration of keratinocytes in DC electric fields. *J Cell Sci* **112**:1967-1978.

[**66**] Somosy Z, Kubasova T, Koteles GJ (1984) Cell membrane polarity in primary human fibroblasts. *Cell Biol Int Rep* **8**:407-413.

[**67**] Heberle J, Riesle J, Thiedemann G, Oesterhelt D, Dencher NA (1994) Proton migration along the membrane surface and retarded surface to bulk transfer. *Nature* **370**:379-382.

[**68**] Scherrer P (1995) Proton movement on membranes. *Nature* **374**:222.

[**69**] Nuccitelli R, Smart T, Ferguson J (1993) Protein kinases are required for embryonic neural crest cell galvanotaxis. *Cell Motil Cytoskeleton* **24**:54-66.

[**70**] Pullar CE, Isseroff RR, Nuccitelli R (2001) Cyclic AMP-dependent protein kinase A plays a role in the directed migration of human keratinocytes in a DC electric field. *Cell Motil Cytoskeleton* **50**:207-217.

[**71**] Pullar CE and Isseroff RR (2005) Cyclic AMP mediates keratinocyte directional

migration in an electric field. *J Cell Sci* **118**:2023-2034.

[**72**] Onuma EK and Hui SW (1988) Electric field-directed cell shape changes, displacement, and cytoskeletal reorganization are calcium dependent. *J Cell Biol* **106**:2067-2075.

[**73**] Trollinger DR, Isseroff RR, Nuccitelli R (2002) Calcium channel blockers inhibit galvanotaxis in human keratinocytes. *J Cell Physiol* **193**:1-9.

[**74**] Kotnik T, Miklavcic D (2000) Analytical description of transmembrane voltage induced by electric fields on spheroidal cells. *Biophys J* **79**:670-679.

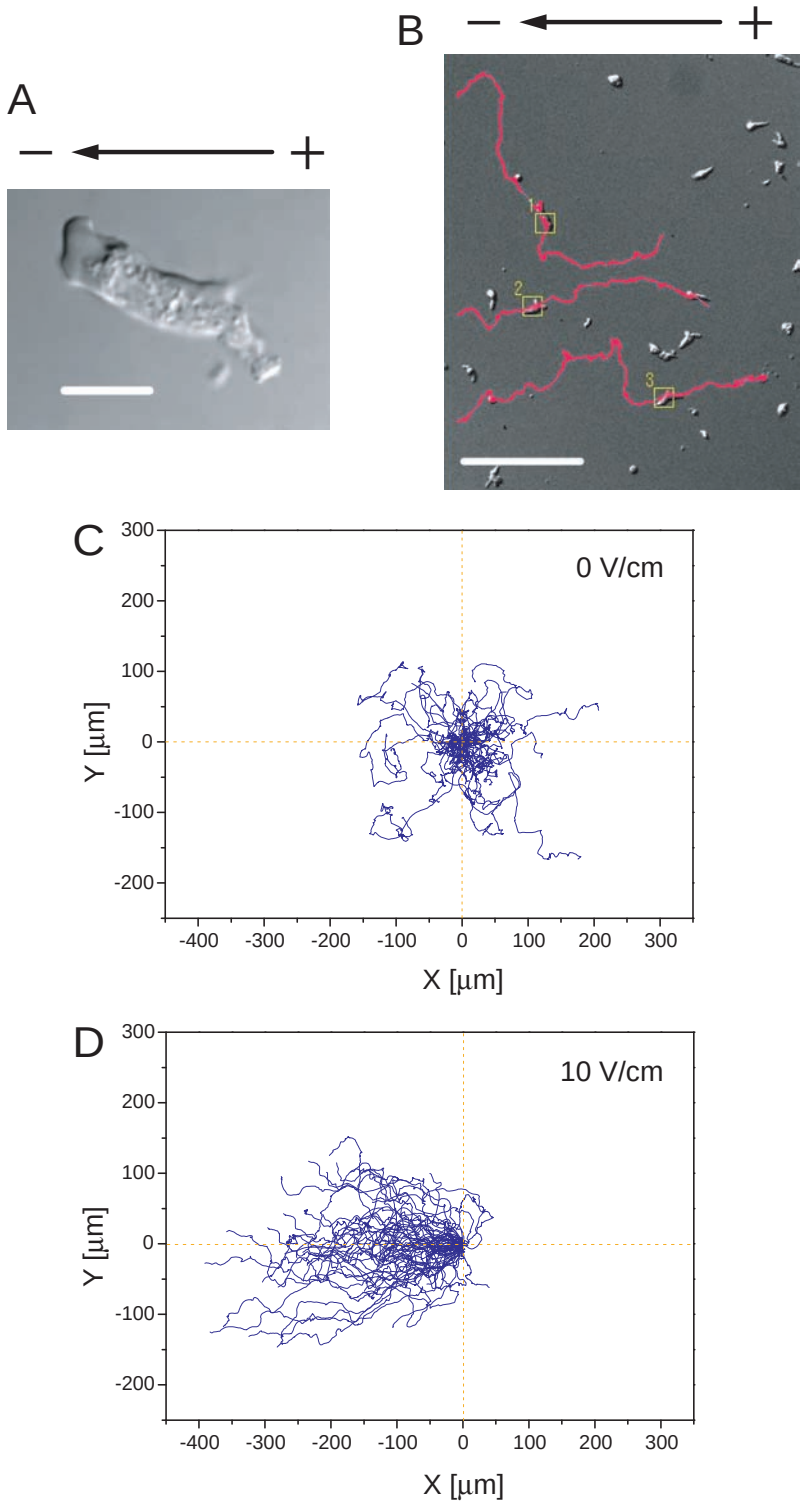

Fig.3-1 Electrotaxis of *Dictyostelium* cells.
(**A**) Typical cell shape of *Dictyostelium* cell under an electric field (10 V/cm). Scale bar, 10 μm. (**B**) Differential interference contrast image of the cells in the chamber in a 10 V/cm electric field. Red lines represent tracking of the cells. Scale bar, 100 μm. (**C**) Tracks of cells with no electric field showing random migration in all directions. (**D**) Tracks of cells in a 10 V/cm electric field, showed directional movements toward the cathode (left side). Both for (**C**) and (**D**), observation time was 30 min.

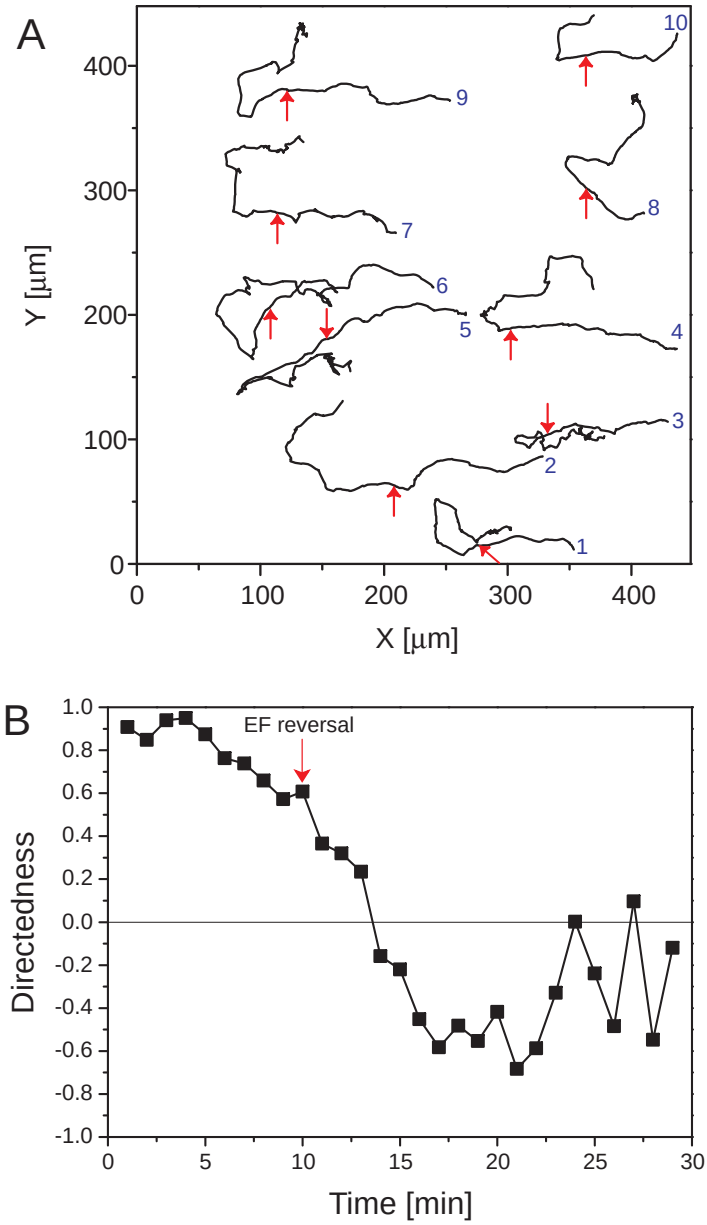

Fig.3-2 Effects of reversing the electric field direction on cell migration.
(**A**) Cell tracks before and after reversal of the electric field. Typical 10 cell tracks are presented. Each cell index is placed near the start position of the respective cell tracks. Arrowheads represent the position where the direction of the electric field was reversed. (**B**) Temporal changes of average directedness upon the reversal. 15 cells was analyzed. After reversing the electric field, cells turn their direction of locomotion within a few minutes.

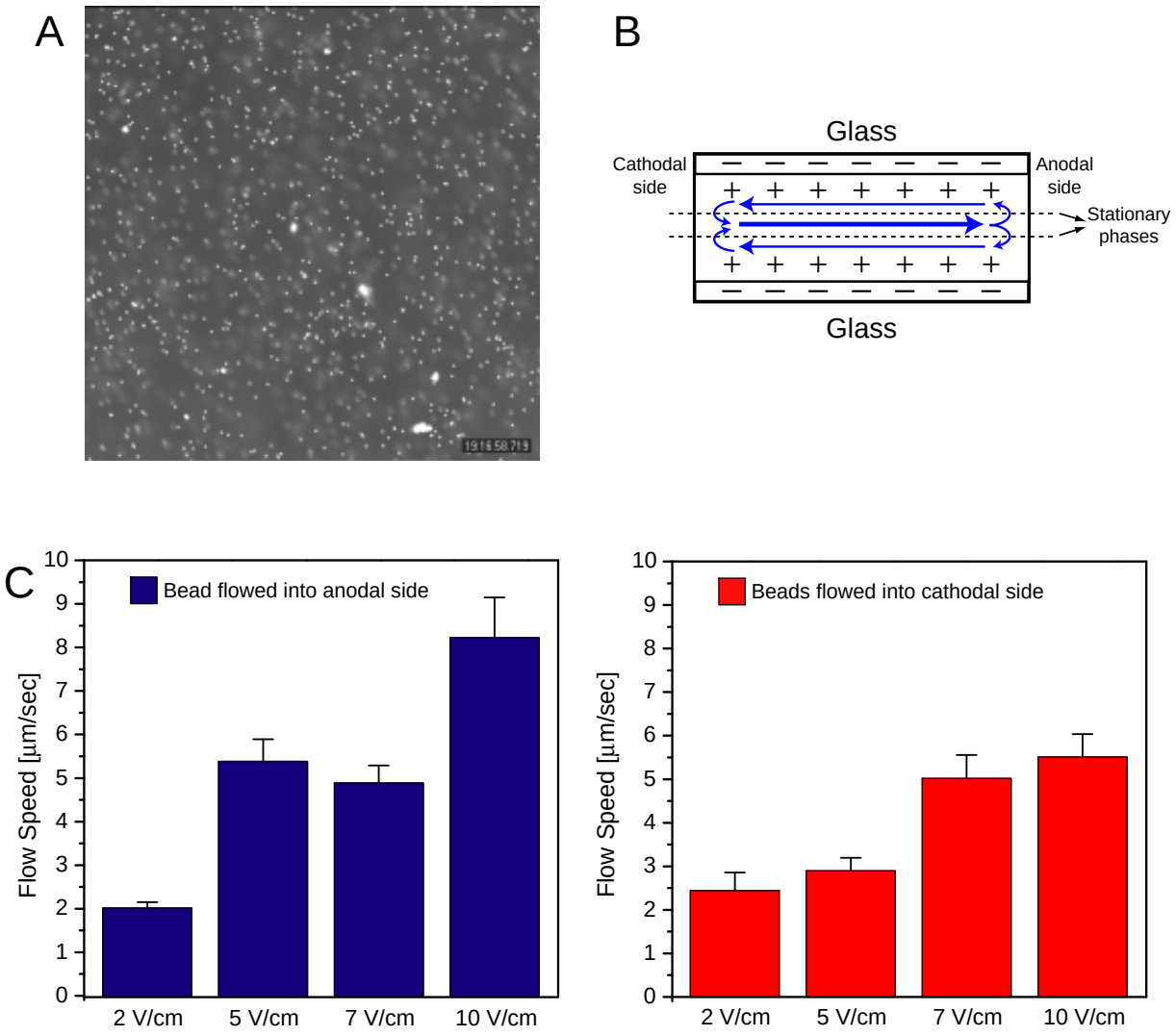

Fig.3-3 Measurement of electric osmotic flow (EOF)
To measure the EOF flow rate, micro beads (ϕ=0.9 μm) were used (**A**). Near the glass surface, EOF flowed into the cathodal side, while it flowed into anodal side in the upper area (**B**). (**C**) EOF flow rate depended on electric field strength. At 10 V/cm, flow rates for cathodal and anodal side was about 5 μm/sec and 8 μm/sec, respectively. Data represent mean±S.E.(n=20-30).

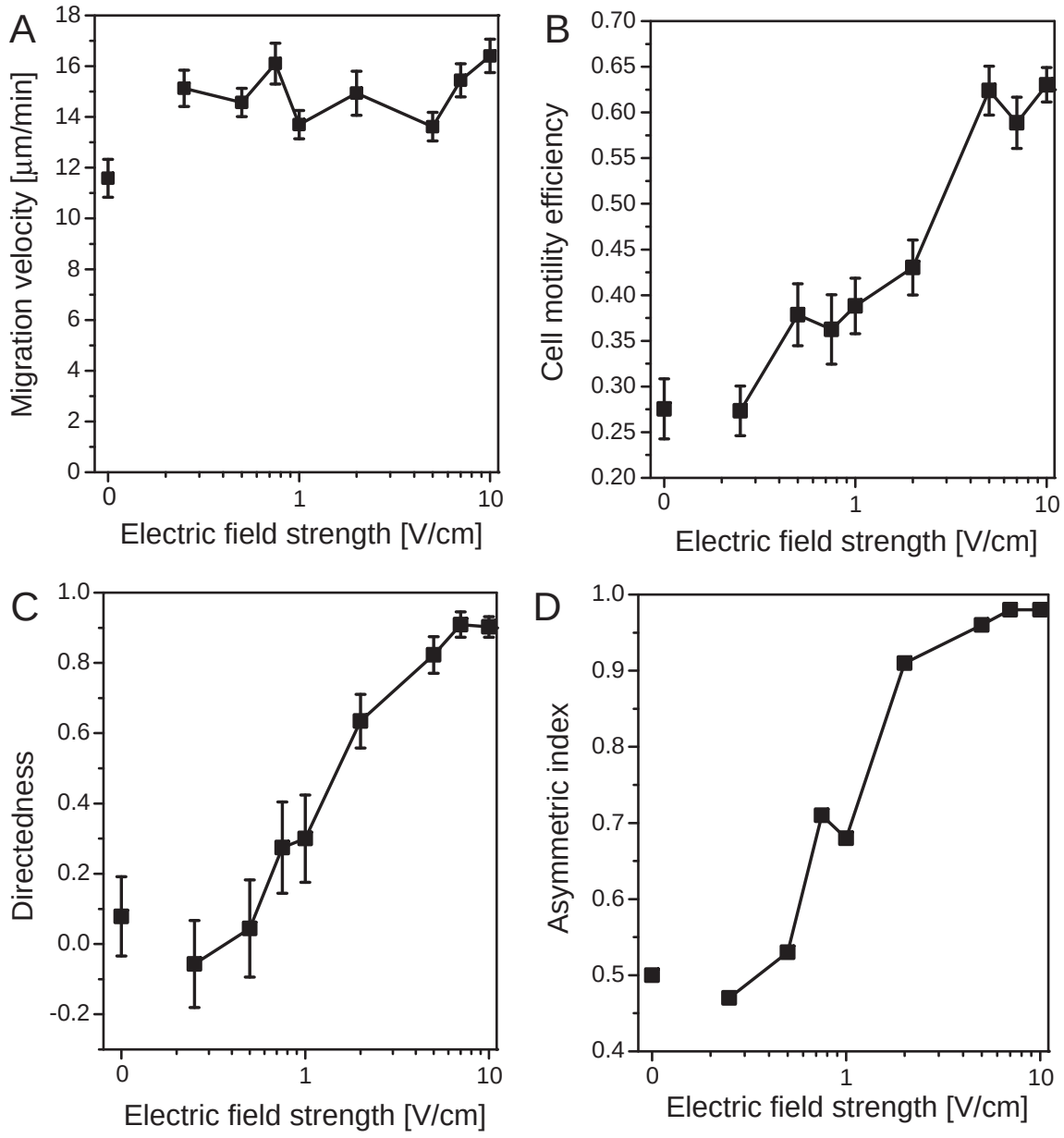

Fig. 3-4 Dependence of cellular motile properties on electric field strength.
Migration velocity (**A**), Cell motility efficiency (**B**), Directedness (**C**) and Asymmetric index (**D**) were analyzed to elucidate the effects of electric fields on cellular motile activities. See "cell migration analysis" in chapter 2 for the calculation details. Migration velocities were almost same at different field strengths, while directedness, asymmetric index and cell motility efficiency increased in a dose dependent manner. Data represent mean±s.e.m. Data were obtained from at least three independent experiments.

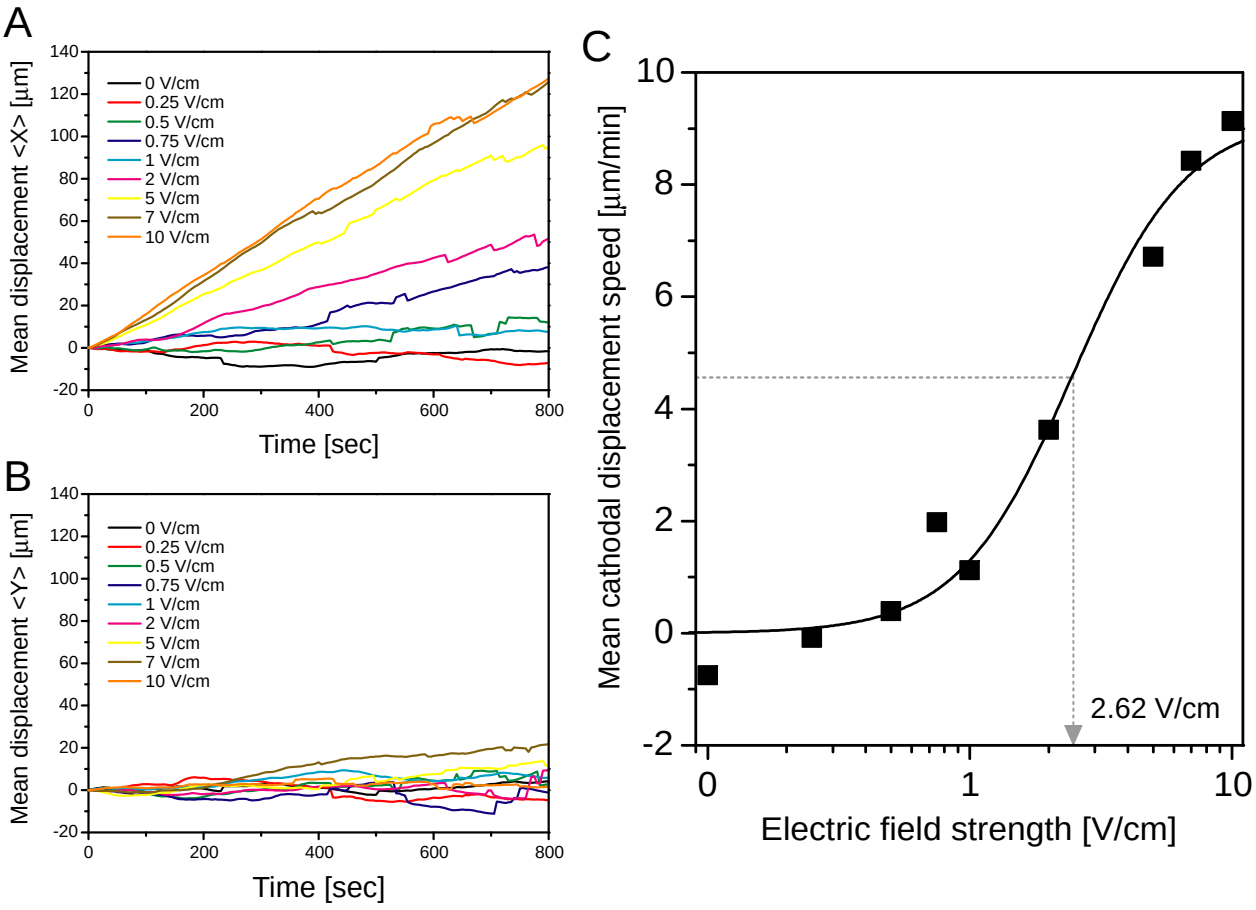

Fig.3-5 Input-output relationship to an electrotactic response of *Dictyostelium* cells.
(**A**) Temporal changes of mean cathodal displacements. (**B**) Temporal changes of mean displacements in the direction perpendicular to the electric field. (**C**) Dependence of mean cathodal displacement speed (MCS) on electric field strength. Solid line represents the fitting curve that was obtained by Equation (3.2) with sigmoidal number n = 2. MCS reaches half-maximum at 2.6 V/cm, which represents cell sensitivity to the electric field.

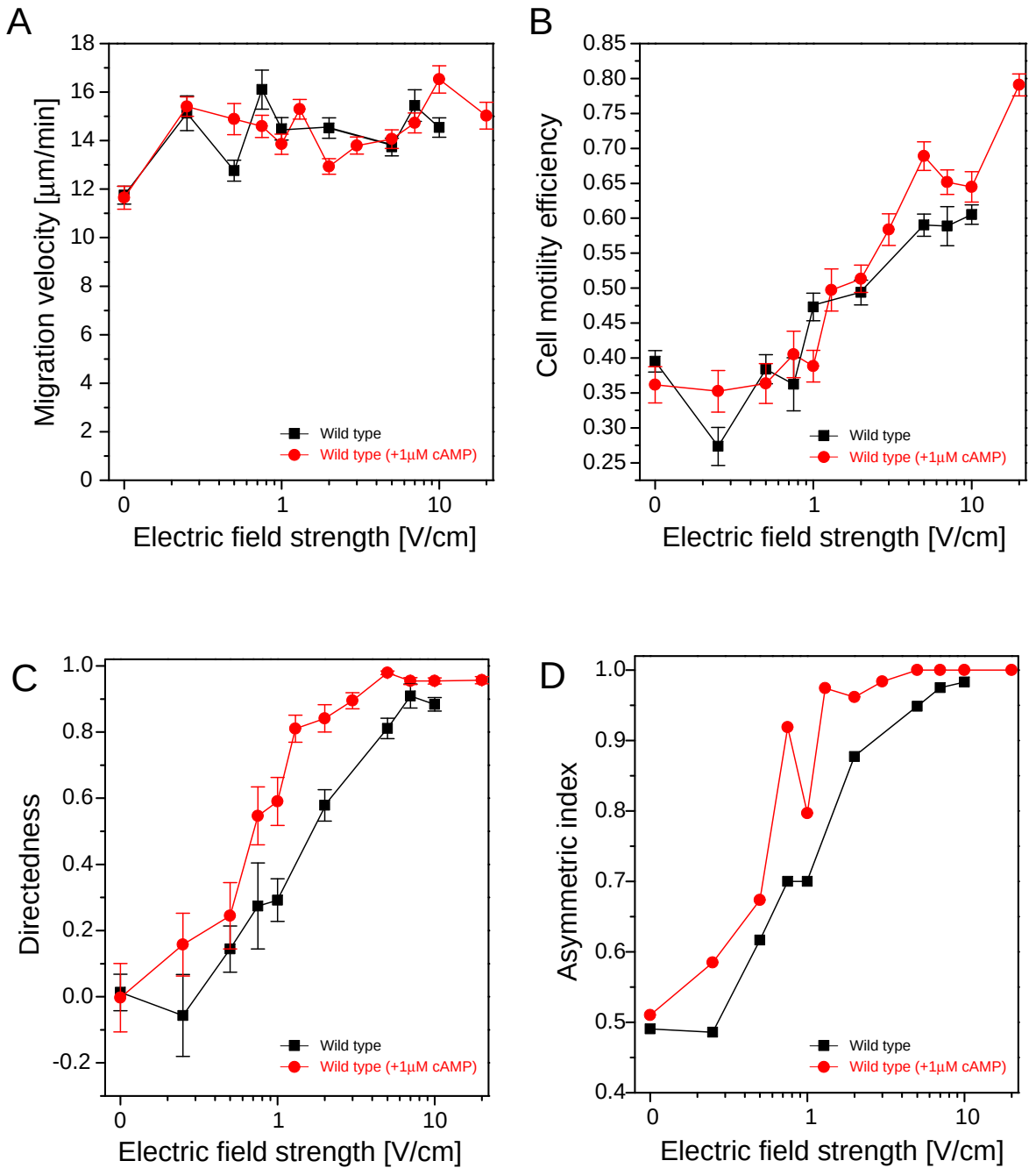

Fig.3-6 Effects of cAMP on electrotactic response

Migration velocity (**A**), Cell motility efficiency (**B**), Directedness (**C**) and Asymmetric index (**D**) were analyzed to elucidate the effects of electric fields on cellular motile activities. See Chapter 2 in "cell migration analysis" for calculations. Migration velocities were similar at different field strengths, while directedness, asymmetric index and cell motility efficiency increased in a dose dependent manner. In the presence of cAMP, cells could sense the direction of the electric field at field strengths lower than that of absence of cAMP. Data represents mean±s.e.m. Data was obtained from at least three independent experiments.

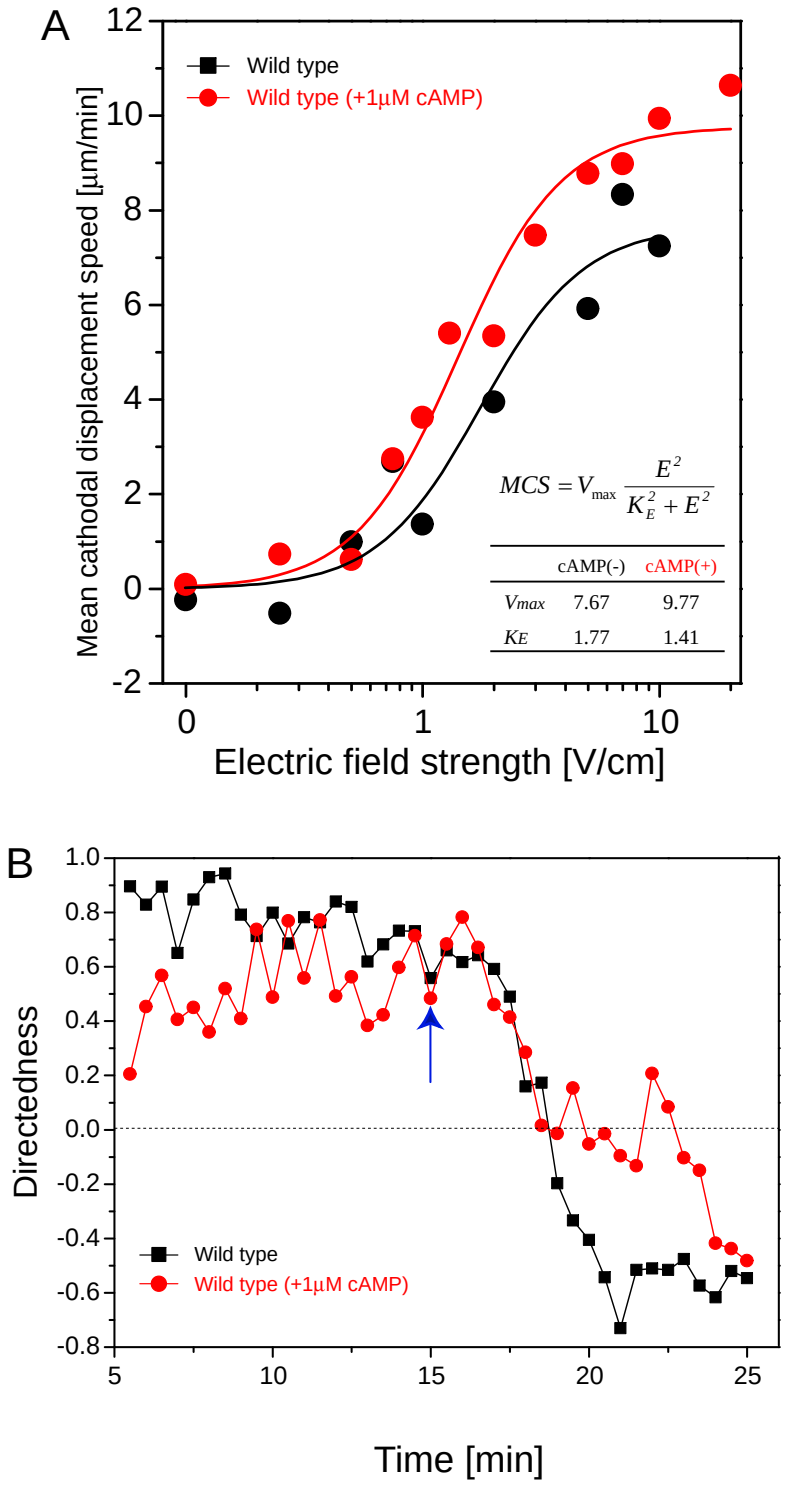

Fig.3-7 Effects of cAMP on electrotactic response.

(**A**) Dependence of mean cathodal displacement speed (MCS) on electric field strength in the absence or presence of cAMP. Solid line represents the fitting curve that was obtained by equation (3.2) with sigmoidal number n = 2. Sensitivity parameter of the cells for electric signal, K_E, is 1.77 in the absence of cAMP and 1.41 in the presence of cAMP, indicating that the sensitivity was enhanced by cAMP stimulation.

(**B**) Reversing the direction of the electric field. The field was reversed after 15 min of electric field application as the point marked by the arrow. Cell migration reversal in the presence of cAMP towards the new cathode side occured more slower than that of no cAMP.

* In (**A**), the values of no cAMP is different from that presented in Fig.3-5C. This is because of the addition of the data.

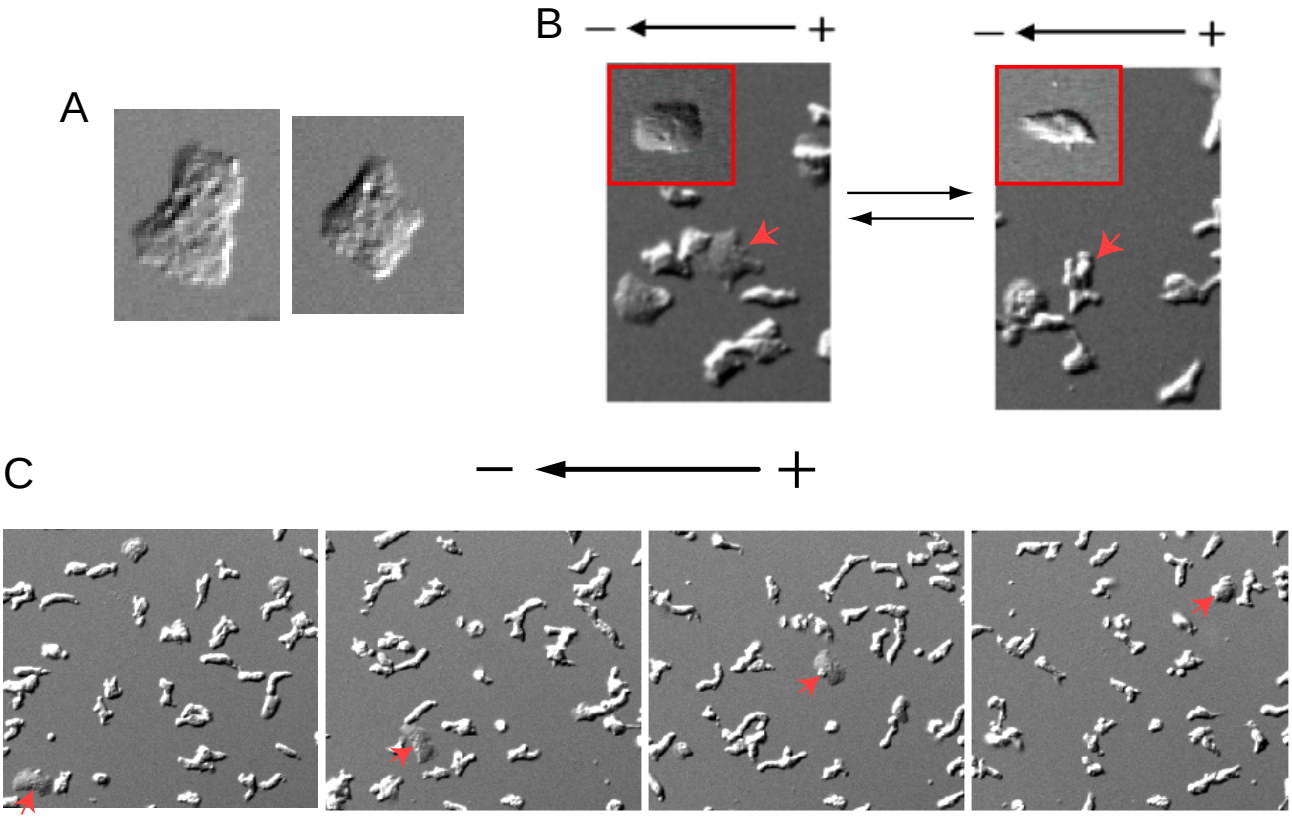

Fig.3-8 Defective electrotaxis.
(**A**) Sprawl-shaped cell was sometimes observed at developmental state.(**B**) Sprawl-shaped cell showed transition between sprawled and polarized shape. Such transition was obsercved within a few minutes. Inlet figures represent the higher magnification images of sprawled and polarized shape.
(**C**) Almost cells migrated towards cathode (left) in dcEF (10 V/cm), however sprawl-shaped cell was indicated by arrow migrated in random direction. Ih this case, this cells migrated towards anode.

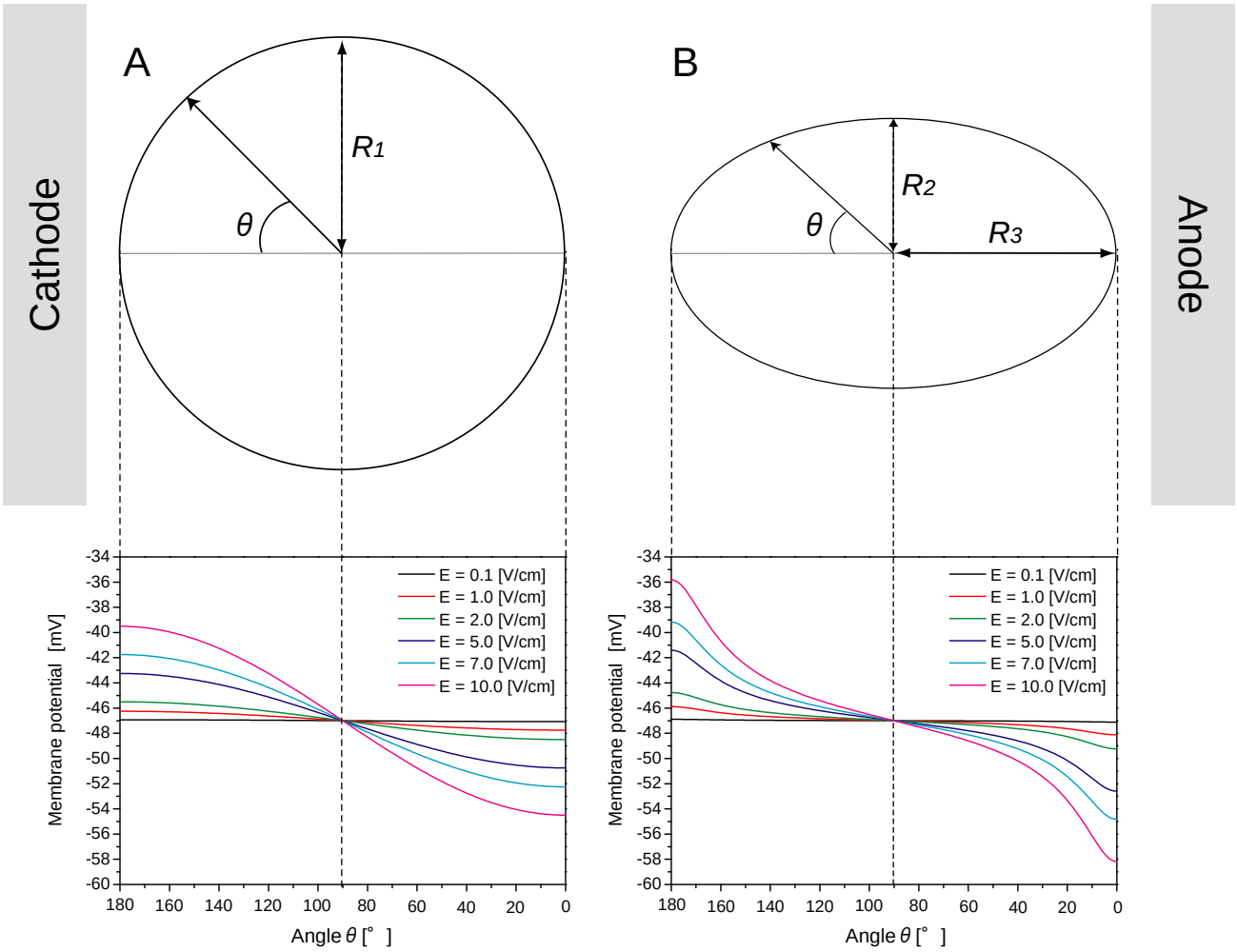

Fig.3-9 Membrane potential distribution.
When external electric fields are applied to cells, membrane potential changes of the area facing the electrode is largest, while membrane potentilal is not change in the area with rectangular to the electric field. Membrane potential depolized at the cathodal side and hyperplarized at the anodal side. Resting membrane potentila of *Dictyostleium* cells is about 47 mV [54]. (**A**) In the spherical cells, potential difference between the cathode and anode is 14.5 mV at 10 V/cm. (**B**) In polarized cells, potential difference is 22.3 mV at 10 V/cm. The membrane potential distribution was calculated by (3.4). R_1=5 μm, R_2=2.5 μm, R_3=10 μm.

3.2 Electrotactic signaling pathway in *Dictyostelium* cells

Abstract

Switching direction of cell movement in response to extracellular guidance cues has been found in various cell types and is an important cellular function for translocation during cellular and developmental processes. Here I show that the preferential direction of migration during electrotaxis in *Dictyostelium* cells can be reversed through the genetic modulation of both guanylyl cyclases (GCases) and the cGMP-binding protein GbpC, in combination with inhibition of phosphatidylinositol-3-OH kinases (PI3K). The PI3K-dependent pathway is involved in cathode-directed migration under direct current electric fields (dcEF). Both the catalytic domain of soluble GCase (sGC) and GbpC also mediate the cathode-directed signaling, while the N-terminal domain of sGC mediates the anode-directed signaling. These observations provide the first identification of the genes required for directional switching in electrotaxis, and suggest parallel processing of electric signals in which multiple signaling pathways act to bias cell movement towards the anode or cathode, determining the direction of migration.

3.2.1 Introduction

Directional cell migration of eukaryotic cells in response to external guidance cues plays crucial roles in many physiological phenomena such as embryogenesis, neurogenesis, immune response, wound healing and regeneration of multicellular organisms, as well as in tactic response of unicellular organisms [1]. Clarifying the molecular basis of determining migration direction has been one of important topics in cell and developmental biology. Cells can exhibit not only attractive but also repulsive migrations in response to external signal. For example, in chemotactic response of neuronal cells, the growth cones exhibit repulsive response for a chemorepellant, while under the presence of membrane-permeable analog of cyclic nucleotides they show attractive turning in response to the same chemoattractant [2]. Further investigations of the mechanism underlying reversal in migration direction have revealed that the ratio between intracellular cyclic AMP (cAMP) and cyclic GMP (cGMP) regulates Ca^{2+} channels responsible for directional selection of migration [3]. In the case of chemotaxis in *Dictyostelium discoideum*, the cells exhibit attraction towards the source of extracellular chemoattractant cAMP, while they exhibit repulsion away from the source

of chemorepellent cAMP analog [4]. Chemoattractants induces the activation of phosphoinositide-3-kinase (PI3K) and phospholipase C (PLC) at the cell surface facing to the higher concentrations, leading to the localized accumulation and depletion of phosphatidylinositol 3,4,5-trisphosphate (PtdIns(3,4,5)P_3) and phosphatidylinositol 4,5-biphosphate (PtdIns[4,5]P_2), respectively, which induces pseudopod formation directionally toward the chemoattractant source. On the other hand, chemorepellent gradients induce the localized inhibition of PLC, leading to the localized accumulation of PtdIns[4,5]P_2. This chemorepellent-elicited reaction is opposite to the chemoattractant-elicited one, which causes the reversal in the polarized localization of the PtdIns lipids, inducing repulsive migration away from the chemorepellent. The proper localization of the PtdIns lipids on membrane is responsible for directional selection of chemotactic migration. Thus, investigations of directional switching in response to external signals have been a quite useful to clarify the molecular mechanisms underlying determination of the migration direction.

In electrotaxis, cells move with a directional preference towards the cathode or anode under direct current electric fields (dcEFs). There is a growing body of evidence that electrotaxis plays important roles in many physiological phenomena [5-9]. Similar to chemotactic responses, preferential direction of migration during electrotaxis varies among cell types and under different experimental condition (See Table 1). Different types of cells show different migration direction. For example, corneal rat epithelial cells, human keratinocytes, osteoblasts, rat prostate cancer cells, lymphocyte and *Xenopus* neurons migrate towards cathode, while corneal stromal fibroblasts, osteoclasts, human granulocyte and macrophage migrate towards anode [5-9]. Even in the same cell type, cells derived from different species exhibit opposite migration

direction in dcEFs; bovine vascular endothelial cells migrated towards cathode, while human vascular endothelial cells migrated towards anode [10, 11]. Furthermore, lens epithelial cells change its migration direction depend on applied electric field strength [12]. However, in spite of the mechanistic importance regarding the coupling between gradient sensing and directional cell migration, the molecules responsible for selecting the migration direction in electrotaxis have not been identified.

To investigate molecular mechanisms underlying determination of the migration direction in electrotaxis, here I used cellular slime mold *Dictyostelium discoideum*. The *Dictyostelium* cells are well-established model organism for elucidating molecular mechanisms of amoeboid movements and its regulations [13-16]. The chemotactic responses have been extensively studied at the molecular and cellular levels, which identify multiple and parallel chemotactic signalling pathways [17-20]. Since *Dictyostelium* cells exhibited strong electrotaxis, they would be useful for studying the mechanism of electrotaxis [21, 22]. Previous reports revealed that upstream components of chemotactic signaling pathways such as cAMP receptor 1 and its coupled heterotrimeric G proteins are not essential for electrotaxis in contrast with chemotaxis [21], although whether downstream components are involved in electrotaxis or not has not been examined. Here, I found that chemotaxis-deficient mutant cells which have defect in guanylyl cyclase (GCase)-dependent signaling pathway exhibited reversal migration in electrotaxis. I further confirm that simultaneous suppression of GCases and PI3K activities caused switching preferential direction of migration from cathode to anode in response to the same electric signals. These observations provide the first identification of the genes required for directional switching in electrotaxis.

3.2.2 Guanylyl cyclase dependent signaling pathway

Defects of KI mutant cells in electrotaxis

First, I examined the effects of electrical signals on a series of mutant cells called KI mutants, originally isolated as chemotaxis-deficient mutants by means of chemical mutagenesis [23]. I used three types of mutants, KI-5, KI-8 and KI-10, for electrotactic assays. Biochemical characterization of these KI mutants during chemotactic responses has revealed that KI-8 cells have virtually no GCase activity while KI-10 and KI-5 cells do have GCases activity but are defective in their chemoattractant-mediated activation of GCase and downstream cGMP-dependent signaling events, respectively [24,25]. With no electric field, wild type and these KI mutant cells moved randomly in all directions with a migration velocity between 6 ~ 26 μm/min (Table 4). Upon electrical stimulation, wild type cells moved toward the cathode, which gradually became obvious with increasing electric field strength. The electrotactic efficiency of the cells reached a maximum at 10 V/cm (Fig. 3-10A, B and I). KI-5 cells moved efficiently toward the cathode at 10 V/cm, showing no defects in electrotaxis (Fig. 3-10C and D). Impaired responses to electrical stimulation were observed clearly in the other KI mutant cells. KI-8 cells moved toward the anode, opposite of wild type cells, at the same dcEF strength (Fig. 3-10E and F). KI-10 cells moved in a random direction (Fig. 3-10G and H). To examine the effects of electric signal on cell motility, we quantitatively analysed motile properties as summarized in Table 4. The dependence of directedness on the dcEF strength for these mutant and wild type cells is shown in Fig. 3-10I, where positive and negative values of the directedness indicate movements towards the cathode and anode, respectively. The preferential direction of migration depended on the mutant types but not on the dcEF strength. Reversal of the preferential direction

relative to the wild type was constantly observed in KI-8 at a range between 1 and 10 V/cm. In addition, detailed migration analysis of KI mutant cells was done by mean cathodal displacement speed (MCS) analysis. It was found that the sensitivity for the electric signal by KI-8 cells was similar to that of wild type cells (K_E= 1.60 V/cm in KI-8, K_E= 1.77 V/cm in wild type) and KI-10 cells were also biased slightly towards cathode, but only at field strength >5 V/cm (Fig. 3-11). Thus, severe defects in the migration direction during electrotaxis were observed in KI-8 and KI-10, but not in KI-5, indicating that the molecular mechanisms for electrotaxis are shared in part with those of chemotaxis. Mutant type-specific directionality in KI mutants during electrotaxis suggests that GCase activity is involved in determining preferential direction. I should note that the responsible mutation(s) in KI mutants has not been identified genetically [23].

Involvement of the guanylyl cyclase dependent pathway in electrotaxis

To test directly whether the GCase-dependent signaling pathway is involved in the electrotaxis of *Dictyostelium* cells, I next examined the effects of genetic disruption of GCases and cGMP-binding proteins on electrotactic response. In *Dictyostelium* cells, two types of GCases, guanylyl cyclase A (GCA) and soluble guanylyl cyclase (sGC), have been identified as responsible for all cGMP production in the cells [26]. cGMP-binding protein C (GbpC) is a major binding target for intracellular cGMP and transmits cGMP signals, which is responsible for regulation of myosin filament formation at the side and tail end of *Dictyostelium* cells [27, 28]. Thus, the GCase and cGMP-binding protein are the upstream and downstream molecules of cGMP, respectively. Upon electrical stimulation (10 $V \cdot cm^{-1}$), both the *gca*$^-$/*sgc*$^-$ and *gbpC*$^-$ cells exhibited an

To confirm the involvements of cGMP production in cathode-directed migration, I prepared the *gca*$^{-}$*/sgc*$^{-}$ cells expressing with either the N-terminal domain or the catalytic domain of sGC because sGC has the two domains responsible for chemotactic signalling (Fig. 2C) [17, 29]. Upon a dcEF (10 V·cm^{-1}), the *gca*$^{-}$*/sgc*$^{-}$ cells expressing the catalytic domain of sGC (*gc* null/sGCΔN) exhibited cathode-directed electrotaxis with an efficiency similar to that of wild type cells, indicating full recovering of cathode-directed electrotaxis only by the catalytic domain of sGC (Fig. 3-12C). On the other hand, the *gca*$^{-}$*/sgc*$^{-}$ cells expressing the N-terminal domain of sGC (*gc* null/sGCΔCat) exhibited no recovering of efficient electrotaxis but rather defects in the cathode-directed electrotaxis (Fig. 3-12C and E). Consistent with this observation, *gbpA*$^{-}$*/gbpB*$^{-}$ cells, which lack the degradation activities of intracellular cGMP, exhibited stronger electrotaxis towards the cathode than that of wild type cells (Fig. 3-12C and F) [27, 28]. Thus, the GCase-dependent cGMP signalling mediates the cathode-directed electrotaxis. However, in contrast to KI-8 cells, the *gca*$^{-}$*/sgc*$^{-}$, *gbpC*$^{-}$ and *gc* null/sGCΔCat cells were still able to move toward the cathode, showing no reversal of preferential direction. Therefore, the GCase-dependent pathway is not solely responsible for cathode-directed electrotaxis, suggesting GCase-independent pathways are additionally involved in the cathode-directed electrotaxis.

3.2.3 Switching direction by simultaneous inhibition of cGMP and PI3K-mediated signaling pathways

Phosphatidylinositol-3-OH kinase (PI3K) is one candidate for the GCase-independent signaling pathway, because its involvements in electrotaxis have been revealed in other cell types [9, 11, 30]. In *Dictyostelium* cells, PI3K is highly localized at the leading edge of moving cells where PI3K catalyses the production of PtdIns(3,4,5)P_3 on the membrane, a key molecule in regulating the localized activation of actin polymerization via interaction with PH-domain-containing proteins such as Akt/PKB [18-20]. To test the possible involvement of PI3K in preferential direction during electrotaxis, I examined the effects of a PI3K inhibitor, LY294002, on the electrotaxis of wild type, *gca*$^-$*/sgc*$^-$, *gbpC*$^-$, *gc* null/sGCΔN and *gc* null/sGCΔCat cells. In wild type cells, treatment with 60μM LY294002 strongly inhibited the velocity of cell migration in medium (see Table 4). To restore the basal speed of cell movement in the presence of LY294002, I added 1μM cAMP to the medium [31, 32]. In wild type cells, treatment with 60μM LY294002 strongly attenuated the cathode-directed electrotaxis, but the ability to move towards the cathode was maintained (Fig. 3-12A, B and C). When *gca*$^-$*/sgc*$^-$ cells were treated with 60μM LY294002, the direction of electrotaxis reversed towards the anode (Fig. 3-12A, B and D). Similar results were found for *gbpC*$^-$ and *gc* null/sGCΔCat cells (Fig. 3-12A, B, D and E, Movie S3 and S4). In particular, the N-terminal domain of GCase enhanced the anode-directed electrotaxis (Fig. 3-13F; *gc* null/sGCΔCat). While *gca*$^-$*/sgc*$^-$ and *gbpC*$^-$ cells did transiently only for about 10 min after dcEF application, the *gc* null/sGCΔCat cells exhibited continuously electrotaxis toward the anode, which is similar to phenotype of KI-8 (Fig. 3-13G). In contrast to *gca*$^-$*/sgc*$^-$, *gbpC*$^-$ and *gc* null/sGCΔCat cells, the *gc* null/sGCΔN cells that express the catalytic domain of sGC exhibited migration in random directions, suggesting a balance between cGMP-dependent cathode-directed electrotaxis and that anode-directed

electrotaxis (Fig. 3-32H, Table 3). These results reveal that simultaneous inhibition of GCase and PI3K activity is required to reverse migration direction. In addition, GCase has dual functions in electrotaxis. That is, the N-terminal and the catalytic domains of GCase are involved in biasing cell migrations under electric fields toward the anode and cathode, respectively.

3.2.4 Dynamics of electrotactic signaling components during electrotaxis

I next examined the intracellular dynamics of both sGC and GbpC distribution in migrating *Dictyostelium* cells under a dcEF (10 $V \cdot cm^{-1}$) using green fluorescent protein (sGC-GFP and GbpC-GFP, respectively). Both proteins were localized at the leading edge of cells migrating towards the cathode (Fig. 3-14A and B). For the PI3K-dependent signaling pathway, I observed PI3K and PtdIns(3,4,5)P3 by fusing PI3K2 and the PH domain of Akt/PKB to GFP (PI3K2-GFP and $PH_{Akt/PKB}$-GFP, respectively). PI3K2 and PtdIns(3,4,5)P3 also localized in a polarized manner at the leading edge of the pseudopod of cells migrating toward the cathode (Fig. 3-14C and D). These distributions of signaling molecules responsible for electrotaxis resemble those observed in chemotactic cells under cAMP gradients [18-20, 29, 33]. When cells were treated with LatrunculinA (5μM), which is a F-actin-depolymerizing reagent, the distinctive localization of these signaling molecules was lost, becoming random with respect to the direction of electric fields (Fig. 3-14E-H). These observations indicate that these signaling molecules from the GCase- and PI3K-dependent pathways are polarized through actin-dependent localization, and suggest that both pathways are involved in enhancing electrotactic efficiency by localizing in pseudopods directed toward the cathode. The presence of sGC, GbpC, PI3K and PIP_3 in the pseudopod could

3.2.5 Discussion

The results I report here provide the first identification of genes required for selection of migration direction in electrotaxis and show that the GCases- and PI3K-dependent signalling pathways work in parallel to bias cell movements toward the cathode. Simultaneous inhibition of both pathways induced switching direction of cell migration toward the anode. Similarity and differences in the molecular mechanisms between electrotaxis and chemotaxis are discussed below.

Previous reports have revealed that chemotaxis in *Dictyostelium* cells is mediated by PI3K, PLA2 and GCase dependent signaling pathway [17-20, 34, 35]. Simultaneous inhibition of these pathways abolishes chemotactic movements completely, while functional signalling in either one of these multiple pathways can restore chemotaxis at least in part, suggesting that these pathways work independently [17]. Similar to chemotaxis, multiple signaling pathways work in parallel for electrotaxis to reorient cells directionally towards the cathode or anode (Table 3). Both the GCase- and PI3K-dependent signaling pathways are involved in cathode-directed electrotaxis. Molecular components of the GCase- and PI3K-dependent signaling pathways localized at the leading edge of migrating cells under dcEF in an actin-dependent manner (Fig. 3-14A-D). Similar results have been observed in chemotactic cells under the chemoattractant gradients, in which a distinctive localization of the signalling components at the leading edge has been implicated to enhance chemotactic efficiency [19, 29]. These results suggest functional sharing of intracellular signaling components for directional cell

migration between chemotaxis and electrotaxis. However, there are some differences between electrotaxis and chemotaxis. First, the localized accumulation of PtdIns(3,4,5)P_3 on membrane facing to the chemoattractant source with actin-independent manner is one of key signaling events in chemotaxis [33], while no localization of PtdIns(3,4,5)P_3 was observed in cells under dcEF when actin cytoskeleton was inhibited (Fig. 3-14E-H). This indicates that PI3K-dependent signaling pathway mediates electrotactic signals in an actin-dependent manner. Because PI3K activity is regulated by a feedback mechanism through a Ras/PI3K/F-actin circuit [32], electric signals may affects on some components of this feedback circuit. Second, sGC is involved in both chemotaxis and electrotaxis, but in a different way. The GC null cells expressing N-terminal domain of sGC (*gc* null/sGCΔCat) can restore chemotaxis, while the cells expressing catalytic active domain of sGC (*gc* null/sGCΔN) is not sufficient for chemotaxis [17]. In contrast to chemotaxis, *gc* null/sGCΔCat cells cannot restore electrotaxis toward the cathode, while catalytic active *gc* null/sGCΔN cells can restore perfectly cathode-directed electrotaxis (Fig. 3-13A). The *gc* null/sGCΔCat cells was rather inhibited to move toward the cathode. Furthermore, with simultaneous inhibition of PI3K, *gc* null/sGCΔCat cells moved efficiently toward the anode. These results indicate that the N-terminal domain and catalytic domain of sGC are involved in anode- and cathode-directed signaling in electrotaxis, respectively. The two domains of sGC with opposite function may be integrated through intramoleculer interactions for directional migration in electrotaxis. Additionally, electrotactic cells sometimes changed their behaviours by application time of electric fields. Wild type and *gc* null/sGCΔCat cells exhibited electrotaxis continuously towards the cathode and anode, respectively, while *gca*$^-$/*sgc*$^-$ and *gbpC*$^-$ cells gradually became random with time

after electric field application (Fig. 3-13G). Such stimulation time-dependent directionality is not obvious in chemotaxis. Although its precise mechanism remains unknown, electrophoresis of membrane protein may be involved in electrotaxis because it requires relative longer field application (at least 5 min longer) [36, 37].

In chemotactic response of growth cones of Xenopus spinal neurons, intracellular Ca^{2+} pattern, which are generated by cyclic nucleotide-activated L-type Ca^{2+} channel, determines whether they exhibit attraction or repulsion to the same external stimulations [3]. In the gradient of netrin-1, the activation of cAMP-dependent signaling pathway induces Ca^{2+} entry resulting attraction, while inhibition of this pathway suppress Ca^{2+} entry resulting repulsion. Thus, intracellular cyclic nucleotides function as key signaling molecules through Ca^{2+} regulation for directional preference. Because the involvement of Ca^{2+} ion in electrotaxis has been demonstrated in many cell types [5-8], I examined the effects of extracellular Ca^{2+} ion on electrotaxis of *Dictyostelium* cells. First, I used $GdCl_3$ (50-100μM) known as a general Ca^{2+} channel inhibitor for electrotactic assay. However, addition of $GdCl_3$ suppressed cell motile activity as previously reported [38]. Instead of inhibitor, cells were inhibited for Ca^{2+} entry from medium by using Ca^{2+} chelator EGTA (5mM). Under this condition, no obvious changes in electrotaxis both of wild type cells toward the cathode and of knockout cells (*gc* null/sGCΔCat) toward the anode, suggesting no involvement of extracellular Ca^{2+} ion in *Dictyostelium* electrotaxis (Fig. 3-15A and B). It would be worth exploring the involvement of other chemotactic signals such as Ras, TORC2, PLCγ and PLA2 in directional control during electrotaxis [18-20]. These studies would further contribute to the understanding of molecular mechanisms involved in the coupling between gradient sensing and directional cell migration.

Table 3 Tug of War like model of electrotaxis in *Dictyostelium* cells

Determining the migration direction of electrotaxis in the presence of a PI3K activity

Cell type	Wild type	*gca*⁻/*sgc*⁻	*gc* null/sGC Δ N	*gc* null/sGC Δ Cat
Migration direction	Cathode	Cathode	Cathode	Cathode
Related signaling pathways		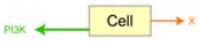		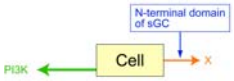

Determining the migration direction of electrotaxis in the absence of a PI3K activity

Cell type	Wild type	*gca*⁻/*sgc*⁻	*gc* null/sGC Δ N	*gc* null/sGC Δ Cat
Migration direction	Cathode	Anode	Random	Anode
Related signaling pathways				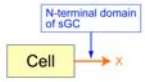

*1) X indicates unidentified signaling pathway for anode-directed migration.

*2) Lengths of arrow suggest the relative strength of biased force.

Table 4 Cell migration properties in a dcEF (1/2)

Cell type	EF stimulation (10 V/cm)	PI3K inhibitor (60 μM LY294002)	cAMP (1 μM)	Number of cells analyzed	Directedness	Migration velocity (μm/min)	Cell motility efficiency	Asymmetric index (cathode : anode)
Wild type	-	-	-	157	0.01±0.06 (random)	11.8±0.4	0.4±0.02	0.49 : 0.51
Wild type	+	-	-	119	0.88±0.02 (cathode)	14.5±0.4	0.61±0.01	0.98 : 0.02

Wild type	+	-	+	43	0.95±0.01 (cathode)	16.5±0.6	0.64±0.02	1 : 0
Wild type	-	+	-	137	0.05±0.06 (random)	2.8±0.2	0.14±0.01	0.5 : 0.5
Wild type	-	+	+	119	0.06±0.07 (random)	7.8±0.2	0.39±0.02	0.49 : 0.51
Wild type	+	+	-	148	0.53±0.05 (cathode)	4.6±0.2	0.26±0.02	0.8 : 0.2
Wild type	+	+	+	99	0.36±0.06 (cathode)	14±0.4	0.54±0.02	0.75 : 0.25
gbpA$^-$/*gbpB*$^-$	+	-	-	110	0.9±0.02 (cathode)	13.7±0.3	0.67±0.01	0.99 : 0.01
KI-5	-	-	-	107	0.11±0.07 (random)	22±0.4	0.39±0.02	0.59 : 0.41
KI-5	+	-	-	103	0.84±0.03 (cathode)	25±0.5	0.64±0.01	0.96 : 0.04
KI-8	-	-	-	132	-0.06±0.06 (random)	5.9±0.2	0.38±0.02	0.47 : 0.53
KI-8	+	-	-	142	-0.62±0.04 (anode)	8.4±0.3	0.5±0.02	0.13 : 0.87
KI-10	-	-	-	125	-0.04±0.06 (random)	25.8±0.3	0.5±0.02	0.49 : 0.51
KI-10	+	-	-	116	0.04±0.07 (random)	26.4±0.6	0.47±0.02	0.53 : 0.47
gca$^-$/*sgc*$^-$	+	-	-	111	0.63±0.05 (cathode)	14.1±0.4	0.45±0.02	0.89 : 0.11
gca$^-$/*sgc*$^-$	+	+	-	100	0.39±0.06 (cathode)	8.1±0.3	0.41±0.01	0.78 : 0.22
gca$^-$/*sgc*$^-$	+	+	+	138	-0.17±0.06 (anode)	8.4±0.2	0.42±0.01	0.39 : 0.61
gc null/sGC Δ N	+	-	-	133	0.83±0.03 (cathode)	9.4±0.4	0.6±0.01	0.95 : 0.05
gc null/sGC Δ N	+	+	+	114	0.01±0.06 (random)	7.0±0.3	0.53±0.02	0.53 : 0.47
gc null/sGC Δ Cat$^-$	+	-	-	105	0.32±0.07 (cathode)	12.5±0.4	0.5±0.02	0.69 : 0.31

Table 4 Cell migration properties in a dcEF (2/2)

Cell type	EF stimulation (10 V/cm)	PI3K inhibitor (60 μM LY294002)	cAMP (1 μM)	Number of cells analyzed	Directedness	Migration velocity (μm/min)	Cell motility efficiency	Asymmetric index (cathode : anode)
gc null/sGC Δ Cat	+	+	+	113	-0.67±0.04 (Anode)	10.6±0.2	0.73±0.01	0.09 : 0.91
gbpC$^-$	+	-	-	139	0.61±0.04 (cathode)	13.3±0.2	0.47±0.02	0.87 : 0.13
gbpC$^-$	+	+	+	190	-0.36±0.05 (anode)	7.8±0.1	0.39±0.01	0.28 : 0.72
gbpC$^-$/*gbpD*$^-$	+	-	-	123	0.77±0.03 (cathode)	9.9±0.4	0.62±0.02	0.94 : 0.06
gbpC$^-$/*gbpD*$^-$	+	+	+	190	-0.21±0.05 (anode)	9.9±0.2	0.65±0.01	0.36 : 0.64

Data are presented as mean±s.e.m. Definition of each parameter is given in chapter 2.

Data for each cell type was collected from 6 to 11 independent experiments.

References

[1] Bray D (2001) *Cell Movements: From Molecules to Motility*. (Garland Publishing, New York)

[2] Song H, *et al*. (1998) Conversion of neuronal growth cone responses from repulsion to attraction by cyclic nucleotides. *Science* **281**:1515-1518.

[3] Nishiyama M, *et al*. (2003) Cyclic AMP/GMP-dependent modulation of Ca2+ channels sets the polarity of nerve growth-cone turning. *Nature* 423:990-995.

[4] Keizer-Gunnink I, Kortholt A, Van Haastert PJ (2007) Chemoattractants and chemorepellents act by inducing opposite polarity in phospholipase C and PI3-kinase signaling. *J Cell Biol* **177**:579-585.

[5] Robinson KR (1985) The responses of cells to electrical fields: a review. *J Cell Biol* 101:2023-2027.

[6] Nuccitelli R (2003) A role for endogenous electric fields in wound healing. *Curr Top Dev Biol* 58:1-26.

[7] Mycielska ME, Djamgoz MB (2004) Cellular mechanisms of direct-current electric field effects: galvanotaxis and metastatic disease. *J Cell Sci* 117:1631-1639.

[8] McCaig CD, Rajnicek AM, Song B, Zhao M (2005) Controlling cell behavior electrically: current views and future potential. *Physiol Rev* 85:943-978.

[9] Lin F, Baldessari F, Gyenge CC, Sato T, Chambers RD, Santiago JG, Butcher EC (2008) Lymphocyte electrotaxis in vitro and in vivo. *J Immunol* **181**:2465-2471.

[10] Li X, Kolega J (2002) Effects of direct current electric fields on cell migration and actin filament distribution in bovine vascular endothelial cells. *J Vasc Res* **39**:391-404.

[11] Zhao M, Bai H, Wang E, Forrester JV, McCaig CD (2004) Electrical stimulation directly induces pre-angiogenic responses in vascular endothelial cells by signaling through VEGF receptors. *J Cell Sci* **117**:397-405.

[12] Wang E, Zhao M, Forrester JV, McCaig CD (2003) Bi-directional migration of lens epithelial cells in a physiological electrical field. *Exp Eye Res* 76:29-37.

[13] Segall JE, Gerisch G (1989) Genetic approaches to cytoskeleton function and the control of cell motility. *Curr Opin Cell Biol* **1**:44–50.

[14] Schleicher M, Noegel AA (1992) Dynamics of the Dictyostelium cytoskeleton during chemotaxis. *New Biol* **4**:461–472.

[15] Eichinger L, Lee SS, Schleicher M (1999) Dictyostelium as model system for studies of the actin cytoskeleton by molecular genetics. *Microsc Res Tech* **47**:124–134.

[16] Fukui Y (2002) Mechanistics of amoeboid locomotion: signal to forces. *Cell Biol Int* **26**:933–944.

[17] Veltman DM, Keizer-Gunnik I, Van Haastert PJ (2008) Four key signaling pathways mediating chemotaxis in Dictyostelium discoideum. *J Cell Biol* **180**:747-753.

[18] Kölsch V, Charest PG, Firtel RA. (2008) The regulation of cell motility and chemotaxis by phospholipid signaling. *J Cell Sci* **121**:551-559.

[19] Janetopoulos C, Firtel RA. (2008) Directional sensing during chemotaxis. *FEBS Lett* **582**:2075-2085.

[20] Kay RR, Langridge P, Traynor D, Hoeller O. (2008) Changing directions in the study of chemotaxis. *Nat Rev Mol Cell Biol* **9**:455-463.

[21] Zhao M, Jin T, McCaig CD, Forrester JV, Devreotes PN (2002) Genetic analysis of the role of G protein-coupled receptor signaling in electrotaxis. *J Cell Biol* 157:921-927.

[22] Sato MJ, *et al*. (2007) Input-output relationship in galvanotactic response of Dictyostelium cells. *BioSystems* **88**:261-272.

[**23**] Kuwayama H, Ishida S, Van Haastert PJ (1993) Non-chemotactic Dictyostelium discoideum mutants with altered cGMP signal transduction. *J Cell Biol* 123:1453-1462.

[24] Liu G, Kuwayama H, Ishida S, Newell PC (1993) The role of cyclic GMP in regulating myosin during chemotaxis of Dictyostelium: evidence from a mutant lacking the normal cyclic GMP response to cyclic AMP. *J Cell Sci* 106:591-595.

[25] Kuwayama H, Viel GT, Ishida S, Van Haastert PJ (1995) Aberrant cGMP-binding activity in non-chemotactic Dictyostelium discoideum mutants. *Biochim Biophys Acta* 1268:214-220.

[26] Roelofs J, Van Haastert PJ (2002) Characterization of two unusual guanylyl cyclases from dictyostelium. *J Biol Chem* 277:9167-9174.

[27] Bosgraaf L, *et al*. (2002) A novel cGMP signalling pathway mediating myosin phosphorylation and chemotaxis in Dictyostelium. *EMBO J* 21:4560-4570.

[28] Bosgraaf L, Van Haastert PJ (2002) A model for cGMP signal transduction in Dictyostelium in perspective of 25 years of cGMP research. *Muscle Res Cell Motil* **23**:781-791.

[29] Veltman DM, Roelofs J, Engel R, Visser AJ, Van Haastert PJ (2005) Activation of soluble guanylyl cyclase at the leading edge during Dictyostelium chemotaxis. *Mol Biol Cell* **16**:976-983.

[30] Zhao M, *et al*. (2006) Electrical signals control wound healing through phosphatidylinositol-3-OH kinase-gamma and PTEN. *Nature* **442**:457-460.

[31] Loovers HM, *et al*. (2006) Distinct roles of PI(3,4,5)P3 during chemoattractant signaling in Dictyostelium: a quantitative in vivo analysis by inhibition of PI3-kinase. *Mol Biol Cell* **17**:1503-1513.

[32] Sasaki AT, *et al*. (2007) G protein-independent Ras/PI3K/F-actin circuit regulates basic cell motility. *J Cell Biol* **178**:185-191.

[33] Parent CA, Devreotes PN (1999) A cell's sense of direction. *Science* **284**:765-770.

[34] Van Haastert PJ, Keizer-Gunnink I, Kortholt A (2007) Essential role of PI3-kinase and phospholipase A2 in Dictyostelium discoideum chemotaxis. *J Cell Biol* **177**:809-816.

[35] Chen L, *et al*. (2007) PLA2 and PI3K/PTEN pathways act in parallel to mediate chemotaxis. *Dev Cell* **12**:603-614.

[36] Jaffe LF (1977) Electrophoresis along cell membranes. *Nature* **265**:600-302.

[37] Fang KS, Ionides E, Oster G, Nuccitelli R, Isseroff RR (1999) Epidermal growth factor receptor relocalization and kinase activity are necessary for directional migration of keratinocytes in DC electric fields. *J Cell Sci* **112**:1967-1978.

[38] Lombardi ML, Knecht DA, Lee J. (2008) Mechano-chemical signaling maintains the rapid movement of Dictyostelium cells. *Exp Cell Res* **314**:1850-1859.

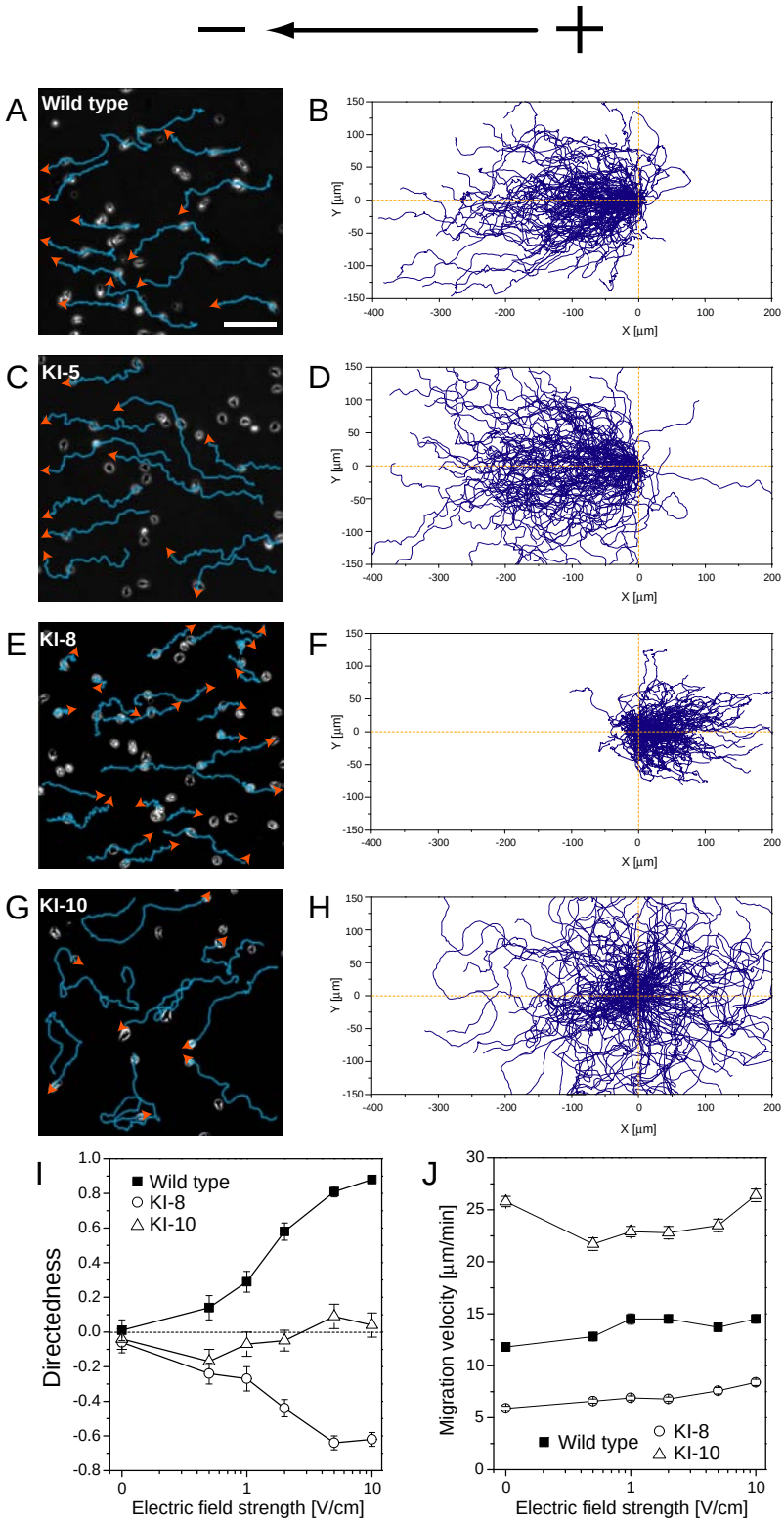

Fig.3-10 Reversal of directional preference during electrotaxis in KI-8 mutant cells.
Migration of wild type cells (**A, B**), mutants KI-5 (**C, D**), KI-8 (**E, F**) and KI-10 (**G, H**) under a dcEF (10 V/cm). Wild type and KI-5 mutant migrated towards the cathode under dcEF, while KI-8 mutant moved towards the anode. KI-10 mutant migrated in random directions. Blue lines and red arrows represent the cell trajectory and its direction of migration, respectively. Scale bar, 100 μm. (**B, D, F, H**) Cell trajectories in dcEF (10 V/cm). The start points of cell migration were accumulated at the origin. (**I**), Dependence of directedness on the dcEF strength: wild type (black closed square), KI-8 (open circle), KI-10 (open triangle). Although migration velocity was specific for cell type, it had minimal dependence on electric field strength (**J**). Data (mean±s.e.m.) for each cell type were quantified from 7-9 independent experiments.

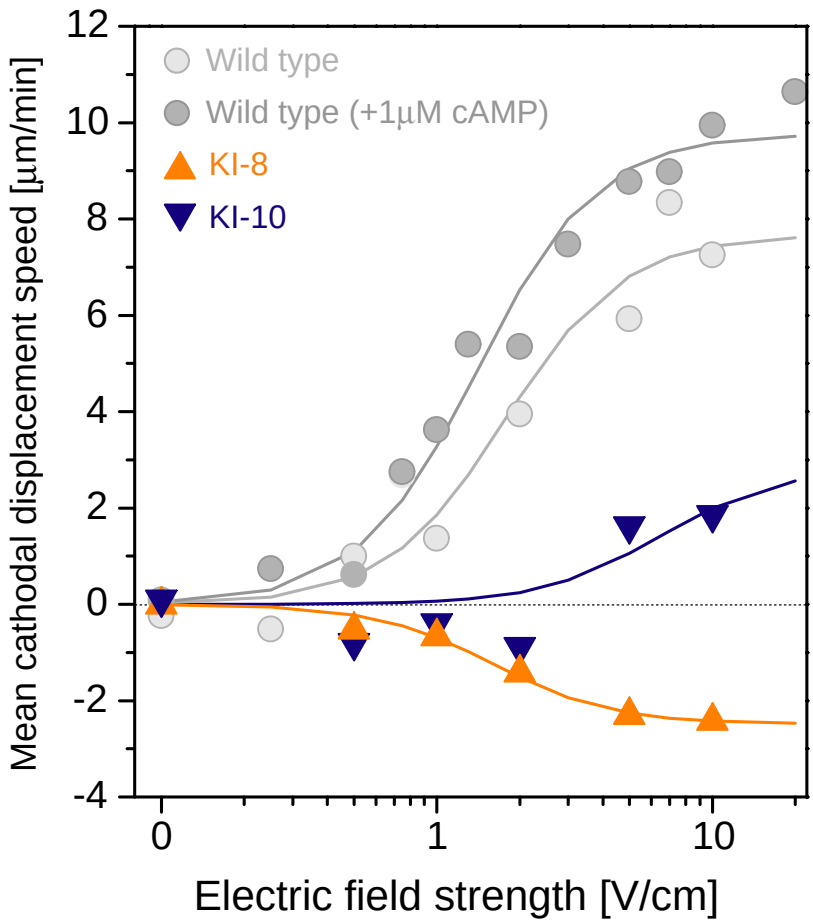

$$MCS = V_{\max} \frac{E^2}{K_E^2 + E^2}$$

	KI-8	KI-10	cAMP(-)	cAMP(+)
Vmax	-2.49	2.84	7.67	9.77
K_E	1.60	6.49	1.77	1.41

Fig.3-11 Input-output relationship to electrotactic response of KI mutant cells.
Dependence of mean cathodal displacement speed (MCS) on electric field strength. Solid line represents the fitting curve that was obtained by equation (3.2) with sigmoidal number *n*=2. MCS reaches half-maximum at different field strength between KI-8 and KI-10 cells, which represents sensitivity of the cells for the electric field. Sensitivity of KI-8 cells for electric signal was similar to that of wild type cell, while KI-10 cells could sense the electric signal only at large field strength.

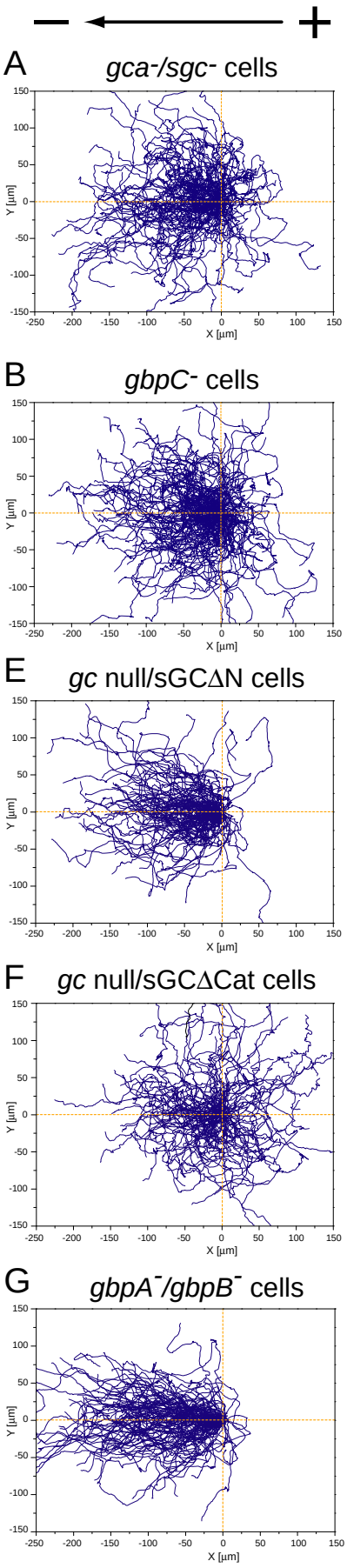

Fig.3-12 Both GCase and PI3K dependent pathways are required for preferential direction during electrotaxis.
Cell migration traces under dcEF (10 V/cm).GCases double knockout cells (*gca*$^-$/*sgc*$^-$) (**A**), cGMP binding protein C knockout cells (*gbpC*$^-$) (**B**), N-terminal domain deletion of sGC in guanylyl cyclase double knockout cells (*gc* null/sGCΔN) (**E**), catalytic domain deletion of sGC in GCases double knockout cells (*gc* null/sGCΔCat) (**F**), and cGMP binding proteins A and B knockout cells (*gbpA*$^-$/*gbpB*$^-$) (**G**). GCase-dependent siganling pathway in *Dictyostleium* cells (**C**). Cell motile properties in dcEF. Directedness (**D**) and Migration velocity (**H**). In all cases, cells were biased towards cathode. Data (mean±s.e.m.) for each cell type were quantified from 7-9 independent experiments.

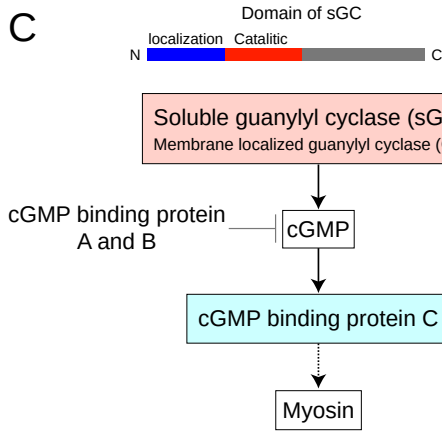

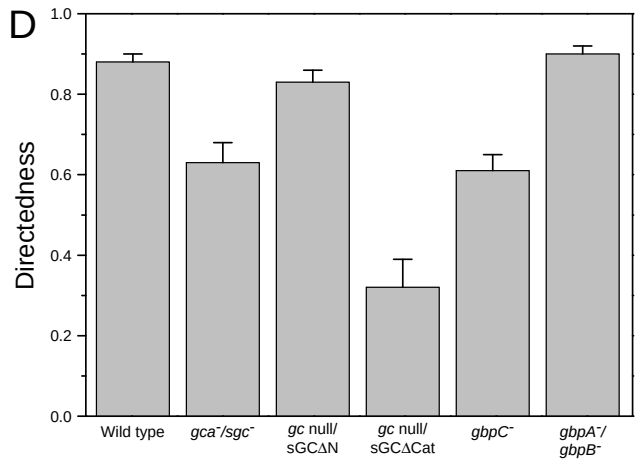

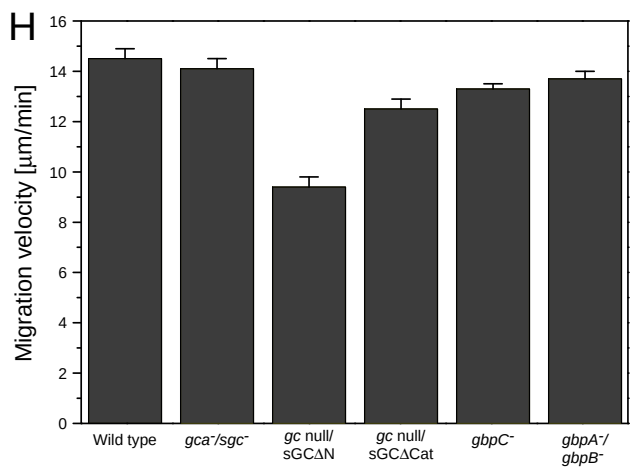

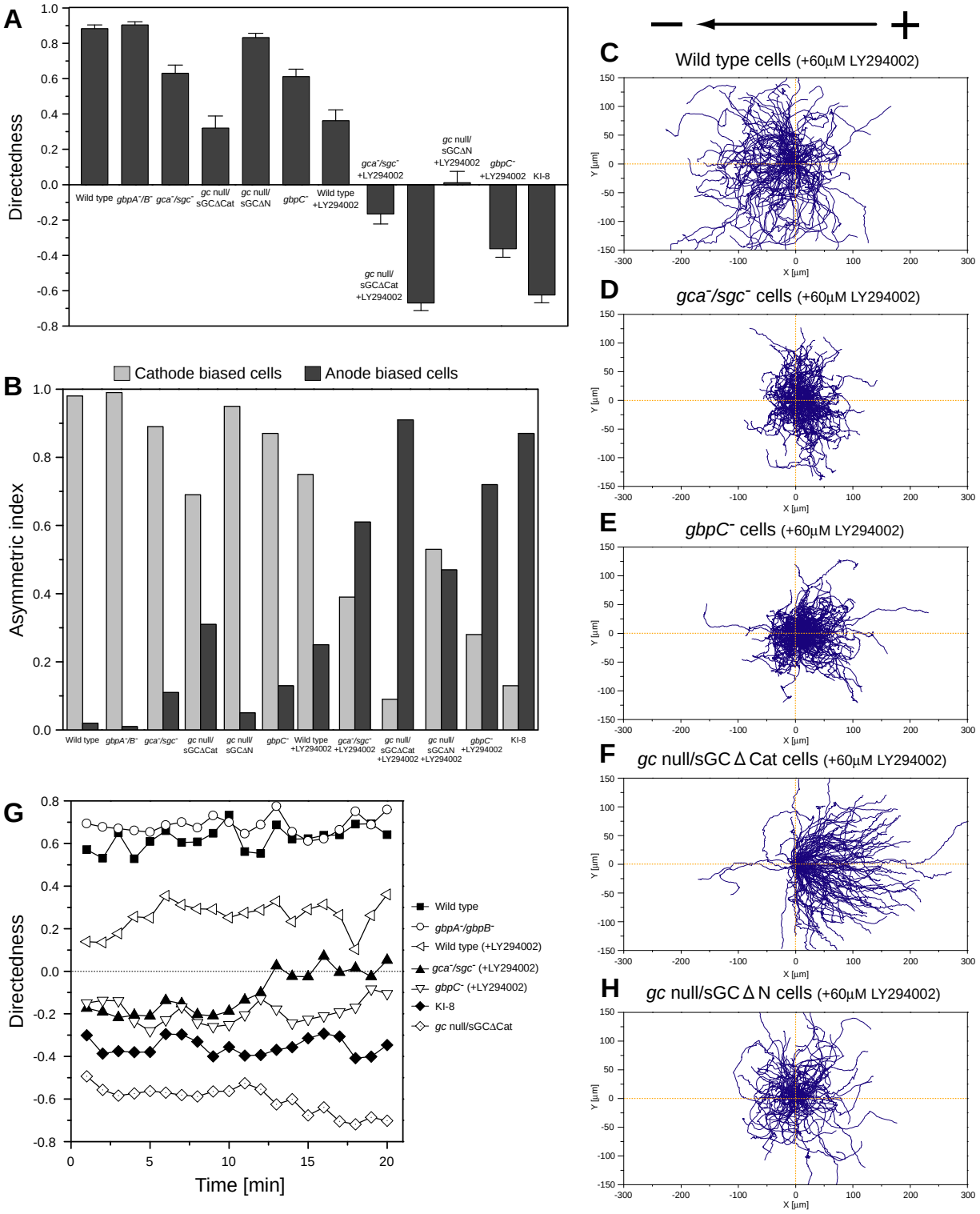

Fig.3-13 Switching direction in electric signal-induced cell migration by cGMP and phosphatidylinositol signaling. Cell motility analysis: directedness (**A**) and asymmetric index (**B**). Cell trajectories of wild type (**C**), *gca⁻/sgc⁻* (**D**), *gbpC⁻* (**E**), *gc* null/sGCΔCat (**F**) and *gc* null/sGCΔN (**H**) cells in the presence of 60μM LY294002, a PI3K inhibitor and 1μM cAMP, under a dcEF (10 V/cm).
When the activity of cGMP and PI3K dependent pathways was suppressed simultaneously, migration direction was reversed (D**, E, F**). (**G**) Time course of directedness in dcEF (10 V/cm). Directedness of cells with respect to the electric field was obtained in 1 min intervals. Reversal of preferential direction was observed in *gca⁻/sgc⁻*, *gbpC⁻* and *gc* null/sGCΔCat cells in dcEF. Data (mean±s.e.m.) for each cell type were quantified from 8-11 independent experiments.

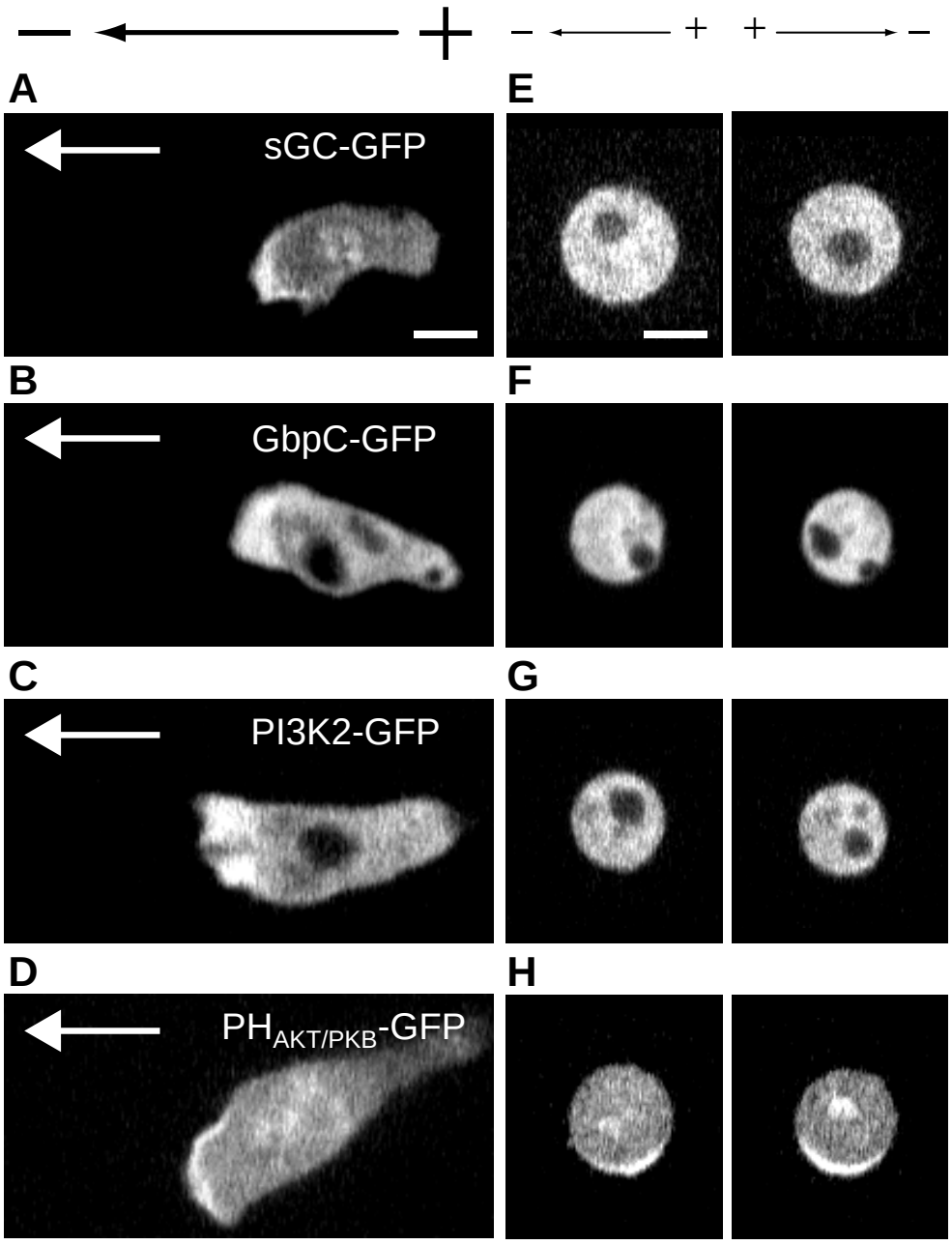

Fig.3-14 Intracellular localization of signaling molecules responsible for electrotaxis under dcEF. Confocal images of cells expressing sGC-GFP (**A**), GbpC-GFP (**B**), PI3K2-GFP (**C**) and $PH_{Akt/PKB}$-GFP (**D**) under dcEF (10 V/cm). White arrow indicates the direction of migration. These signaling molecules were polarized in cells migrating toward the cathode under dcEF, while such an asymmetric distribution was not observed in Latrunculin A (5 μM) treated cells (**E to H**). Right panels correspond to the signaling molecules presented in left panels. Scale bar, 5 μm.

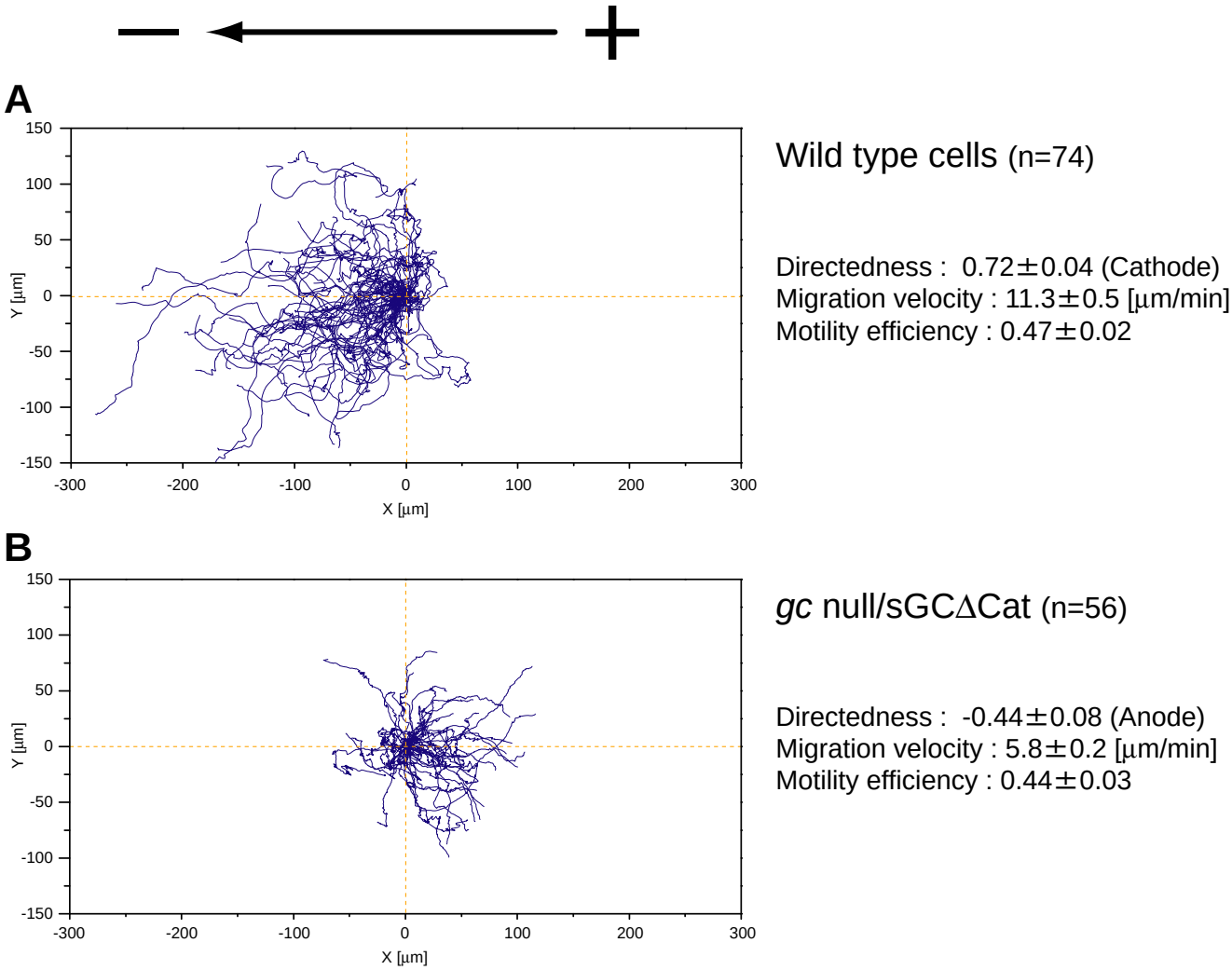

Fig.3-15 Influx of external Ca^{2+} is not necessary for electrotaxis in *Dictyostelium* cells.
Cell trajectories of cathode directed-migration of wild type cells in the presence of 5mM EGTA (**A**) and anode directed-migration of *gc* null/sGCΔCat cells treated with 60µM LY294002 in cobination with 1µM cAMP in the presence of 5mM EGTA (**B**). In both cases, caffeine was not applied. Althogh motile activity was decerased in both cases, migration direction was not affected by the absence of external Ca^{2+}.
Data (mean±s.e.m.) for each cell type were quantified from 3-9 independent experiments.

4 Future direction and outlook

4.1 Effects of oscillating EF on cell migration

To investigate the mechanism of the intracellular signaling network, it is important to reveal the relationship between signal inputs and outputs quantitatively under different conditions: the absence of a signal input, presence of a stable signal input and oscillating signal input (Fig. 1-1). This thesis describes the results from the first two categories. In direct current electric fields (dcEFs), *Dictyostelium* cells exhibit electrotactic migration toward the cathode. Input-output relationship of electrotaxis in *Dictyostelium* cells can be described by a simple phenomenological equation (chapter 3.1). I found that the electric signal is transmitted into the motile apparatus through both phosphatidylinositol-3-OH kinase (PI3K) and guanylyl cyclase (GCase) dependent signaling pathways (chapter 3.2).

I have already begun to examine the third group by observing the effects of oscillating EF on cell migration (Fig. 4-1 and 4-2). In the absence of an EF, migration velocity was about 11.8 μm/min, as shown in Fig. 3-4A. When oscillating electric signals, alternative current electric fields (acEFs) were applied to the cells, migration velocity increased and reached maximum (17.1 μm/min) at around 5 kHz, but began to decrease at over 7 kHz acEF. Moreover, when a dcEF (average field strength; 2 V/cm) was oscillated (±1 V/cm, 100 Hz), a cell population with faster velocity (about 1.4 times) appeared (Fig. 4-2C). While migration velocity increased, directedness was relatively unchanged. As a result, the arrival efficiency, which was calculated by multiply directedness and migration velocity, in dcEF+acEF was higher than that of the dcEF alone due to its higher migration velocity (Fig. 4-2D). Since it has been reported that migration velocity is controlled by the intracellular proton concentration regulated by Na/H exchangers in *Dictyostelium* cells [1], it would be worth examining whether the activity of Na/H exchanger is affected or not by application of acEFs [2]. A theoretical model has proposed that electro-chemical coupling generated by acEFs accelerates ion pump activity [3]. However, acEFs affect on living cells are quite different form that of dcEF [4,5] and are therefore worthy of both theoretical and experimental investigations.

4.2 Model of cell migration

Even in the absence of external directional cue such as electric field, cells migrate in a random direction spontaneously (Fig. 3-1C). When electric signal is presented, such spontaneous cell movement is biased towards particular direction (Fig. 3-1D). Here, I have tried to construct the model, which describes these spontaneous and tactic movement of *Dictyostelium* cells with a collective view. First, I succeeded in applying a generalized Langevin model to the experimental data of cell migration in the absence of directional cue (Fig. 4-3A). Then, I have tried to construct further developed model, which describe the electrotactic movement by introducing the bias term to a generalized Langevin equation of spontaneous movement (Fig. 4-3B). These generalized Langevin equations composed of decay, memory, noise and bias terms. Since what kinds of cellular mechanism are corresponded to these terms is remain unknown, to identify these molecular basis is needed.

4.3 Voltage sensitive protein

Another attractive approach to investigate the intracellular signaling pathway by electrical stimulation is utilizating voltage sensitive proteins. It has been gradually realized that many proteins have voltage sensitivity. For example, novel adenylyl cyclases found in *Paramecium* and *Tetrahymena* are ion channel/enzyme fusion proteins [6]. Also, muscarinic receptors (m2R and m1R), which are part of the G-proteins coupled receptor (GPCR) family, show voltage sensitivity itself even without the voltage sensor domain (VSD). It has been reported that the binding of a ligand to the receptor is correlated with the membrane potential change [7].

A major breakthrough in this field is the discovery of voltage sensitive phosphatase (VSP) (Fig. 4-4A). VSP is found in the *Ascidian Ciona intestinalis* by genome searching [8]. This protein consists of a canonical transmembrane VSD and a cytoplasmic domain of phosphoinositide phosphatase, which is homologous to the phosphatase and tensin homologues deleted on chromosome 10 (PTEN). When the membrane potential depolarizes, VSP is activated and then produces PIP_2, which is derived from the hydrolysis of PIP_3 [9]. These findings suggest that membrane potential change directly couples with biochemical signaling pathways and that bioelectricity

influences physiological function in more diverse ways than previously thought. VSP potentially allows us to experimentally control the intracellular signaling pathways activated by electrical stimulation to achieve results at speeds and specificity, which to date are unachievable. I have already prepared the VSP expressing *Dictyostelium* cells to try to manipulate phosphatidylinositol signaling pathway by electric signal (Fig. 4-4B)

References

[**1**] Van Duijn B, Inouye K (1991) Regulation of movement speed by intracellular pH during Dictyostelium discoideum chemotaxis. *Proc Natl Acad Sci U S A* **88**:4951-4955.

[**2**] Patel H, Barber DL (2005) A developmentally regulated Na-H exchanger in Dictyostelium discoideum is necessary for cell polarity during chemotaxis. *J Cell Biol* **169**:321-329.

[**3**] Markin VS, Liu D, Gimsa J, Strobel R, Rosenberg MD, Tsong TY (1992) Ion channel enzyme in an oscillating electric field. *J Membr Biol* **126**:137-145.

[**4**] Cho MR, Thatte HS, Lee RC, Golan DE (1994) Induced redistribution of cell surface receptors by alternating current electric fields. *FASEB J* **8**:771-776.

[**5**] Cho MR, Thatte HS, Lee RC, Golan DE (1996) Reorganization of microfilament structure induced by ac electric fields. *FASEB J* **10**:1552-1558.

[**6**] Weber JH, Vishnyakov A, Hambach K, Schultz A, Schultz JE, Linder JU (2004) Adenylyl cyclases from Plasmodium, Paramecium and Tetrahymena are novel ion channel/enzyme fusion proteins. *Cell Signal* **16**:115-125.

[**7**] Ben-Chaim Y, Chanda B, Dascal N, Bezanilla F, Parnas I, Parnas H (2006) Movement of 'gating charge' is coupled to ligand binding in a G-protein-coupled receptor. *Nature* **444**:106-109.

[**8**] Murata Y, Iwasaki H, Sasaki M, Inaba K, Okamura Y (2005) Phosphoinositide phosphatase activity coupled to an intrinsic voltage sensor. *Nature* **435**:1239-1243.

[**9**] Iwasaki H, Murata Y, Kim Y, Hossain MI, Worby CA, Dixon JE, McCormack T, Sasaki T, Okamura Y (2008) A voltage-sensing phosphatase, Ci-VSP, which shares sequence identity with PTEN, dephosphorylates phosphatidylinositol 4,5-bisphosphate. *Proc Natl Acad Sci U S A* **105**:7970-7975.

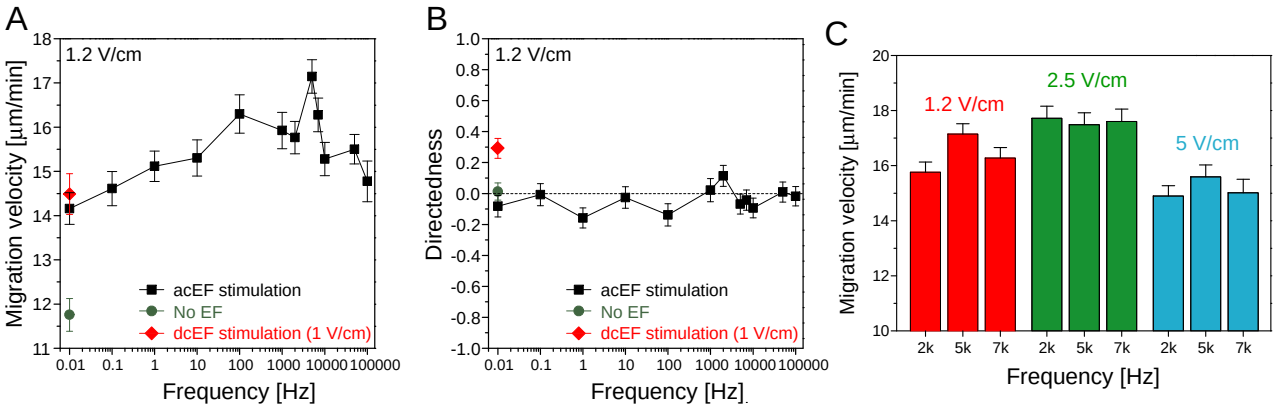

Fig.4-1 Cell motile properties under alternative current electric fields.
Migration velocity (A) and Directedness (B) were analyzed to elucidate the effects of alternative current electric fields (acEFs) on cell motile activities. Directedness was almost constant at different frequencies indicating that input signal was symmetrical. On the other hand, migration velocities were depend on frequency. It reached maximum at around 5 kHz and decreased at more high frequency region. (C) Such increasing of migration velocity also showed slight dependency in applied field strength.
Data was obtained from at 5 independent experiments. Data represents mean±s.e.m.

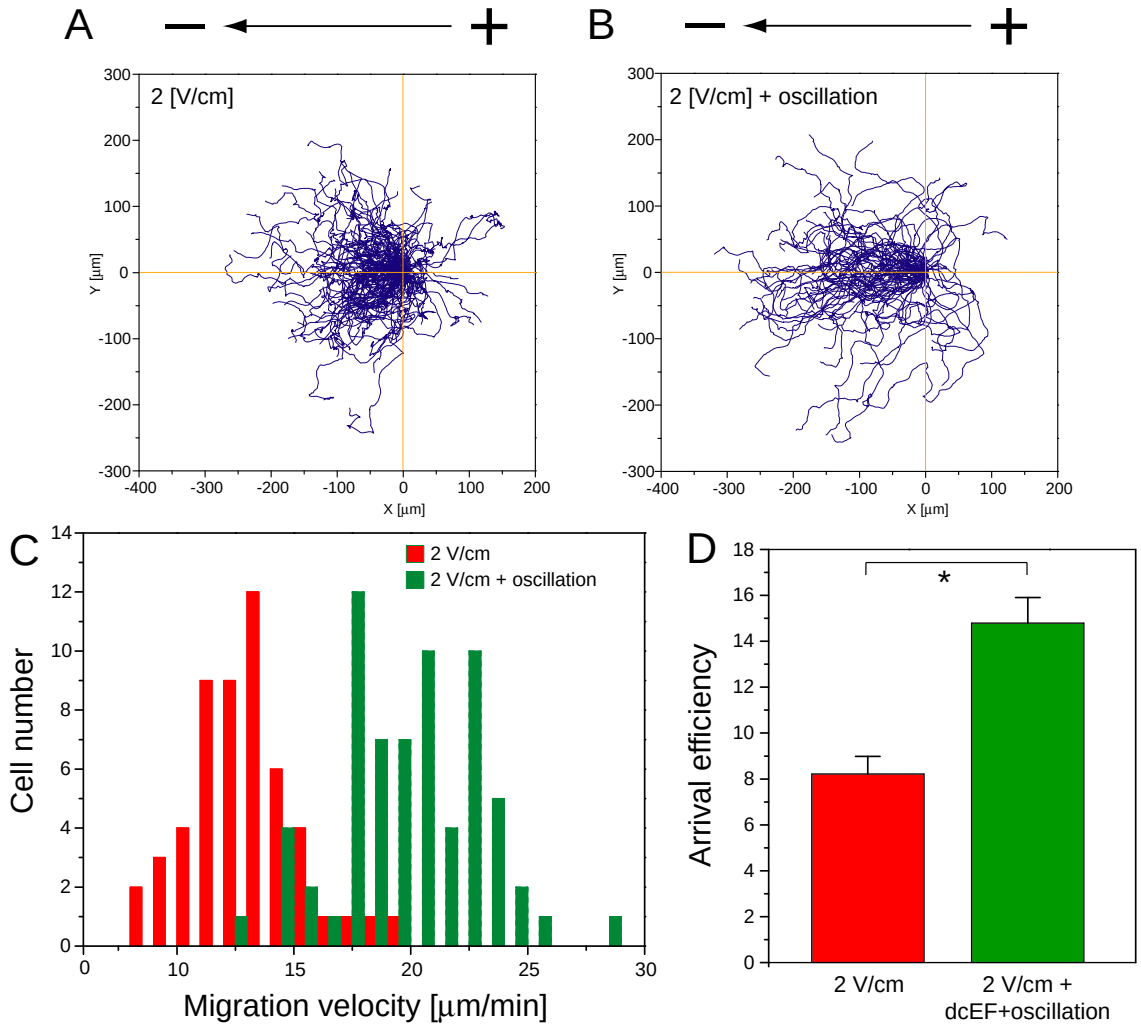

Fig.4-2 Effects of oscillating EF on electrotaxis.
Cell trajectory in dcEF (2 V/cm) (**A**) and dcEF with oscillation (±1 V/cm. 100Hz) (**B**). Cell population with high migration velocity (average 19.8±0.4 μm/min) appeared under dcEF with oscillation (**C**).
Arraival efficiency was calculated by multiplying directedness and migrtion velocity.
Arrival efficiency in the presence of oscillation was about two times higher than that of absence of one indicating that cells could arrive at certain point more efficiently (**D**).
*P < 0.01, unpaired Student's t-test.

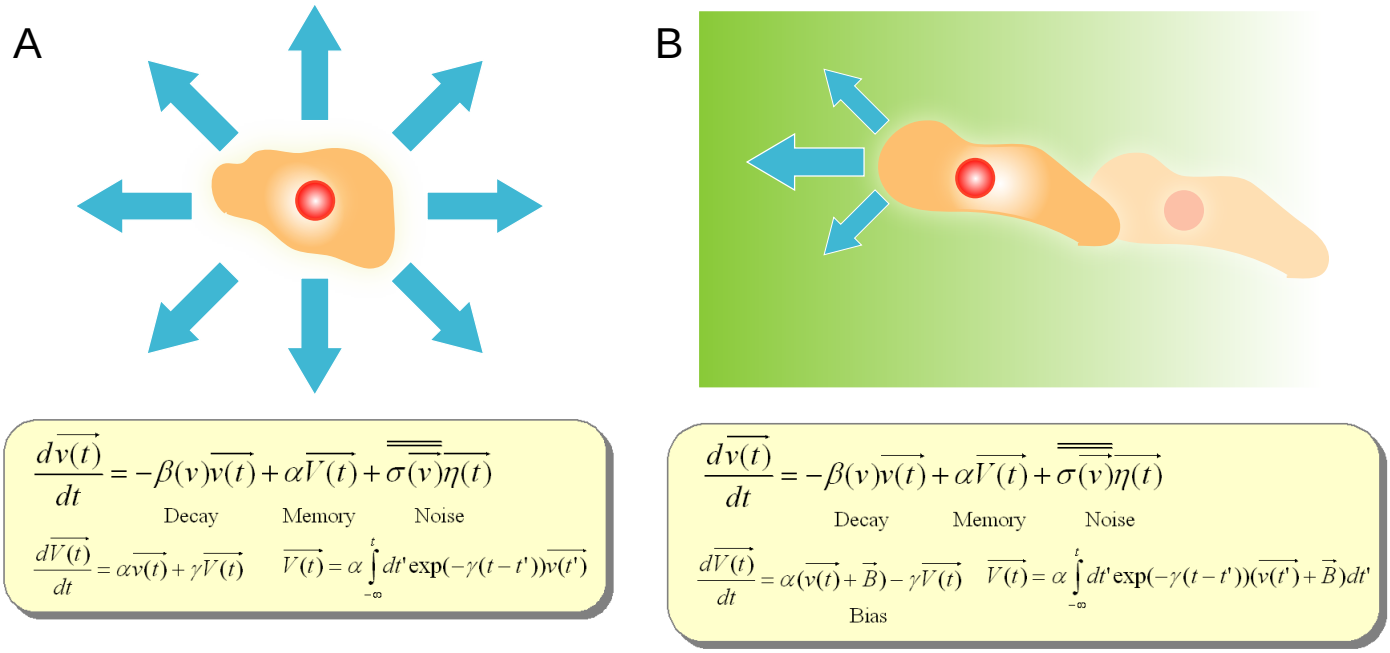

Fig.4-3 Model of spontaneous and tactic cell migration.
Spontaneous (**A**) and electrotactic (**B**) cell migraion models based on a generalized Langevin equation. These models composed of decay, memory, noise and bias term. Here, white gaussian noise is used as a noise term. Simulation of these models produce cell migraiton trajectory and its migration properties such as distribuation of migration velocity and angular are agree with that off experimental data.

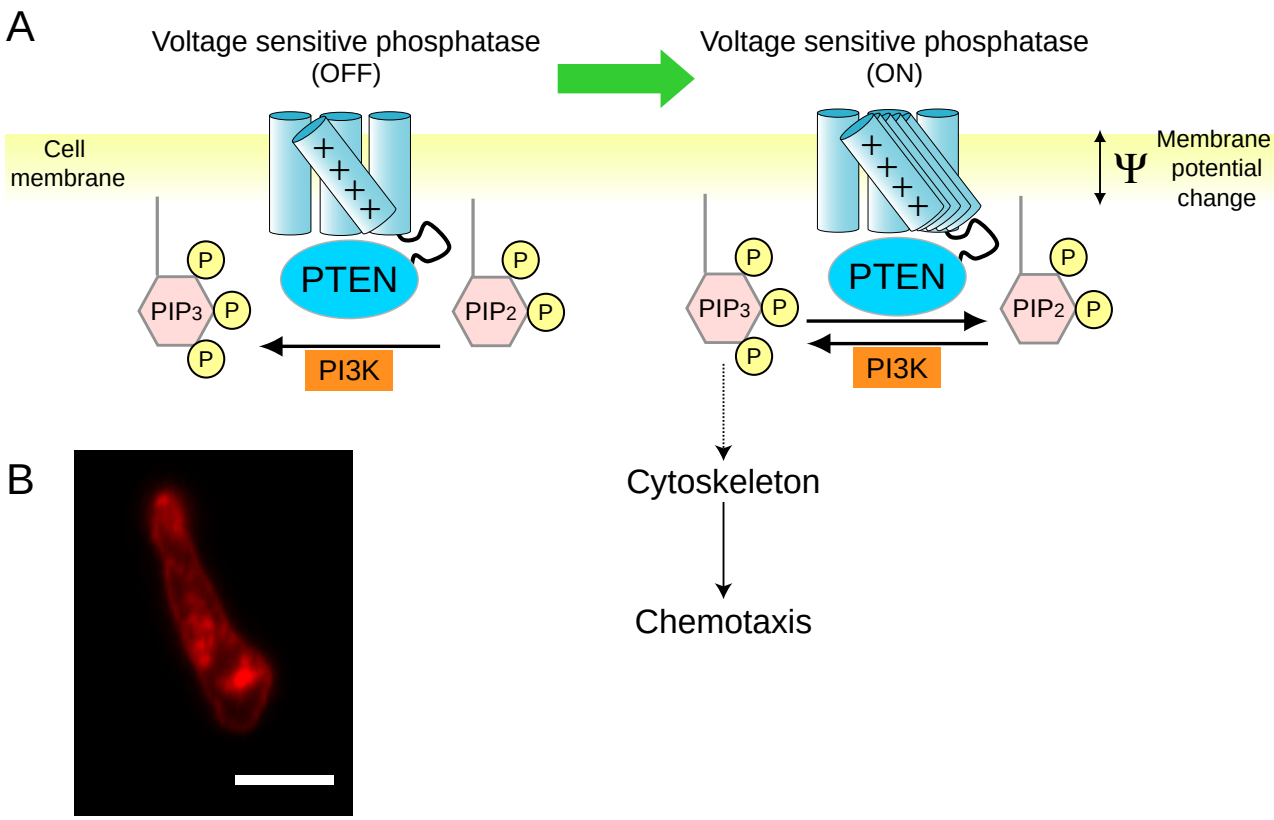

Fig.4-4 Voltage sensitive phosphatase. (**A**) Voltage sensitive phosphatase (VSP) is constructed of three regions, voltage sensitive domain (VSD), phosphatase domain and those linker. VSD and phosphatase domains are resemble for voltage dependent ion channel and phosphatase and tensin homologue deleted on chromosome 10, respectively. When membrane potential depolarize, VSP is activated and dephosphorylates PIP_3. Unlike PTEN, VSP dephosphorylates from PIP_3 to PIP. (**B**) The *Dictyostelium* cells lacking PTEN (*pten*$^-$) were transfected with VSP gene. Fluorescence imaging showed that VSP-Halo tag protein expressed in *Dictyostelium* cells was distributed in membrane uniformly. Scale bar, 5 μm.

Publication list

学術雑誌等又は商業誌における論文（査読あり）

[**1**] Neurite outgrowth on fluorinated polyimide film micropatterned by ion irradiation
Y. Okuyama, M. Sato, S. Nagaoka, H. Kawakami, Y. Suzuki, M. Iwaki
Nuclear Insruments and Methods in Physics Research Section B **206**, p543-547. (2003).

[**2**] Input-output relationship in galvanotactic response of Dictyostelium cells.
MJ. Sato, M. Ueda, H. Takagi, TM. Watanabe, T. Yanagida, M. Ueda
Biosystems **88**, p261-272. (2007).

[**3**] Biologically-inspired stochastic vector matching for noise-robust information processing
M. Ueda, M. Ueda, H. Takagi, MJ. Sato, T. Yanagida, I. Yamashita, K. Setsune
Physica A **387**, p4475-4481 (2008).

[**4**] Functional analysis of spontaneous cell movement under different physiological conditions
H. Takagi, MJ. Sato, T. Yanagida, M. Ueda
PLoS One **3**:e2648. (2008).

[**5**] Switching direction in electric signal-induced cell migration by cGMP and phosphatidylinositol signaling
M.J. Sato, H. Kuwayama, W. van Egmond, A.L.K. Takayama, H. Takagi, P. van Haastert, T. Yanagida, M. Ueda
submitted to *Proc Natl Acad Sci U S A.* **106**, pp6667-6672 (2009).

学術雑誌等又は商業誌における解説、総説

[**1**] 高木拓明、佐藤雅之 細胞性粘菌の自発運動解析、物性研究 2007 年 3 月号 vol.87 no.6 p.907-913 (2007).
[**2**] Fluctuations and Noises in Biosciences. T. Yanagida, Y. Miyanaga, M. Sugawa and

MJ. Sato NOISE ANS FLUCTUATIONS, New York, AIP Conference proceedings, Munecazu T. *et al. Ed*, Vol.**922**, pp10-15 (2007).

学会発表

[**1**] M. Sato (2003) “Constructive Brain Science”, 21COE International Symposium, Future Directions for Analyzing Cell and Molecular Functions, SESSION IV、平成 15 年 9 月 16 日—9 月 17 日,仙台国際センター.

[**2**] 佐藤雅之、上田昌宏、桑山秀一、柳田敏雄(2004) “細胞性粘菌 における走電性応答の解析”, 第 6 回細胞性粘菌研究会, 平成 16 年 3 月 8 日—3 月 9 日, 東京大学山上会館.

[**3**] 佐藤雅之、上田昌宏、桑山秀一、高木拓明、柳田敏雄(2004) “細胞性粘菌の走電性における cAMP 刺激の効果”, 第 7 回細胞性粘菌研究会, 平成 16 年 11 月 26 日—11 月 27 日, 立命館大学エポック 21.

[**4**] 佐藤雅之、上田昌宏、桑山秀一、高木拓明、柳田敏雄(2004) “細胞性粘菌の走電性における cAMP 刺激の効果”, 日本生物物理学会第 42 回年会, 平成 16 年 12 月 13 日—12 月 15 日, 国立京都国際会館.

[**5**] M. Sato, M. Ueda, H. Takagi and T. Yanagida (2005) “Effects of cAMP stimulation on efficiency of galvanotaxis in *Dictyostelium discoideum*.”, Biophysical Society 2005 annual Meeting, 平成 17 年 2 月 12 日—2 月 16 日, アメリカ・カリフォルニア.

[**6**] 佐藤雅之、上田昌宏、桑山秀一、高木拓明、柳田敏雄(2005) “細胞性粘菌の走電性におけるPI3 キナーゼ経路の関与”, 日本生物物理学会第 43 回年会, 平成 17 年 11 月 23 日—11 月 25 日, 札幌コンベンションセンター.

[**7**] M. Sato, M. Ueda, H. Kuwayama, H. Takagi and T. Yanagida (2005) “Directional migration of *Dictyostelium* amoeba in an electric field”, Biocomp2005, Hotel Lloyd's Baia, 平成 17 年 12 月 10 日—12 月 18 日, イタリア.

[**8**] 佐藤雅之、桑山秀一、高木拓明、柳田敏雄、上田昌宏(2006) “細胞性粘菌における走電性応答の解析”, 平成 18 年生体運動研究合同班会議, 平成 18 年 1 月 6

日—1 月 8 日, 東京大学弥生講堂.

[**9**] H. Takagi and M. J. Sato (2006) “Analysis of spontaneous cell motion”, 9th Tamura symposium, Frontiers in Dynamics physical and biological systems, 平成 18 年 5 月 22 日—5 月 24 日, 東京大学小柴ホール.

[**10**] 佐藤雅之、高木拓明(2006) “細胞性粘菌の走電性運動のメカニズム”, FCS研究会「細胞の運動と知能」,平成 18 年 6 月 8 日—6 月 9 日, 名古屋大学東山キャンパスベンチャービジネスラボラトリー.

[**11**] H. Takagi, M. J. Sato, T. Yanagida, and M. Ueda (2006) “Dynamics of spontaneous cell motion in the developmental process of Dictyostelium cells”, Japanese-Korean Joint Meating for Mathematical Biology, 平成 18 年 9 月 16 日—9 月 18 日, 九州大学.

[**12**] M. J. Sato, H. Kuwayama, H. Takagi, T. Yanagida and M. Ueda. (2006) “Directional reversal of electrotactic movements in cyclic GMP metabolic mutants”, 日本生物物理学会第 44 回年会, 平成 18 年 11 月 12 日—11 月 16 日, 沖縄コンベンションセンター.

[**13**] 佐藤雅之、高木拓明(2007) “遊走する細胞と運動制御”, 交通流数理研究会第 12 回交通流のシュミレーション, 平成 18 年 12 月 1 日—12 月 2 日, 大阪大学サイバーメディアセンター.

[**14**] M. Sato, H. Kuwayama, H. Takagi, T. Yanagida and M. Ueda (2007) “Directional Cell Movement in an electric field”, The 9th International Symposium on Future Medical Engineering based on Bio-nanotechnology, 平成 19 年 1 月 7 日—1 月 9 日, 仙台国際センター.

[**15**] 高木拓明、佐藤雅之、柳田敏雄、上田昌宏(2007) “細胞性粘菌における自発運動の解析”, 平成 19 年生体運動研究合同班会議, 平成 19 年 1 月 7 日—1 月 9 日, 金沢市文化ホール.

[**16**] M. J. Sato, H. Kuwayama, H. Takagi, T. Yanagida and M. Ueda (2007) “Reversal of directional preference during electrotaxis through defects in guanylyl cyclase and phosphatidylinositol-3-OH kinase.”, Gordon Research Conference on Gradient Sensing & Directed Cell Migration, 平成 19 年 1 月 28 日-2 月 2 日, アメリカ・カリフォルニア.

[**17**] 佐藤雅之、桑山秀一、高木拓明、柳田敏雄、上田昌宏(2007) “細胞性粘菌における走電性応答の解析”, 第 9 回細胞性粘菌研究会, 平成 19 年 2 月 17 日—2 月 18 日, 富山大学黒田講堂.

[**18**] MJ. Sato, H. Kuwayama, H. Takagi, T. Yanagida and M. Ueda (2007) “Directional Cell Movement in an Electric Field”, ELECTRO-CHEMICAL SIGNALING BY MEMBRANE PROTEINS, 平成 19 年 3 月 14 日—3 月 16 日, 岡崎カンファレンスセンター

[**19**] 高木拓明, 佐藤雅之, 柳田敏雄, 上田昌宏(2007) “細胞性粘菌の発生過程における自発運動の解析”, 日本物理学会 2007 年春季大会, 平成 19 年 3 月 18 日—3 月 21 日, 鹿児島大学.

[**20**] 佐藤雅之(2007) “電気シグナルに応答する細胞性粘菌”, 生命分子の集合原理に基づく分子情報科学研究ネットワーク拠点スクーリング, 平成 19 年 12 月 11 日—12 月 12 日, 九州大学箱崎キャンパス.

[**21**] 佐藤雅之、柳田敏雄、上田昌宏(2007) “振動する電気シグナルの細胞運動への影響”, 日本生物物理学会 45 回年会, 平成 19 年 12 月 21 日—12 月 23 日, パシフィコ横浜.

[**22**] 高木拓明, 佐藤雅之, 柳田敏雄, 上田昌宏(2007) “細胞性粘菌における走電性運動の解析”, 日本生物物理学会 45 回年会, 平成 19 年 12 月 21 日—12 月 23 日, パシフィコ横浜.

[**23**] 高山愛理, 佐藤雅之, 新井由之, 柳田敏雄, 上田 昌宏(2007) “走電性時の細胞性粘菌におけるPI3 キナーゼとグラニル酸シクラーゼ依存情報伝達経路の細胞内ダイナミクス”, 日本生物物理学会 45 回年会, 平成 19 年 12 月 21 日—12 月 23 日, パシフィコ横浜.

[**24**] H.Takagi, M.J. Sato, T. Yanagida, M. Ueda (2008) “Spontaneous cell movement and galvanotactic response in Dictyostelium cells”, Biophysical society 2008 annual meeting, 平成 20 年 2 月 2 日—2 月 6 日, アメリカ・カリフォルニア州.

[**25**] A. Takayama, M.J. Sato, Y. Arai, T. Yanagida, M. Ueda (2008) “Behavior of signaling molecules in electrotaxis of Dictyostelium cells”, Biophysical society 2008 annual meeting, 平成 20 年 2 月 2 日—2 月 6 日, アメリカ・カリフォルニア州.

[**26**] M.J. Sato, WN. van Egmond, H. Takagi, P.J.M. van Haastert, T. Yanagida and M. Ueda (2008) “Switching direction in electric signal-induced cell migration by cGMP and phosphatidylinositol signaling”, Gordon Research Conference on Bioelectrochemistry, 平成 20 年 7 月 19 日-7 月 25 日, アメリカ・メイン州.

Acknowledgement

I would like to express my deep and sincere gratitude to my supervisor, Professor Toshio Yanagida, Ph.D., Graduate School of Frontier Biosciences, Osaka University. His wide knowledge and his suggestion have been of great value for me. I am deeply grateful to my supervisor, Professor Masahiro Ueda, Ph.D., Head of the CREST project, for his detailed, constructive comments for planning of experiment and for his important support throughout this work. I wish to express my warm and sincere thanks to Hiroaki Takagi, Ph.D. (Nara Medical University) and Tatsuo Shibata, Ph.D. (Hiroshima University). They help me in the aspect of theoretical and analytical framework of this work and they always encouraged me to progress the work. Collaborator, Hidekazu Kuwayama, Ph.D. (Tsukuba University), Wouter Van Egmond and Peter van Haastert, Ph.D. (Groningen University) kindly gave essential various types of cell lines for this work and these promoted my study extensively. I also thank Peter Karagiannis for reading the manuscript and correcting the manuscript. I also wish to thank SBC group member and Yanagida Lab.'s member for technical suggestion and useful discussion. I wish to express my warm and sincere thanks to Professor Hiroshi Hamada Ph.D., Nobuhiko Yamamoto, Ph.D., Graduate School of Frontier Biosciences, Osaka University and Yasushi Okamura Ph.D., Department of medicine, Osaka University for evaluating this work and gave many useful comments on this work. During Ph.D course, my parents gave financial support to me and always encouraged me. Here, I would like to express my deep gratitude for my parents and Satomi Tetsumoto. This work is supported by Research Fellowships of the Japan Society for the Promotion of Science for Young Scientists, Japan and supported by MEXT's Leading Project.

Masayuki J. Sato